NONLINEAR OSCILLATIONS OF HARMONICALLY EXCITED AUTOPARAMETRIC SYSTEMS

A Thesis Submitted
in Partial Fulfilment of the Requirements
for the Degree of

DOCTOR OF PHILOSOPHY

by

HIMANSHU HATWAL

to the

DEPARTMENT OF MECHANICAL ENGINEERING
INDIAN INSTITUTE OF TECHNOLOGY KANPUR
SEPTEMBER, 1981

To
My parents

CERTIFICATE

This is to certify that the present work "NONLINEAR OSCILLATIONS OF HARMONICALLY EXCITED AUTOPARAMETRIC SYSTEMS" has been carried out under our supervision and has not been submitted elsewhere for the award of a degree.

A. Ghosh
Professor
Department of Mech. Engg.
I.I.T. Kanpur
INDIA

A.K. Mallik
Assistant Professor
Department of Mech. Engg.
I.I.T. Kanpur
INDIA

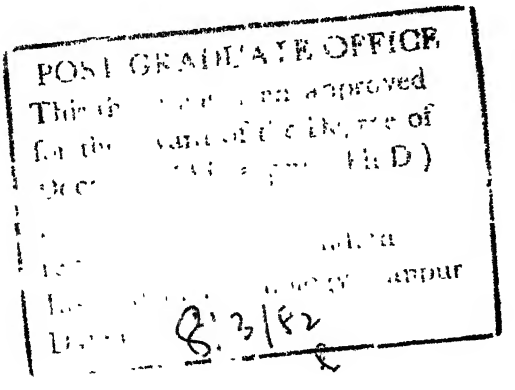

ACKNOWLEDGEMENT

The author expresses his deep sense of appreciation and gratitude to his advisors Dr. A.Ghosh and Dr.A.K.Mallik who have guided this work from conception to completion.

The author gratefully acknowledges the help from Mr. R.M.Jha and Mr.M.M.Singh in the experimental work.

The author would like to recall his deep sense of gratitude to his friends Messers Nirmal Roberts, E.S.Reddy, M.C.Prakash and I.K.Bhatt for their cooperation in various stages.

Thanks are also due to Mr.J.D.Verma, Mr. P.P.Singh and Mr.Ayodhya Prasad to produce the work in the present form.

Finally, I acknowledge my great indebtedness to Mrs. Meena Ghosh and Mrs. Kaberi Mallik for giving me homely care during my illness.

CONTENTS

LIST OF FIGURES

LIST OF PRINCIPAL SYMBOLS

A	:	Nondimensional amplitude of the primary mass
B	:	Amplitude of oscillations of the pendulum
h	:	Step size of integration
$J_n(\ )$	:	Bessel's coefficient of order n
l	:	Length of the pendulum
M	:	Mass of the primary
m	:	Mass of the pendulum
P	:	Nondimensional amplitude of the exciting force
p	:	Forcing frequency nondimensionalized with respect to natural frequency of the primary mass
$\bar{p}$	:	Forcing frequency nondimensionalized with respect to natural frequency of the locked mass
q	:	Ratio of natural frequencies of the pendulum and the locked mass
q_1	:	Ratio of natural frequencies of the gravity controlled pendulum and the locked mass
q_2	:	Ratio of natural frequencies of the spring controlled pendulum and the locked mass
R	:	Ratio of the pendulum mass and the primary mass
$\bar{t}$	:	Nondimensional time
$\bar{x}$	:	Nondimensional displacement of the primary mass
Y	:	Amplitude of base displacement of the primary mass
$\bar{Y}$	:	Nondimensional amplitude of the base displacement

Z : Amplitude of longitudinal motion of the elastic pendulum

$\bar{z}$: Nondimensional longitudinal displacement of the elastic pendulum

α, β : Coefficients of Mathieu equation

δ : Tuning ratio of the auxiliary mass damper

ζ_1 : Damping ratio of the primary mass

$\bar{\zeta}_1$: Damping ratio of the locked mass

ζ_2 : Damping ratio of the pendulum

θ : Angular displacement of the pendulum

μ : Damping ratio of the auxiliary mass damper

Φ_0, Φ_1, Φ_2 : Phase angles

ω : Forcing frequency

SYNOPSIS

NONLINEAR OSCILLATIONS OF HARMONICALLY EXCITED AUTOPARAMETRIC SYSTEMS

A Thesis Submitted
In Partial Fulfilment of the Requirements
for the Degree of
DOCTOR OF PHILOSOPHY
by
HIMANSHU HATWAL
to the
DEPARTMENT OF MECHANICAL ENGINEERING
INDIAN INSTITUTE OF TECHNOLOGY KANPUR
SEPTEMBER, 1981

As the title suggests, this thesis presents a study on nonlinear oscillations of harmonically excited autoparametric systems. Two different types of systems are investigated. The first one has two degrees of freedom. It comprises of a spring - mass - dashpot primary system and a secondary system which is a damped rigid pendulum hinged to the primary mass. The second type of system, having three degrees of freedom, is very similar to the first one except that in this case the secondary consists of an elastic pendulum. In both cases the primary mass is excited by a harmonic force of constant amplitude. The linear natural frequencies of both the systems are adjusted so as to cause internal resonance.

The work is broadly divided in five sections. The first four sections are devoted to the study of systems of the first type. The last section deals with only the absorber action of the secondary in both types of systems (i.e., with rigid and elastic pendulum).

The first part deals with the harmonic responses under small excitation. Two types of restoring couples on the pendulum are considered. In the first case the restoring couple is entirely due to gravity field, when the pendulum can execute continuous revolutions. In the second case a linear torsional spring, preventing continuous revolutions of the pendulum, provides the entire restoring couple. With a harmonic forcing function, the steady state responses are also expected to be harmonic. As such the method of harmonic balance is used. The stability characteristics are studied by perturbing the approximate solutions. Whenever necessary, the analytical results are successively refined with the help of higher order approximations by including higher order nonlinearities. The approximate results are verified by numerically integrating the equations of motion.

With both types of pendulums (spring controlled and gravity controlled) it is observed that for an excitation amplitude greater than a critical value (which depends on other system parameters) the responses no longer remain harmonic in certain frequency ranges.

Integrated results show that with the spring controlled pendulum the responses still remain periodic, whereas, the gravity controlled pendulum may result in nonperiodic responses. For the system having a spring controlled pendulum, the stable harmonic motion bifurcates to one unstable harmonic motion and another stable amplitude modulated periodic state. This bifurcation is found to be associated with a jump in the amplitude values. Rest of the thesis is devoted only to the system with a gravity controlled pendulum.

Higher values of the excitation parameter are dealt with in the second part of the thesis. In the regions of unstable harmonic solutions, numerical integrations are carried out to study the nature of the responses. Depending on the frequency, the following two types branching of the stable harmonic motion are obtained:

i) With a moderate excitation the stable harmonic motion branches out to one (or more) unstable harmonic state(s) and one (or more) amplitude modulated periodic motion(s). The amplitude modulated states (depending on the initial conditions) are weakly stable and the modulation period can vary over a wide range. In this branching the amplitudes do not increase sharply.

ii) The stable harmonic motion branches out to one (or more) unstable harmonic state(s) and another chaotic state. This branching is associated with sharp increase in the amplitudes.

The approximate method is not applicable in the chaotic regime and the results are obtained by only numerical integration, which do not converge and the responses are completely nonperiodic. Thus the responses, though remaining bounded, can not be described uniquely.

In the third part of this work statistical description of the nonperiodic responses is attempted with the proposition that in such cases the actual physical experiment would yield random responses and the integrated results represent these. Mean square values and PSD's are obtained by using different step sizes of integration and initial conditions. These values are found not to differ much and as such are considered as meaningful descriptions of the responses. The nature of the PSD functions for the primary and the secondary is investigated; no attempt, however, is made to correlate the statistical descriptions with the system parameter combinations.

In the fourth part of the thesis some experimental results are reported. The major objective of these experiments is to verify qualitatively the analytical results presented earlier. In the experiment, a harmonic

base excitation, instead of a force excitation, is given to the primary system. This does not alter the basic characteristics of the system investigated earlier. It is seen that for certain combinations of parameters the system responses indeed become random and for these parameter combinations the numerical integrations also do not converge.

The vibration neutralizing effect of the pendulum is studied in the last part. The rigid pendulum in the two degree-of-freedom system is shown to exhibit limited absorber action. The range and scope of this absorber are discussed. The optimum value of the absorber damping is found to depend upon the level of excitation amplitude. Lastly, the absorber action of a damped elastic pendulum is studied briefly. It is shown that with a nonoptimal auxiliary mass damper, the peaks in the responses may be suppressed by providing the secondary with an additional degree of freedom in rotation.

CHAPTER I

INTRODUCTION

1.1 INTRODUCTION AND LITERATURE SURVEY

Vibratory systems, in practice, are all nonlinear, but within certain limits they can, in many ways, be depicted in approximate fashion by a linear autonomous system for which the complete solution can be obtained in closed form. Unlike linear systems, nonlinear systems and non-autonomous linear systems do not lend themselves to general solutions. Moreover, many intricate features of the nonlinear systems are lost in the process of linearization. Systems of special interest are those possessing periodic solutions. Since the qualitative and the quantitative characteristics of such systems can not be obtained in totality, some approximate methods are called for to analyse these. Because of lack of generalized analysis, different types of nonlinear equations exhibit different interesting features. A special class of nonlinear systems includes parametric and autoparametric systems.

Parametric vibration refers to the oscillatory motion that occurs in a system as a result of time-dependent (usually periodic) coefficients in the governing differential equation (i.e. nonautonomous equations). In such cases the time dependence is explicit, which implies an

external energy source (pump). Parametric oscillations may stabilize a system which is statically unstable or may destabilize a statically stable system. The standard second order homogeneous linear equations with periodically time varying coefficients have the form of Mathieu - Hill equations [1, 2]. According to linear theory, the oscillations in the regions of instability increase unboundedly and rapidly. These growths are checked due to nonlinearities of the system and the oscillations may become periodic. Various types of nonlinearities in a dynamical system are listed in reference [3].

For a two degree-of-freedom system, the autoparametric oscillations arise due to nonlinear coupling between the governing equations rather than the explicit time-dependence of the coefficients. This type of system is termed an autoparametric system (because no external pumping is required) or a system with internal resonance (because certain combinations of linear natural frequencies of the two modes cause resonance). The term autoparametric is more appropriate because unlike other resonances (which are observed at discrete frequencies only) these systems exhibit resonance over a frequency range - a characteristic of the parametric oscillations.

A system, besides having parametric (or autoparametric) oscillations, may be subjected to external

inputs appearing as nonhomogeneous terms in the equations. An excellent review of parametric vibrations is given in reference [4 - 8]. Other useful references may be found in [9, 10] .

In the present work the autoparametric vibrations of a simple and an elastic pendulum are studied. A simple pendulum with an oscillating support has been used extensively to explain parametric instability. The response characteristics of this system have also been studied in detail; to quote a few references, Skalak and Yarymovytch [11], Caughey [12, 13], and Struble [14, 15] studied the steady state responses of a pendulum with a vertically or horizontally oscillating support. In these analyses only the first nonlinear term was retained. Chester [16] investigated the same system with both horizontal and vertical motions of the support.

The pendulum as a part of a two-degree-of-freedom autoparametric system has also been studied. The autoparametric instability and energy transfer associated with coupled differential equations of a beam-pendulum system have been investigated [17 - 19]. A similar system with a small external excitation was studied in [20]. Free oscillations of an elastic pendulum, with the linear natural frequencies in the longitudinal and angular motions adjusted so as to cause internal resonance, were investigated in

[21 - 24]. Ryland and Meirovitch[25] determined the stability boundaries of a swinging spring with an oscillating support.

A part of the system, under investigation in this work, is a hinged pendulum capable of executing large motions. With first order approximation, the equations of motion have quadratic nonlinearities. Such equations have been studied in detail under the conditions of internal resonance. It is well known that with harmonic excitation of these systems, the stable periodic solutions may branch out to one unstable and two stable periodic solutions; this is associated with jumps in the amplitude values. It was shown in [26, 9] that if the excitation frequency is in the neighbourhood of the lower natural frequency (which is half of the other), another branching of the stable periodic solution may take place without any jump. In this case one unstable periodic solution and another stable amplitude modulated motion are obtained. Such phenomena have also been observed by Miles [27] in a system with two equal linear natural frequencies and with cubic nonlinearities, and by Yamamoto and Yasuda [28] in a system with one linear natural frequency twice the other and having quadratic and cubic nonlinearities. Sethna and Bajaj [29] derived the conditions on the system parameters at which the stable periodic motion bifurcates into an unstable periodic motion

and an amplitude modulated motion at the excitation frequency. In the course of present study also, such amplitude modulated motions are found but with the difference that there may exist more than one set of amplitudes at which the modulation occurs and that these states are weakly stable. Moreover, another branching of the stable periodic states is observed where besides one (or more) unstable periodic state(s) a nonperiodic state is obtained. The latter state reveals almost random motion of the system.

The deterministic systems, with simple mathematical models, producing random or chaotic motions have long been observed in various biological, economic, social and physical sciences and have been reviewed by May [30]. Lorenz [31] called this general phenomenon the "butterfly effect" : even if the atmosphere could be described by a deterministic model, the fluttering of a butterfly's wings could alter the initial conditions, and thus (in the chaotic regime) alter the long term predictions. Holmes [32] + studied a nonlinear oscillator for which complicated nonperiodic motions arise. He called these motions as strange attractors, studied their structure by means of the Poincare map and developed a necessary criterion for strange attractor motions which determines the minimum

---

+ References [32 - 34] were noticed towards the end of this thesis.

forcing amplitude as a function of forcing frequency. As a mechanical example, Moon and Holmes [33] examined the non-linear forced vibrations of a cantilever beam which is buckled by magnetic forces. Moon [34] later presented an experimental criterion on the forcing amplitude and frequency for strange attractor motions and developed a heuristic formula. The basic system in [32 - 34] had two stable and one unstable static equilibrium positions. For fixed damping and frequency, the motion for small forcing amplitudes was periodic (about either of the stable fixed point) but became chaotic for larger forcing amplitudes, with the solution jumping from one equilibrium to the other. For sufficiently large forces the oscillations encompassed all three fixed points of the unforced system resulting in periodic motions. The present work shows a possibility of such chaotic motions with a two degree-of-freedom system where one mode is parametrically excited and the unforced system has only one static equilibrium position.

Lastly a few applications of the parametric phenomenon have also been reported in the literature. In electrical devices this phenomenon has been exploited considerably [35]. Rodgers [36, 37] suggested the mechanical amplifiers based on the parametric phenomenon, which was further studied by Eisinger and Merchant [38, 39]. Haxton and Barr [20] suggested an autoparametric vibration absorber

(which is rather a neutralizer). Curiously the practicability of such absorbers was not explored further. Unlike the conventional auxiliary mass damper which gives linear response characteristics, the auxiliary system (which is a cantilever beam with a concentrated mass at the free end) considered in [20] was excited because of nonlinear coupling. The range of frequency over which the cantilever beam oscillates was determined from the instability zones of its static equilibrium position. The response characteristics of such systems obviously depend on the force amplitude. In the present work a similar system (with a hinged pendulum instead of a cantilever beam) is studied in detail for different levels of excitations (harmonic) and is shown to exhibit many interesting features.

Two major approaches to the solution of nonlinear differential equations are (i) the qualitative methods and (ii) the quantitative methods. Only the latter approach is used since we are interested in the quantitative analysis as well. Some of the popular methods are methods of averaging due to Krylov - Bogoliubov - Mitropolski [40] and Struble [41], method of multiple scales [42] and method of harmonic balance [3]. These methods have found interesting and wide applications to study various phenomena in nonlinear differential equations with or without excitation. The method of harmonic balance is not very suitable for the study of free oscillations where a priori

knowledge of the solution is not available. For forced oscillations with harmonic inputs, however, this method is more straightforward to study the nature and amplitudes of the harmonic responses. Most of the results in this thesis are obtained using the method of harmonic balance.

1.2 OBJECTIVE AND SCOPE OF THE PRESENT WORK

Nonlinear systems are mostly analysed for small oscillations. The objective of the present work is to study an autoparametric system under harmonic excitation with no restrictions on the amplitudes. The system comprises of a primary, which is a spring - mass - dashpot system, and a secondary, which is a damped rigid pendulum hinged to the primary mass. The characteristics of the spring and the dashpots are assumed to be linear. The primary mass is excited by a harmonic force and its linear natural frequency is taken as twice that of the pendulum so as to cause internal resonance.

In Chapter 2 the existence and characteristics of the harmonic responses of this system are studied. Approximate results are obtained by using the method of harmonic balance. The accuracy of the solutions are checked by considering different orders of approximations. Stability of the harmonic motion is checked by perturbing the solutions. To check the validity of the approximate results

the equations of motion are numerically integrated. Further to study the effect of allowing the pendulum to make complete revolutions, two types of restoring couples on the pendulum are considered. In the first case the restoring couple is entirely due to gravity field, when the pendulum can execute continuous revolutions. In the second case a linear torsional spring, preventing continuous revolutions of the pendulum, provides the entire restoring couple. In both cases it is observed that for an excitation amplitude greater than a critical value (which depends on other system parameters) the responses no longer remain harmonic in certain frequency ranges. From the integrated results it is seen that the responses with the spring controlled pendulum still remain periodic, whereas, the gravity controlled pendulum results in nonperiodic responses.

For excitation amplitudes greater than this critical value, further analysis is carried out in Chapter 3 with the gravity controlled pendulum only. The major objective in this chapter is to determine the regions of stable harmonic solutions and the behaviour of the responses when the harmonic solutions are unstable. To this end, the regions of stable and unstable harmonic solutions are obtained by the approximate method. By plotting these regions in the forcing amplitude and frequency plane, it is observed that there are two separate regions where the

harmonic solutions are unstable. Numerical integrations reveal that only in one of these regions, and for a limited range of forcing amplitude, frequency and initial conditions, the response may be amplitude modulated. For other cases (where harmonic solutions are unstable) the responses are seen to be completely nonperiodic. For this reason the approximate solutions are not attempted in these ranges of unstable solutions. Rather the emphasis is placed on the results obtained by numerical integrations.

For these cases, the integrated responses are seen to be nonperiodic and nonconvergent. Based on physical arguments, an attempt is made to interpret these nonconvergent results. It is proposed that in such cases the actual physical experiment would yield random responses and that the integrated results represent these. With this consideration, the statistical analysis of the integrated responses is undertaken in Chapter 4. We try to establish the randomness of the responses through autocorrelation and power spectral density functions. For obtaining these statistical quantities the hypothesis of stationarity is assumed. An attempt is also made to justify this hypothesis by performing run tests.

The statistical analysis in Chapter 4 is carried out with the expectation that the actual physical system (for certain combinations of parameters) would also result

in nonreproducible and nonperiodic (i.e. random) responses. With this point of view an experiment is performed and the results are presented in Chapter 5. The objective of the experiment is only to verify the existence of random responses of the deterministic system with a harmonic excitation. No statistical analysis of the experimental results is attempted.

In Chapter 6 the objective is to study the vibration - neutralizing effect of the pendulum. The pendulum, as a parametrically excited secondary system, is indeed found to neutralize the vibrations of the primary mass, which is acted upon by an external force. The range and scope of this absorber action are discussed. Further, based on these results, the absorber action of a damped elastic pendulum is studied briefly.

CHAPTER 2

RESPONSE OF A TWO DEGREE - OF - FREEDOM AUTOPARAMETRIC SYSTEM TO HARMONIC EXCITATION

2.1 INTRODUCTION

In this chapter the forced oscillation of a two degree - of - freedom autoparametric system is studied. The system under investigation is shown in Fig. 2.1. The excitation is considered to be harmonic and the range of the amplitude is limited so as to produce a harmonic response of the system. The system comprises of a primary, consisting of a linear spring - mass - dashpot and a secondary, consisting of a damped rigid pendulum. The primary mass is excited by a harmonic force. The linear natural frequencies of the primary and the secondary are adjusted so as to cause internal resonance. The range of excitation frequency considered is such that the pendulum is parametrically excited. Two types of restoring couples on the pendulum are investigated. In the first case, the restoring couple is only due to gravity, whereas in the second a torsional spring provides the entire restoring couple.

The responses are evaluated approximately by using the methods of harmonic balance [3] and multiple time scale (MTS) [42]. While using MTS method only the first order approximation is used and the results are compared with the

first order approximate results obtained by harmonic balance method. It is shown that with the harmonic excitation, where the responses are also expected to be harmonic (and hence a priori knowledge of the solution is intuitively available), the results obtained by the first order harmonic balance are accurate as compared to those obtained by using the same order approximation in MTS method.

Solutions are also obtained by including higher order approximations in harmonic balance. Stability of the obtained solutions is investigated by perturbation technique and using Floquet's theory[9] . The results obtained by different order approximations are compared. It is shown that the first order approximation not only gives quantitatively inaccurate results in some cases but may even fail to predict the stability characteristics properly. The approximate results are also verified by numerical integrations of the equations of motion.

For certain combinations of parameters the second order approximate results are found to be unstable. Only the existence of such combinations of parameters is shown in this chapter. The study of the responses under such situations is undertaken in the next chapter.

2.2 SYSTEM DESCRIPTION AND EQUATIONS OF MOTION

Figure 2.1 shows the two degree - of - freedom system in which the primary consists of the mass M, the linear spring of stiffness k_1 and the viscous dashpot of damping coefficient c_1. The secondary system comprises of a simple pendulum of length l under gravity field and hinged to mass M. The mass of the pendulum bob is m and k_2 refers to the torsional spring resisting the angular motion of the pendulum. The pendulum motion is damped by a viscous damper of coefficient c_2. The primary mass is excited by a harmonic force $F \cos \omega t$.

The equations of motion of the system are

$$(M + m)\ddot{x} + c_1\dot{x} + k_1 x - ml(\ddot{\theta}\sin\theta + \dot{\theta}^2\cos\theta) = F\cos\omega t \qquad (2.1)$$

and $$ml^2\ddot{\theta} + c_2\dot{\theta} + k_2\theta + (mgl - ml\ddot{x})\sin\theta = 0, \qquad (2.2)$$

where x represents the displacement of M ; θ, the rotation of the pendulum, the dot implies the derivative with respect to time t and F and ω are, respectively, the amplitude and frequency of the excitation. Equations (2.1) and (2.2) can be written as

$$(1 + \frac{m}{M})\ddot{x} + 2\zeta_1\Omega_1\dot{x} + \Omega_1^2 x - \frac{m}{M}l(\ddot{\theta}\sin\theta + \dot{\theta}^2\cos\theta) = \frac{F}{M}\cos\omega t \qquad (2.3)$$

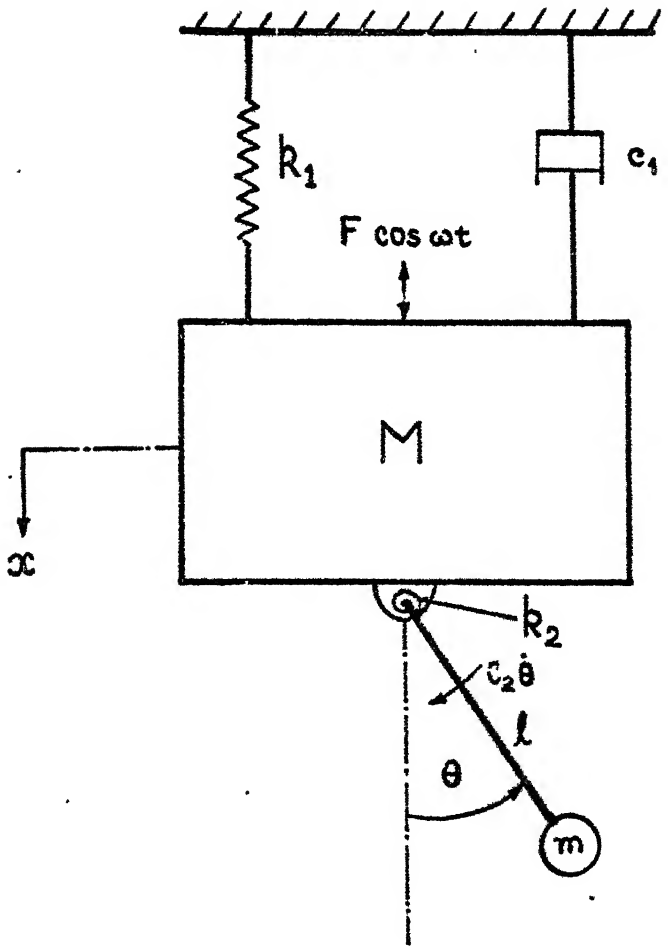

FIG. 2.1 TWO DEGREE-OF-FREEDOM AUTOPARAMETRIC SYSTEM

$$\text{and } \ddot{\theta} + 2\,\zeta_2\,\omega_2\,\dot{\theta} + \Omega_3^2\,\theta + \left(\zeta_2^2 - \frac{\ddot{x}}{l}\right)\sin\theta = 0, \qquad (2.4)$$

respectively, where

$$\Omega_1 = \sqrt{\frac{k_1}{M}} \text{ is the natural frequency of the primary,}$$

$$\zeta_1 = \frac{c_1}{2\,M\,\Omega_1} \text{ is the damping ratio of the primary,}$$

$$\Omega_2 = \sqrt{\frac{g}{l}} \text{ is the linear natural frequency of the pendulum under gravity only,}$$

$$\Omega_3 = \sqrt{\frac{k_2}{ml^2}} \text{ is the natural frequency of the pendulum with spring control only,} \qquad (2.5)$$

$$\omega_2 = \sqrt{\Omega_2^2 + \Omega_3^2} \text{ is the linear natural frequency of the pendulum under combined control of spring torque and gravity}$$

$$\text{and } \zeta_2 = \frac{c_2}{2\,ml^2\,\omega_2} \text{ is the damping ratio of the pendulum.}$$

When the pendulum does not oscillate, the system responds like a locked mass with the natural frequency as

$$\omega_1 = \sqrt{\frac{k_1}{M + m}} \qquad (2.6)$$

Equations (2.3) and (2.4) are written in the nondimensional form as

$$(1 + R)\, p^2 \bar{x}'' + 2\, \zeta_1\, p\, \bar{x}' + \bar{x} - p^2 R\, (\theta'' \sin\theta + \theta'^2 \cos\theta) = P \cos \bar{t} \qquad (2.7)$$

and $$p^2 \theta'' + \frac{2\, \zeta_2\, q\, p}{\sqrt{1 + R}}\, \theta' + \frac{q_2^2}{1 + R}\, \theta + \left(\frac{q_1^2}{1 + R} - p^2 \bar{x}'' \right) \sin\theta = 0 , \qquad (2.8)$$

respectively, where the variables are nondimensionalised as

$$\bar{x} = \frac{x}{l} \quad \text{and} \quad \bar{t} = \omega t \qquad (2.9)$$

The prime denotes the derivative with respect to the non-dimensional time $\bar{t}$ and the following nondimensionalisations are used for the parameters:

$$R = \frac{m}{M} \text{ is the mass ratio,} \quad p = \frac{\omega}{\Omega_1} , \quad P = \frac{F}{k_1 l},$$

$$q = \frac{\omega_2}{\omega_1} , \quad q_1 = \frac{\Omega_2}{\omega_1} , \quad q_2 = \frac{\Omega_3}{\omega_1} \qquad (2.10)$$

and $$q = \sqrt{q_1^2 + q_2^2}$$

At the excitation frequency equal to the locked mass natural frequency, p is given by

$$p = \frac{1}{\sqrt{1 + R}} \qquad (2.11)$$

When the system oscillates like a locked mass, i.e., $\theta = 0$ for $\bar{t} \geq 0$, its motion is governed by

$$(1 + R)\, p^2 \bar{x}_L'' + 2\zeta_1\, p\, \bar{x}_L' + \bar{x}_L = P \cos \bar{t} \qquad (2.12)$$

where $\bar{x}_L$ is the locked mass response nondimensionalised

with respect to 1 . The steady state solution of (2.12) is

$$\bar{x}_L = A_L \cos (\bar{t} - \Phi_o) , \tag{2.13}$$

where

$$A_L = \frac{P}{\sqrt{\left[1 - p^2 (1 + R)\right]^2 + (2 \zeta_1 p)^2}} \tag{2.14a}$$

is the nondimensional amplitude of the locked mass and

$$\Phi_o = \tan^{-1}\left[\frac{2 \zeta_1 p}{1 - p^2 (1 + R)} \right] \tag{2.14b}$$

2.3 APPROXIMATE SOLUTIONS BY METHOD OF HARMONIC BALANCE AND STABILITY OF THE SOLUTIONS

Equations (2.7) and (2.8) form a set of coupled nonlinear differential equations where the pendulum is parametrically excited. The solution is attempted in the neighbourhood of the primary unstable region of (2.8), i.e., with $\frac{q^2}{p^2 (1 + R)} \approx \frac{1}{4}$, when the static equilibrium position of the pendulum becomes unstable. Hereafter the static equilibrium position of the pendulum will be referred to as the zero solution of θ . Furthermore, the range of excitation frequency considered is around the natural frequency of the locked mass system, i.e. $p/\sqrt{1 + R} \approx 1$ (from (2.11)), and q is taken as $\frac{1}{2}$.

As the excitation is harmonic, the steady state solution of the primary mass is also assumed to be harmonic with the same frequency ω . The solution being sought near the primary unstable region of (2.8), the pendulum motion is taken as harmonic with frequency $\frac{\omega}{2}$. Thus the solutions are assumed to be of the form

$$\bar{x} = A \cos (\bar{t} + \Phi_1) \qquad (2.15)$$

and $$\theta = B \cos (\frac{\bar{t}}{2} + \Phi_2) \qquad (2.16)$$

For accurate analysis higher harmonics should be considered in (2.15) and (2.16), in particular when the amplitudes are large. Substitution of (2.15) and (2.16) in (2.7) and (2.8) shows that some terms of order B^3, B^5 etc. are neglected as they are associated with higher harmonics. But since we are investigating the existence and the stability of the harmonic responses with a harmonic excitation, the analysis is carried out with the form given by (2.15) and (2.16).

First the boundaries of the primary unstable region are determined with the one term approximation given by (2.16).

2.3.1 Approximate Boundaries of the Primary Unstable Region

For determining the primary unstable region, $\sin \theta$ is replaced by θ in (2.8) rendering it to the following form:

$$p^2 \theta'' + \frac{2 \zeta_2 p q}{\sqrt{1 + R}} \theta' + \left[\frac{q^2}{1 + R} - p^2 \bar{x}_L'' \right] \theta = 0, \quad (2.17)$$

where $\bar{x}_L$ is obtained from (2.13) and (2.14).

Substitution of (2.16) in (2.17) yields the first order approximate equation for the bounding frequencies of the primary unstable zone as

$$\left(\frac{q^2}{1 + R} - \frac{p^2}{4} \right)^2 + \frac{(\zeta_2 p q)^2}{1 + R} = \frac{p^4 A_L^2}{4}, \quad (2.18)$$

where A_L is given by (2.14).

For $q = \frac{1}{2}$, (2.18) gives the bounds of p for the primary unstable zone as

$$p^2_{bound} = \frac{1}{1 + R} \left[(Q + 1) \pm \sqrt{Q^2 + 2Q} \right], \quad (2.19)$$

where $$Q = -\left(\frac{\zeta_1^2}{1 + R} + \zeta_2^2 \right) + \sqrt{P^2 + \left(\frac{\zeta_1^2}{1 + R} - \zeta_2^2 \right)^2}$$

The condition for these values of p_{bound} to be real is

$$P > \frac{2 \zeta_1 \zeta_2}{\sqrt{1 + R}} \quad (2.20)$$

2.3.2 Approximate Steady State Solutions

The steady state solutions of the equations of motion, (2.7) and (2.8), are assumed to be harmonic. The assumed forms are given by (2.15) and (2.16). Substituting (2.15) and (2.16) into (2.7) and (2.8) and equating

the coefficients of the sine and the cosine terms, the following four equations in terms of the four unknowns A, B, Φ_1 and Φ_2 are obtained:

$$(v_1^2 + v_2^2)\, v_4 + v_3^2 + 2\, v_3 [\, \{1 - p^2 (1 + R)\}\, v_1 + (2\ \zeta_1\, p)\, v_2] = P^2 , \qquad (2\ 21)$$

$$A^2 = v_1^2 + v_2^2 , \qquad (2.22)$$

$$\tan 2\Phi_2 = \frac{[1 - p^2 (1 + R)]\, v_2 - (2\ \zeta_1\, p)\, v_1}{[1 - p^2 (1 + R)]\, v_1 + (2\ \zeta_1\, p)\, v_2 + v_3} \qquad (2.23)$$

$$\text{and} \quad \tan (2\ \Phi_2 - \Phi_1) = \frac{v_2}{v_1} , \qquad (2.24)$$

where $v_1 = \dfrac{\frac{B}{4} - \frac{q_2^2}{p^2 (1 + R)} B - \frac{q_1^2}{p^2 (1 + R)} 2 J_1 (B)}{J_1 (B) - J_3 (B)}$,

$$v_2 = \frac{\zeta_2\, q\, B}{p \sqrt{1 + R}\, [J_1 (B) + J_3 (B)]} ,$$

$$v_3 = \frac{p^2 R B}{8} [\, 2\, \{J_1 (B) - J_3 (B)\} + B\, \{J_0 (B) + 2 J_2 (B) + J_4 (B)\}] ,$$

$$v_4 = [\, 1 - p^2 (1 + R)\,]^2 + (\, 2\ \zeta_1\, p\,)^2 ,$$

and $J_n (B)$ is the Bessel's coefficient of order n arising out of expansions of the terms like $\sin \{B \cos (\frac{t}{2} + \Phi_2)\}$ [43].

Equation (2.21) is a polynomial in B. In the first order approximation, terms of order B only are retained in J_n (B)'s. Equation (2.21) then reduces to a biquadratic equation in B which can be solved in closed form. In the second order approximation, terms up to B^3 are included in J_n (B)'s and terms up to B^5 are retained in the third order approximation. In such cases the polynomial equation (2.21) can be solved only numerically. After evaluating B from (2.21), other unknowns A, Φ_2 and Φ_1 are obtained from (2.22), (2.23) and (2.24), respectively.

2.3.3 Stability of the Approximate Steady State Solution

The stability of the assumed solutions, (2.15) and (2.16), is investigated by providing small perturbations to them. Thus the perturbed solutions are

$$\bar{x} = A \cos (\bar{t} + \Phi_1) + x_1 \qquad (2.25)$$

and $$\theta = B \cos (\frac{\bar{t}}{2} + \Phi_2) + x_2 , \qquad (2.26)$$

where x_1 and x_2 refer to the small perturbations. Substituting these equations into (2.7) and (2.8) the perturbed equations are obtained as

$$(1 + R) p^2 x_1'' + 2 \zeta_1 p x_1' + x_1 - p^2 R [f_1 (\bar{t}) x_2'' + f_2 (\bar{t}) x_2' + f_3 (\bar{t}) x_2] = 0 \qquad (2.27)$$

$$\text{and} \quad p^2 x_2'' + \frac{2 \zeta_2 p q}{\sqrt{1+R}} x_2' + \left[\frac{q_2^2}{1+R} + f_4(\bar{t}) \right] x_2 - p^2 f_1(\bar{t}) x_1'' = 0 , \tag{2.28}$$

respectively, where

$$f_1(\bar{t}) = \sin\left[B \cos\left(\frac{\bar{t}}{2} + \Phi_2 \right) \right] ,$$

$$f_2(\bar{t}) = -B \sin\left(\frac{\bar{t}}{2} + \Phi_2 \right) \cos\left[B \cos\left(\frac{\bar{t}}{2} + \Phi_2 \right) \right] ,$$

$$f_3(\bar{t}) = -\frac{B}{4} \cos\left(\frac{\bar{t}}{2} + \Phi_2 \right) \cos\left[B \cos\left(\frac{\bar{t}}{2} + \Phi_2 \right) \right] - \frac{B^2}{4} \sin^2\left(\frac{\bar{t}}{2} + \Phi_2 \right) \sin\left[B \cos\left(\frac{\bar{t}}{2} + \Phi_2 \right) \right]$$

$$\text{and} \quad f_4(\bar{t}) = \left[\frac{q_1^2}{1+R} + p^2 A \cos(\bar{t} + \Phi_1) \right] \cos\left[B \cos\left(\frac{\bar{t}}{2} + \Phi_2 \right) \right] \tag{2.29}$$

Equations (2.27) and (2.28) are linear equations with periodic coefficients. The functions $f_i(\bar{t})$'s in (2.29) are computed with the values of A, B, Φ_1 and Φ_2 obtained by the approximate results. The order of the terms of B, in expansions of $f_i(\bar{t})$'s, are kept same as those in (2.21). Floquet's theory[9] is used to investigate the stability of (2.27) and (2.28). These equations are expressed as four first-order differential equations in the following form:

$$\{w'\} = [\hat{f}(\bar{t})]\{w\},$$

where $\{w\} = \{x_1 \quad x_2 \quad x_1' \quad x_2'\}^T$

$\hat{f}(\bar{t})$ is a periodic matrix with period 4π. Therefore, if $[W(\bar{t})]$ is a fundamental matrix solution, $[W(\bar{t}+4\pi)]$ is also a fundamental matrix solution. Let these be related by

$$[W(\bar{t}+4\pi)] = [S][W(\bar{t})] \tag{2.30}$$

To generate $[S]$ numerically, (2.30) is integrated with initial conditions $[W(0)] = [I]$ for one period of oscillation, where $[I]$ is the identity matrix. Then

$$[S] = [W(4\pi)] \tag{2.31}$$

The eigenvalues, λ_i, of $[S]$ are the roots of

$$|[S] - \lambda[I]| = 0 \tag{2.32}$$

The steady state solutions, (2.15) and (2.16), are stable if $|\lambda_i| < 1$ for $i = 1$ to 4.

Though numerically this process is involved, this is justified since in some cases the higher order approximations are required to predict the true stability behaviour.

2.3.4 First Order Approximation by Harmonic Balance

In the first order approximation, terms of order B only are retained in $J_n(B)$'s in (2.21) to (2.24). These equations then become

$$(p^4 R B^2)^2 + 16 p^4 R B^2 v_5 + 64 \left[v_4 v_6 - \frac{p^2 p^4}{4} \right] = 0, \tag{2.33}$$

$$A^2 = \frac{4}{p^4} \left[\left(\frac{p^2}{4} - \frac{q^2}{1+R} \right)^2 + \frac{(\zeta_2 p q)^2}{1+R} \right], \tag{2.34}$$

$$\tan 2\Phi_2 = \frac{\left[1 - p^2 (1+R)\right] \frac{\zeta_2 p q}{\sqrt{1+R}} - 2 \zeta_1 p \left(\frac{p^2}{4} - \frac{q^2}{1+R} \right)}{v_5 + \frac{p^4 R B^2}{4}} \tag{2.35}$$

$$\text{and} \quad \tan (2\Phi_2 - \Phi_1) = \frac{\zeta_2 p q}{\sqrt{1+R}} \Big/ \left(\frac{p^2}{4} - \frac{q^2}{1+R} \right), \tag{2.36}$$

respectively, where

$$\left.\begin{aligned} v_5 &= \left[1 - p^2 (1+R) \right] \left(\frac{p^2}{4} - \frac{q^2}{1+R} \right) \\ &\quad + (2 \zeta_1 p) \frac{\zeta_2 p q}{\sqrt{1+R}} \\ \text{and} \quad v_6 &= \left(\frac{p^2}{4} - \frac{q^2}{1+R} \right)^2 + \left(\frac{\zeta_2 p q}{1+R} \right)^2 \end{aligned}\right\} \tag{2.37}$$

Equation (2.33) gives two roots of B^2 as

$$B^2 = \frac{8}{p^4 R} \left[- v_5 \pm \sqrt{v_5^2 + \frac{p^2 p^4}{4} - v_4 v_6} \right] \tag{2.38}$$

Equation (2.18), giving the bounding frequencies of the primary unstable region, can also be obtained by putting $B = 0$ in (2.33). It can be shown that the inequality $\frac{p^2 p^4}{4} - v_4 v_6 > 0$ holds within the primary unstable region when (2.38) yields only one real root of B as

$$B^2 = \frac{8}{p^4 R}\left[- v_5 + \sqrt{v_5^2 + \frac{p^2 p^4}{4} - v_4 v_6}\right] \qquad (2.39)$$

Upto certain values of p, on either side of the primary unstable region, (2.38) yields two real roots of B if

$$v_5^2 + \frac{p^2 p^4}{4} - v_4 v_6 > 0 \qquad (2.40)$$

Moreover, in these ranges of frequency the zero solution of θ is stable. Such frequency zones are termed as 'overhangs'. The inner boundaries of these overhangs are simply the boundaries of primary unstable region. The outer bounding frequencies for the overhang regions are obtained from (2.40) as

$$\left.\begin{aligned} p^2 &= \frac{1}{1+R}\left[Q_1 \pm \sqrt{Q_1^2 - 1}\right], \\ \text{where} \quad Q_1 &= 1 + \frac{p^2}{2\left(\frac{\zeta_1^2}{1+R} + \zeta_2^2\right)} \end{aligned}\right\} \qquad (2.41)$$

It is obvious from (2.41) that if $\zeta_1 = \zeta_2 = 0$, the overhang regions cover the entire frequency range (of course excluding the primary unstable region). The first

order approximation yields same overhang regions for the gravity controlled and the spring controlled pendulums, which obviously is not true. It is shown later that the first order approximation gives only a rough estimate of the overhang regions.

2.4 MULTIPLE TIME SCALE METHOD : FIRST ORDER APPROXIMATION

To determine the suitability of harmonic balance method for the present problem, results are also obtained by another powerful approximate method namely multiple time scale method [42]. The results obtained by these two methods are compared only for first order approximations. To this end (2.7) and (2.8) are written as

$$\bar{p}^2\ \bar{x}'' + 2\ \bar{\zeta}_1\ \bar{p}\ \bar{x}' + \bar{x} - \bar{p}^2\ \frac{R}{1+R}\ (\theta'' \sin\theta + \theta'^2 \cos\theta) = P \cos \bar{t} \qquad (2.42)$$

and $$\bar{p}^2 \theta'' + 2\ \zeta_2\ \bar{p}\ q\ \theta' + q^2 \theta + q_1^2 (\sin\theta - \theta) - \bar{p}^2\ \bar{x}''\ \sin\theta = 0\ , \qquad (2.43)$$

respectively, where

$$\bar{p} = p\ \sqrt{1+R} = \frac{\omega}{\omega_1} \qquad (2.44)$$

and $$\bar{\zeta}_1 = \frac{\zeta_1}{\sqrt{1+R}}$$

Introducing ϵ, a small dimensionless paramet the solutions are assumed as

$$\bar{x}\,(\bar{t}\,) = \varepsilon\,\bar{x}_1\,(T_0, T_1) + \varepsilon^2\,\bar{x}_2\,(T_0, T_1) \qquad (2.45)$$

and $$\theta\,(\bar{t}\,) = \varepsilon\,y_1\,(T_0, T_1) + \varepsilon^2\,y_2\,(T_0, T_1), \qquad (2.46)$$

where

$$T_0 = \bar{t}\,, \quad T_1 = \varepsilon\,\bar{t} \qquad (2.47)$$

To order the forcing and damping terms so that they appear in the same perturbation equation as the nonlinear terms, we introduce

$$\left.\begin{aligned} \bar{\zeta}_1 &= \varepsilon\,\mu_1, \\ \zeta_2 &= \varepsilon\,\mu_2 \\ \text{and}\quad P &= 2\,\varepsilon^2\,\bar{P} \end{aligned}\right\} \qquad (2.48)$$

Further, the solutions are sought for ω near ω_1 and for the frequency ratio $q = \frac{1}{2}$, when

$$\left.\begin{aligned} \bar{p} &= 1 + \varepsilon\,\sigma \\ \text{and}\quad q &= \frac{1}{2} \end{aligned}\right\} \qquad (2.49)$$

Substituting (2.45) - (2.48) in (2.42) and (2.43) and equating coefficients of like powers of ϵ

$$D_o^2\,\bar{x}_1 + \bar{x}_1 = 0 \qquad (2.50)$$

$$D_o^2\,y_1 + \frac{y_1}{4} = 0 \qquad (2.51)$$

$$\begin{aligned} D_o^2\,\bar{x}_2 + \bar{x}_2 = &- 2\,\sigma\,D_o^2\,\bar{x}_1 - 2\,D_o\,D_1\,\bar{x}_1 - 2\,\mu_1\,D_o\,\bar{x}_1 \\ &+ \frac{R}{1+R}\left[(D_o^2\,y_1)\,y_1 + (D_o\,y_1)^2\right] \\ &+ 2\,\bar{P}\cos\bar{t} \end{aligned} \qquad (2.52)$$

$$\text{and} \quad D_o^2 y_2 + \frac{y_2}{4} = -2\sigma \; D_o^2 y_1 - 2 D_o D_1 y_1 - \mu_2 D_o y_1 + (D_o^2 \bar{x}_1) y_1 \;, \tag{2.53}$$

where $D_o \equiv \frac{\partial}{\partial T_o}$, $D_o^2 \equiv \frac{\partial^2}{\partial T_o^2}$ and $D_1 \equiv \frac{\partial}{\partial T_1}$.

The solutions of (2.50) and (2.51) are expressed as

$$\bar{x}_1 = A(T_1) \exp(i T_o) + A^*(T_1) \exp(-i T_o)$$
$$\text{and} \quad y_1 = B(T_1) \exp\left(\frac{i T_o}{2}\right) + B^*(T_1) \exp\left(-\frac{i T_o}{2}\right) \tag{2.54}$$

respectively, where A^* and B^* are the complex conjugates of A and B. Substitution of (2.54) in (2.52) and (2.53) yields the solvability condition as

$$2\sigma A - 2 i D_1 A - 2 i \mu_1 A - \frac{B^2 \bar{R}}{2(1+R)} + \bar{P} = 0$$
$$\text{and} \quad \frac{\sigma B}{2} - i D_1 B - i \frac{\mu_2 B}{2} - A \bar{B} = 0 \tag{2.55}$$

Introducing the polar coordinates

$$A(T_1) = \frac{1}{2} a(T_1) \exp\left[i \gamma_1(T_1)\right]$$
$$\text{and} \quad B(T_1) = \frac{1}{2} b(T_1) \exp\left[i \gamma_2(T_1)\right] \tag{2.56}$$

in (2.55) and separating the real and the imaginary parts

$$\left.\begin{aligned} D_1 a &= -\mu_1 a + \frac{R}{1+R} \frac{b^2}{8} \sin(\gamma_1 - 2\gamma_2) - \bar{P} \sin\gamma_1 \\ a D_1 \gamma_1 &= -\sigma a + \frac{R}{1+R} \frac{b^2}{8} \cos(\gamma_1 - 2\gamma_2) - \bar{P} \cos\gamma_1 \\ D_1 b &= -\frac{\mu_2 b}{2} - \frac{ab}{2} \sin(\gamma_1 - 2\gamma_2) \\ \text{and} \quad D_1 \gamma_2 &= -\frac{\sigma}{2} + \frac{a}{2} \cos(\gamma_1 - 2\gamma_2) \end{aligned}\right\} \tag{2.}$$

For steady state solutions

$$D_1 a = D_1 \gamma_1 = D_1 b = D_1 \gamma_2 = 0 \qquad (2.58)$$

and hence (2.57) yield

$$a^2 = \sigma^2 + \mu_2^2 \qquad (2.59)$$

$$\text{and } b^2 = \frac{8(1+R)}{R}\left[(\sigma^2 - \mu_1\mu_2) \pm \sqrt{\bar{P}^2 - \sigma^2(\mu_1+\mu_2)^2}\right] \qquad (2.60)$$

To check the stability of the steady state solution the coordinates are perturbed as

$$\left.\begin{aligned} a &= a_o + a_1 \ , \\ b &= b_o + b_1 \ , \\ \gamma_1 &= \gamma_{10} + \gamma_{11} \\ \text{and } \gamma_2 &= \gamma_{20} + \gamma_{21} \ , \end{aligned}\right\} \qquad (2.61)$$

where suffix 0 implies the steady state values. Substituting (2.61) into (2.57), expanding for small a_1, b_1 etc. and keeping only the linear terms in a_1, b_1 etc. the following equations are obtained:

$$\begin{aligned} D_1 a_1 = &- \mu_1 a_1 + \left[\frac{R}{1+R}\frac{b_o}{4}\sin(\gamma_{10} - 2\gamma_{20})\right] b_1 \\ &+ \left[\frac{R}{1+R}\frac{b_o^2}{8}\cos(\gamma_{10} - 2\gamma_{20}) - \bar{P}\cos\gamma_{10}\right]\gamma_{11} \\ &- \left[\frac{R}{1+R}\frac{b_o^2}{4}\cos(\gamma_{10} - 2\gamma_{20})\right]\gamma_{21} \end{aligned} \qquad (2.62a)$$

$$D_1 \gamma_1 = -\left[\frac{R}{1+R}\frac{b_o^2}{8}\cos(\gamma_{10}-2\gamma_{20}) - \bar{P}\cos\gamma_{10}\right]\frac{a_1}{a_o^2}$$
$$+\left[\frac{R}{1+R}\frac{b_o}{4a_o}\cos(\gamma_{10}-2\gamma_{20})\right]b_1$$
$$-\left[\frac{R}{1+R}\frac{b_o^2}{8a_o}\sin(\gamma_{10}-2\gamma_{20}) - \bar{P}\sin\gamma_{10}\right]\gamma_{11}$$
$$+\left[\frac{R}{1+R}\frac{b_o^2}{4a_o}\sin(\gamma_{10}-2\gamma_{20})\right]\gamma_{21} \qquad (2.62b)$$

$$D_1 b_1 = -\left[\frac{b_o}{2}\sin(\gamma_{10}-2\gamma_{20})\right]a_1 - \left[\frac{a_o b_o}{2}\cos(\gamma_{10}-2\gamma_{20})\right]\gamma_{11}$$
$$+\left[a_o b_o\cos(\gamma_{10}-2\gamma_{20})\right]\gamma_{21} \qquad (2.62c)$$

$$D_1 \gamma_2 = \left[\frac{1}{2}\cos(\gamma_{10}-2\gamma_{20})\right]a_1 - \left[\frac{a_o}{2}\sin(\gamma_{10}-2\gamma_{20})\right]\gamma_{11}$$
$$+\left[a_o\sin(\gamma_{10}-2\gamma_{20})\right]\gamma_{21} \qquad (2.62d)$$

The stability of the steady state motion depends on the eigenvalues of the coefficient matrix on the right - hand side of (2.62). These eigenvalues, λ_i, are the roots of the polynomial

$$\lambda^4 + d_1\lambda^3 + d_2\lambda^2 + d_3\lambda + d_4 = 0, \qquad (2.63)$$

where $d_1 = 2\mu_1 + \mu_2$,

$$d_2 = \mu_1(\mu_1 + 2\mu_2) + \sigma^2 + \frac{R}{1+R}\frac{b_o^2}{8a_o^2}\sigma^2 ,$$

$$d_3 = \frac{R}{1+R}\frac{b_o^2}{8a_o^2}\left[\mu_2^3 + (5\mu_2 + 3\mu_1 + 2)\sigma^2\right]$$
$$+ (\mu_1^2 + \sigma^2)\mu_2$$

and $d_4 = \frac{R}{1+R} \frac{b_o^2}{8} \left[\frac{R}{1+R} \frac{b_o^2}{8} - (\sigma^2 - \mu_1 \mu_2) \right]$

As d_1, d_2 and d_3 are positive, the necessary condition of stability is

$$d_4 > 0 \qquad (2.64)$$

This implies that in (2.60) the plus sign before the quantity under the square root gives the stable root and the minus sign gives the unstable root.

2.5 RESULTS AND DISCUSSIONS

The results are obtained with $R = 0.2$, $\zeta_1 = 0.02$, $\zeta_2 = 0.05$, $q = 0.5$ and varying the other parameters q_1, q_2, P and p in a suitable manner. Initially the first order approximate results, obtained by MTS and harmonic balance, are discussed. Then the higher order approximate results, obtained by harmonic balance only, are presented. The approximate solutions are compared with the numerically integrated results. For this, (2.7) and (2.8) are numerically integrated using Gill's modification of the classical Runge - Kutta method [44] . With the period of forcing function as 2π , a step size of $\frac{\pi}{40}$ is found to give good results. All the results in this section are obtained with this step size. Inside the primary unstable region, the initial conditions are taken as $\bar{x}(0) = \bar{x}'(0) = \theta'(0) = 0$ and $\theta(0) = 0.05$. In the overhang regions

the integrations are performed by changing the frequency, p, in steps when the solution has reached steady state.

2.5.1 First Order Approximate Results

In the first order approximation, the amplitudes of $\bar{x}$ and θ are calculated by harmonic balance using (2.34) and (2.38). The same are also obtained by using MTS with (2.59) and (2.60). It is obvious that so far as the first order approximation is concerned the results depend only on the value of q and not on the individual values of q_1 and q_2. In fact the first order approximation (by both the methods) essentially gives the solution of the approximate equations of motion. These approximate equations, obtained by putting $\sin\theta = \theta$ and $\cos\theta = 1$ in (2.7) and (2.8), are

$$(1 + R)\, p^2\, \bar{x}'' + 2\, \zeta_1\, p\, \bar{x}' + \bar{x} - p^2 R\, (\theta''\theta + \theta'^2) = P \cos \bar{t} \qquad (2.65)$$

and $$p^2 \theta'' + \frac{2\, \zeta_2\, p\, q}{\sqrt{1 + R}}\, \theta' + \left(\frac{q^2}{1 + R} - p^2\, \bar{x}'' \right) \theta = 0 \qquad (2.66)$$

Equations of this form with quadratic nonlinearities have been studied in detail, for example, in references [9, 26].

Figures 2.2 and 2.3 show the amplitudes A and B, respectively. The results obtained by MTS are shown by the curves 1 - 1 and those by harmonic balance are given by

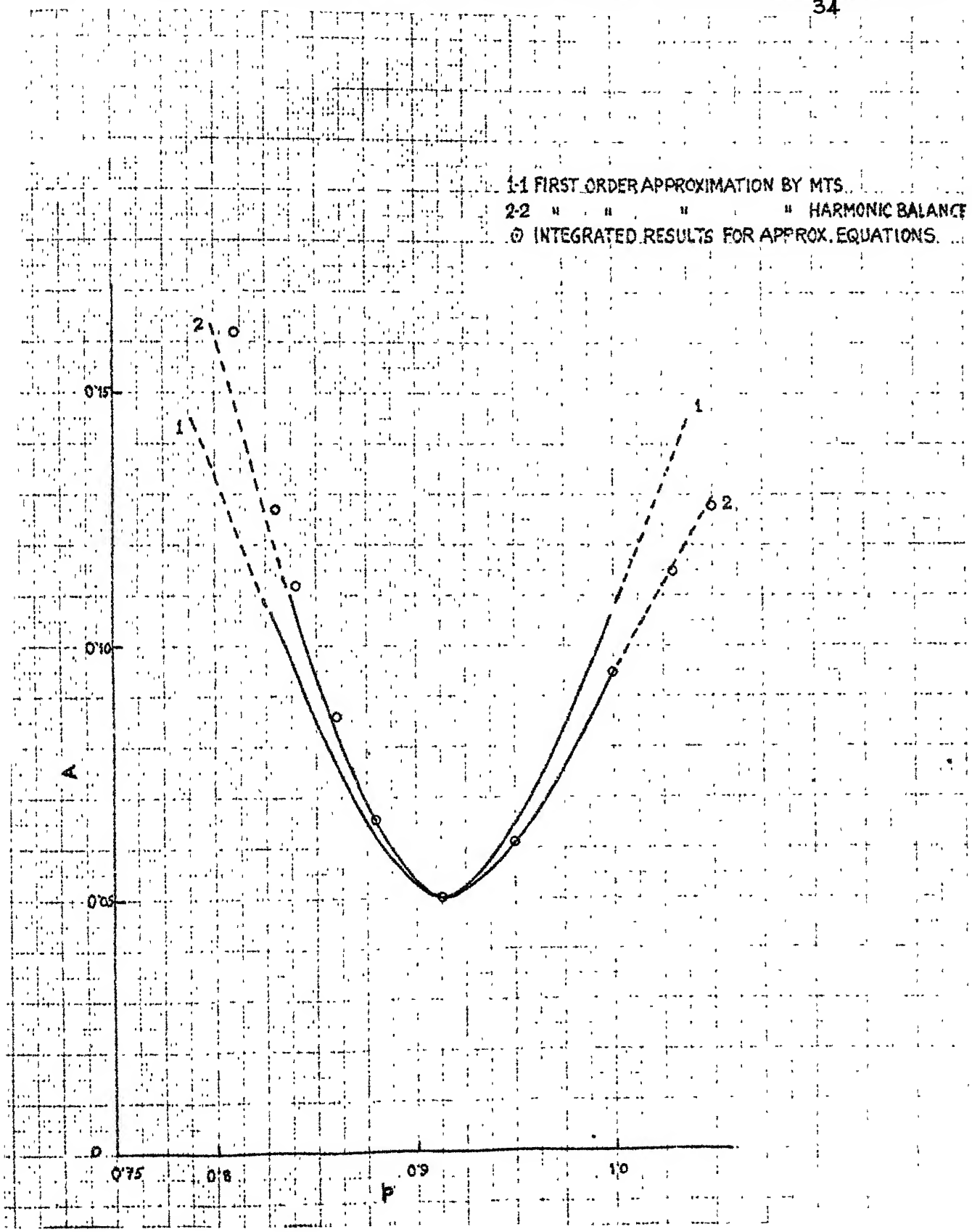

FIG. 2.2 VARIATION OF AMPLITUDE OF PRIMARY MASS WITH EXCITATION FREQUENCY : FIRST ORDER APPROXIMATE RESULTS, P = 0.02

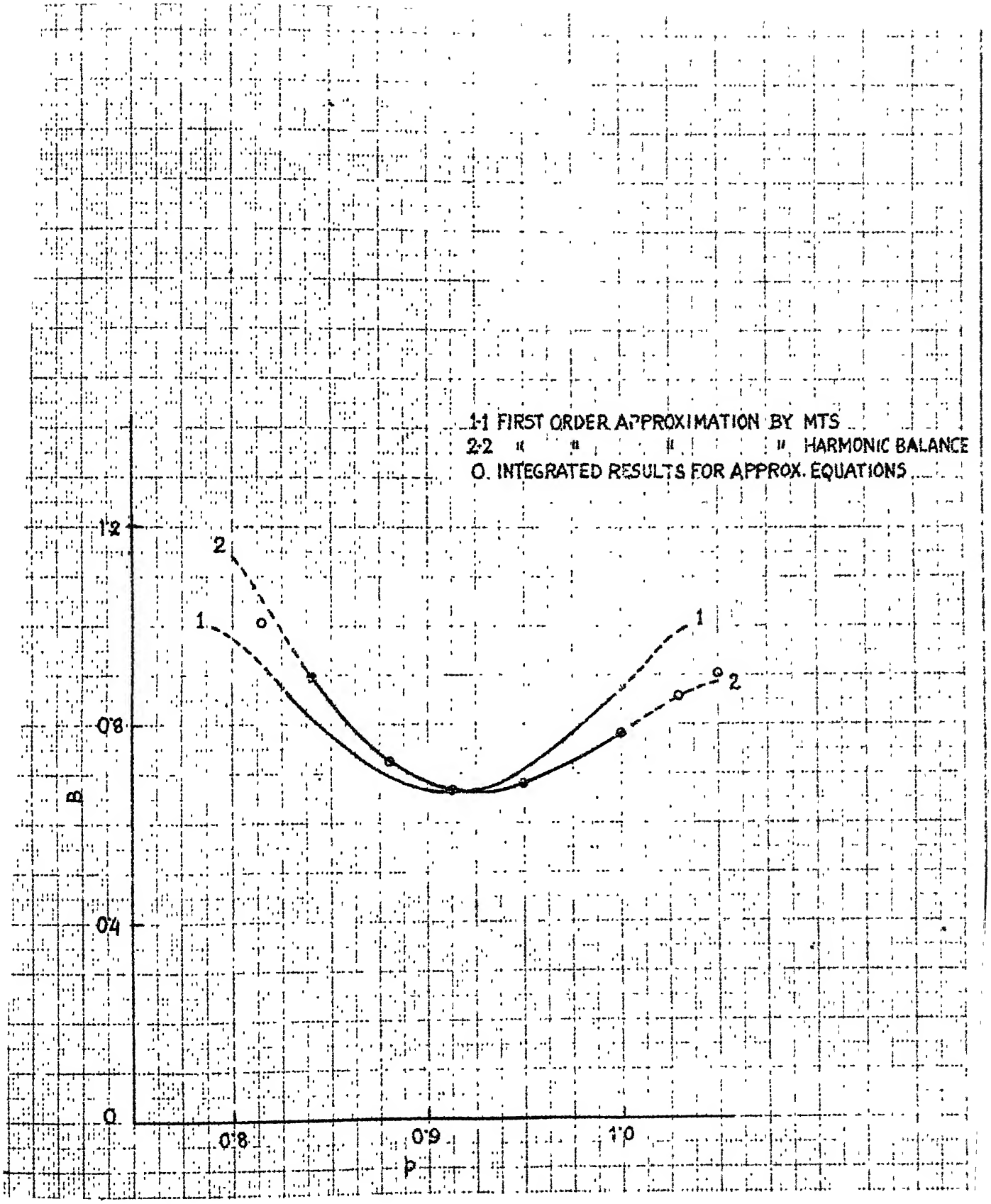

FIG. 2.3 VARIATION OF AMPLITUDE OF PENDULUM WITH EXCITATION FREQUENCY : FIRST ORDER APPROXIMATE RESULTS, P = 0.02

the curves 2 - 2. The firm lines show the amplitudes with frequencies lying inside the primary unstable region and the dotted lines indicate the stable solutions in the overhang regions. In MTS the stability condition is given by (2.64), which states that the upper branch in the overhang (shown by dotted lines in Fig. 2.3) is stable and the lower branch (not shown in this figure) is unstable. It is obvious from (2.59) that no separate lower branch exists in Fig. 2.2. The stability of the solutions obtained by harmonic balance is checked with (2.32) and the results are same as those obtained by MTS. The responses obtained by integration of (2.65) and (2.66) are also found to be harmonic and the amplitudes are indicated by the circled points in Figs. 2.2 and 2.3.

Both MTS and harmonic balance yield same results at $p = 0.913$ ($\bar{p} = 1.0$). While the response curve obtained from MTS is symmetrical about $p = 0.913$, that by harmonic balance is not so. The results by these two methods start deviating as p is varied away from 0.913 on either side. The harmonic balance results are seen to be closer to the integrated results. This is due to the fact that in harmonic balance no approximation is made on the frequency range, whereas MTS gives results in a narrow frequency band as given by (2.49). In fact, the same approximation on the range of frequency makes (2.34) and (2.38) same as

(2.59) and (2.60), respectively.

If the excitation parameter is increased the amplitudes will also be large and the first order approximation will no more be valid. Moreover, it is obvious that with large amplitudes the nature of the pendulum motion (and hence the motion of the primary mass) will depend on the type of the restoring couple it is subjected to - a feature which can not be revealed by the first order approximation. Since the frequency range of interest are quite wide, the subsequent higher order approximations are carried out by the method of harmonic balance only.

2.5.2 Higher Order Approximations by Harmonic Balance

In the first order approximation only one value of A is obtained in the overhang regions as given by (2.34) and (2.59). Further, the first order approximation renders A independent of the excitation parameter, P, as also noted in references [9, 20]. In the former reference this was referred to as saturation phenomenon. This saturation phenomenon is the consequence of the first order approximation and not a system characteristic. This is revealed from Fig. 2.4 which shows the first order approximate results obtained by (2.34) and (2.59) and the integrated results of (2.65) and (2.66) at the locked mass natural frequency ($p = 0.913$). All these results are same (shown by the dotted line in Fig. 2.4) and show the saturation phenomenon for $P > 0.0018$.

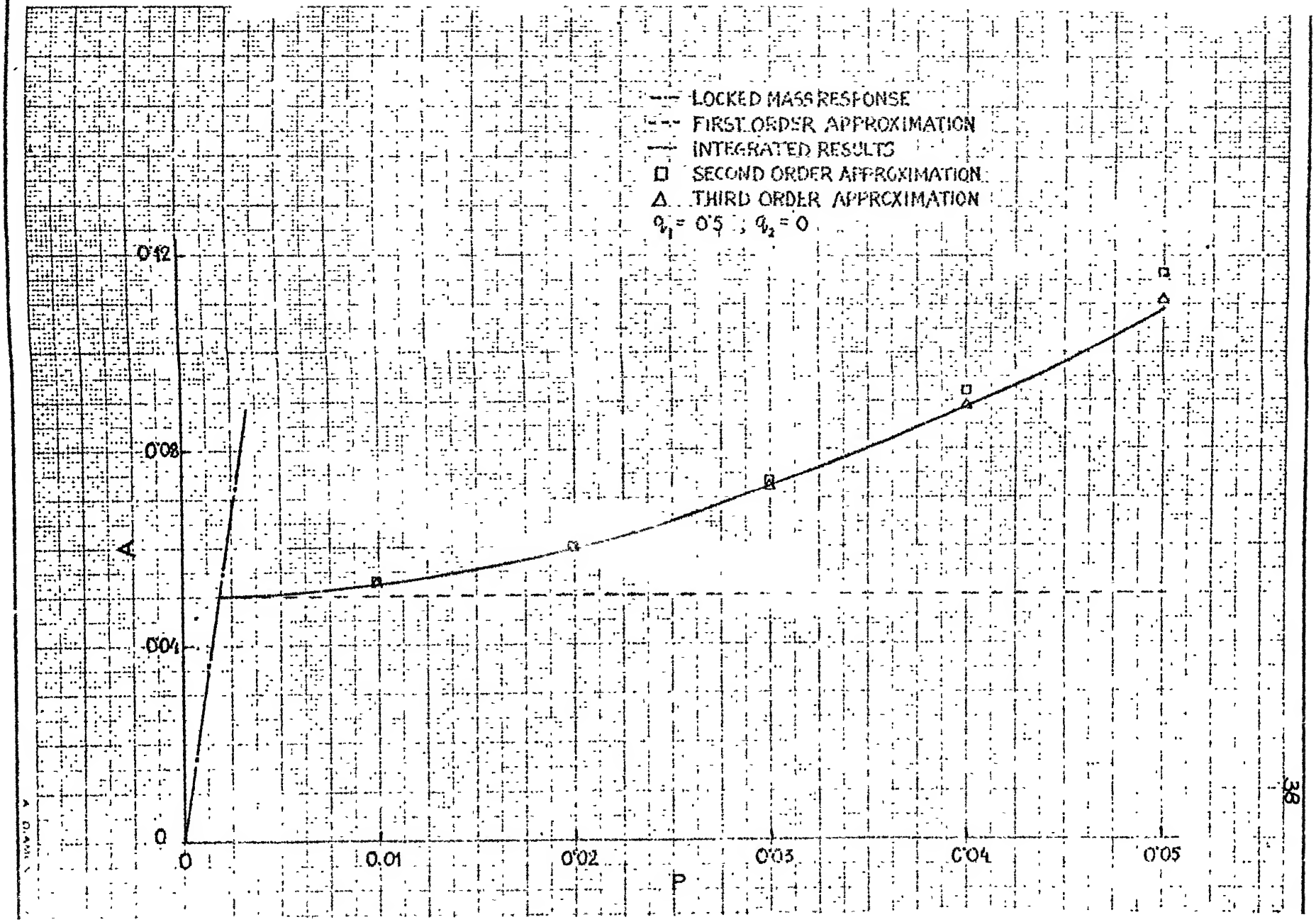

FIG. 2.4 VARIATION OF AMPLITUDE OF PRIMARY MASS WITH EXCITATION AMPLITUDE : p = 0.913

The chain dotted line shows the amplitude of the locked mass response. For $P < 0.0018$ (i.e., $P < \frac{2\zeta_1\zeta_2}{\sqrt{1+R}}$ vide (2.20)) the static equilibrium position of the pendulum is stable. Only for $P > 0.0018$ the pendulum motion affects the primary response. Also included in this figure are the results obtained by the second and the third order approximations (using (2.21) and (2.22)) and by integration of the original equations of motion (i.e. (2.7) and (2.8)). It can be seen that in these cases the amplitude, A, is no longer independent of P and varies almost linearly with P for small values of the excitation.

Figures 2.5 and 2.6 show the variations of the amplitudes, B and A, respectively, with the nondimensional forcin frequency, p. The curve 1 - 1 indicates the steady state amplitudes obtained by numerical integration of (2.7) and (2.8) with $q_1 = \frac{1}{2}$, $q_2 = 0$ (i.e., the gravity controlled pendulum) and the curve 2 - 2 shows the integrated results with $q_1 = 0$, $q_2 = \frac{1}{2}$ (i.e., the spring controlled pendulum). The circled and the squared points indicate the stable amplitudes obtained by the first order and the second order approximations, respectively. The primary unstable region obtained by (2.19) is represented by PUR, where the approximate solutions yield only one stable steady state. The dotted lines indicate the stable amplitudes in the overhang regions, where the zero solution of θ is also stable.

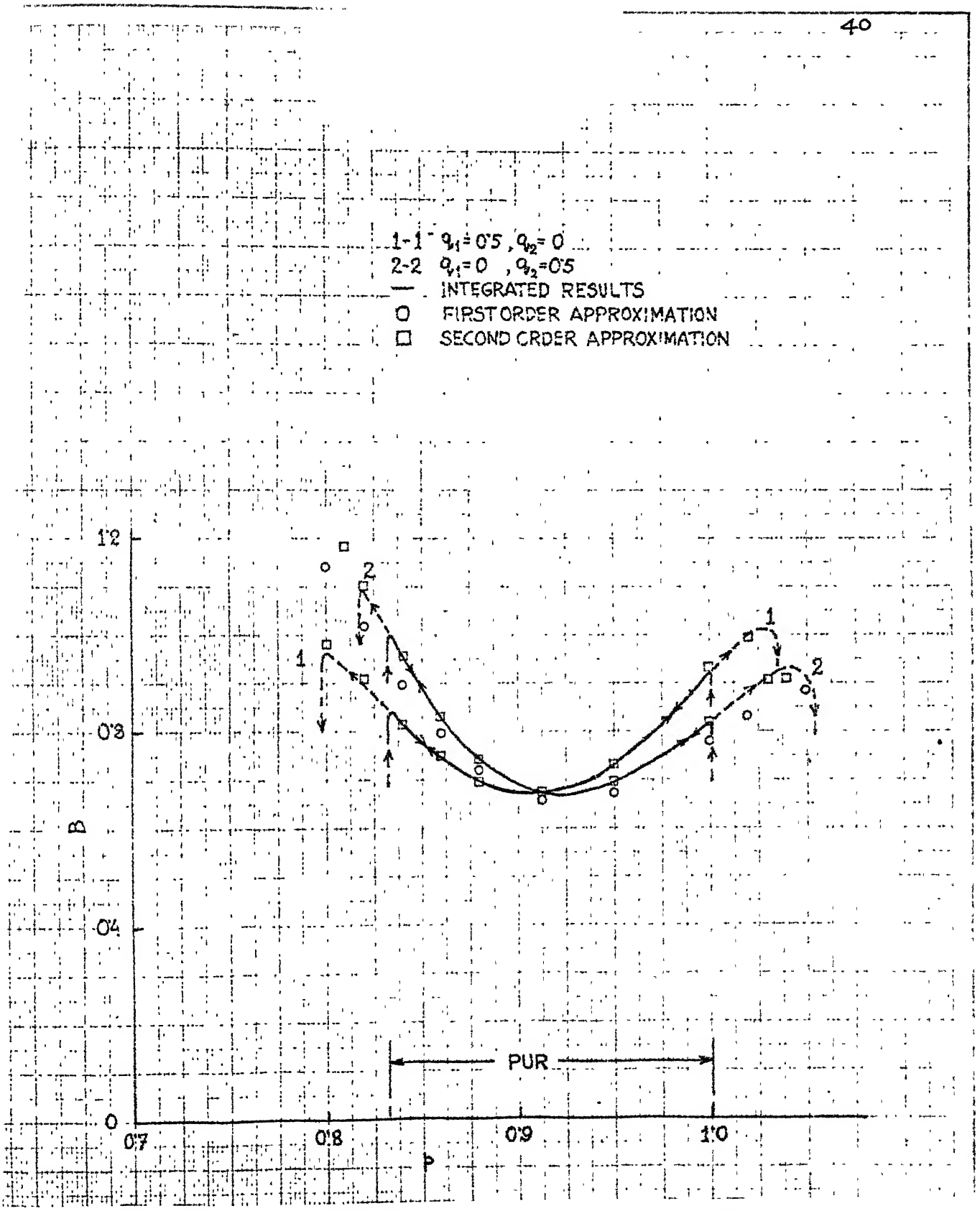

FIG. 2.5 VARIATION OF AMPLITUDE OF PENDULUM WITH EXCITATION FREQUENCY : P = 0.02

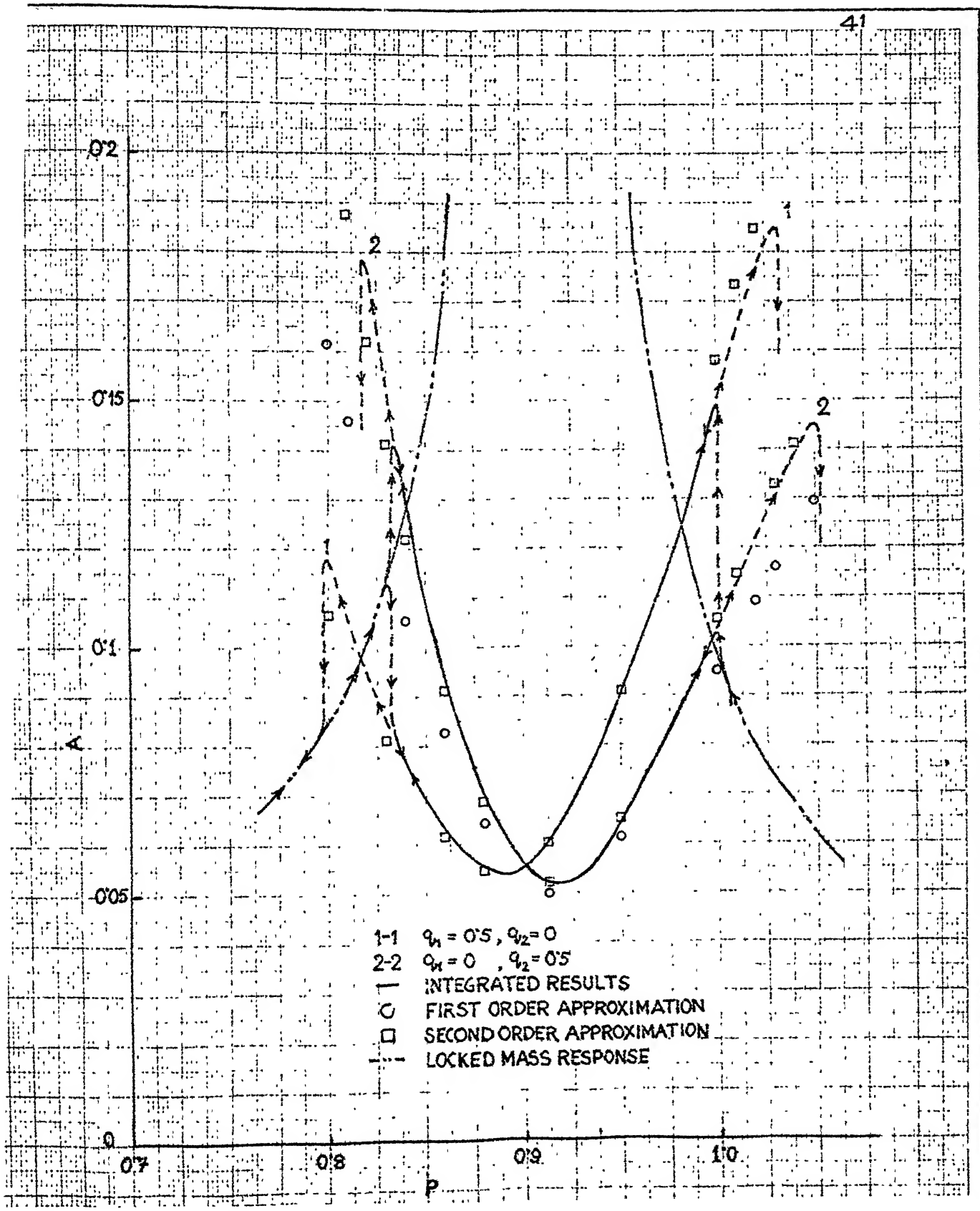

FIG. 2.6 VARIATION OF AMPLITUDE OF PRIMARY WITH EXCITATION FREQUENCY : P = 0.02

The jumps at the ends of the overhangs are shown by arrows. The unstable solutions in the overhangs are not shown. The extent of the overhang region obviously depends on the type of the pendulum's controlling torque. It is evident that both the amplitudes (A and B) are obtained very accurately by using the second order approximation. The integrated responses are also found to be completely harmonic.

If the excitation parameter, P, is increased beyond a certain value, the steady state solutions are seen to deviate from being periodic with a predominant first harmonic as assumed in (2.15) and (2.16). This critical value of P depends on the values of other parameters. In such cases the characteristics of the solutions are different depending on whether the restoring couple on the pendulum is due to gravity (i.e., $q_2 = 0$) or due to the torsional spring (i.e., $q_1 = 0$). These two cases are separately discussed below.

(1) Case I : $q_1 = \frac{1}{2}$, $q_2 = 0$

The approximate results with P = 0.05 are presented in Figs. 2.7 and 2.8, where the numerically integrated results are also shown by firm lines. The first, second and third order approximate stable solutions are shown by the circled, squared and triangled points, respectively. The second and the third order approximate results have negligible difference up to p = 0.95 and match well with the

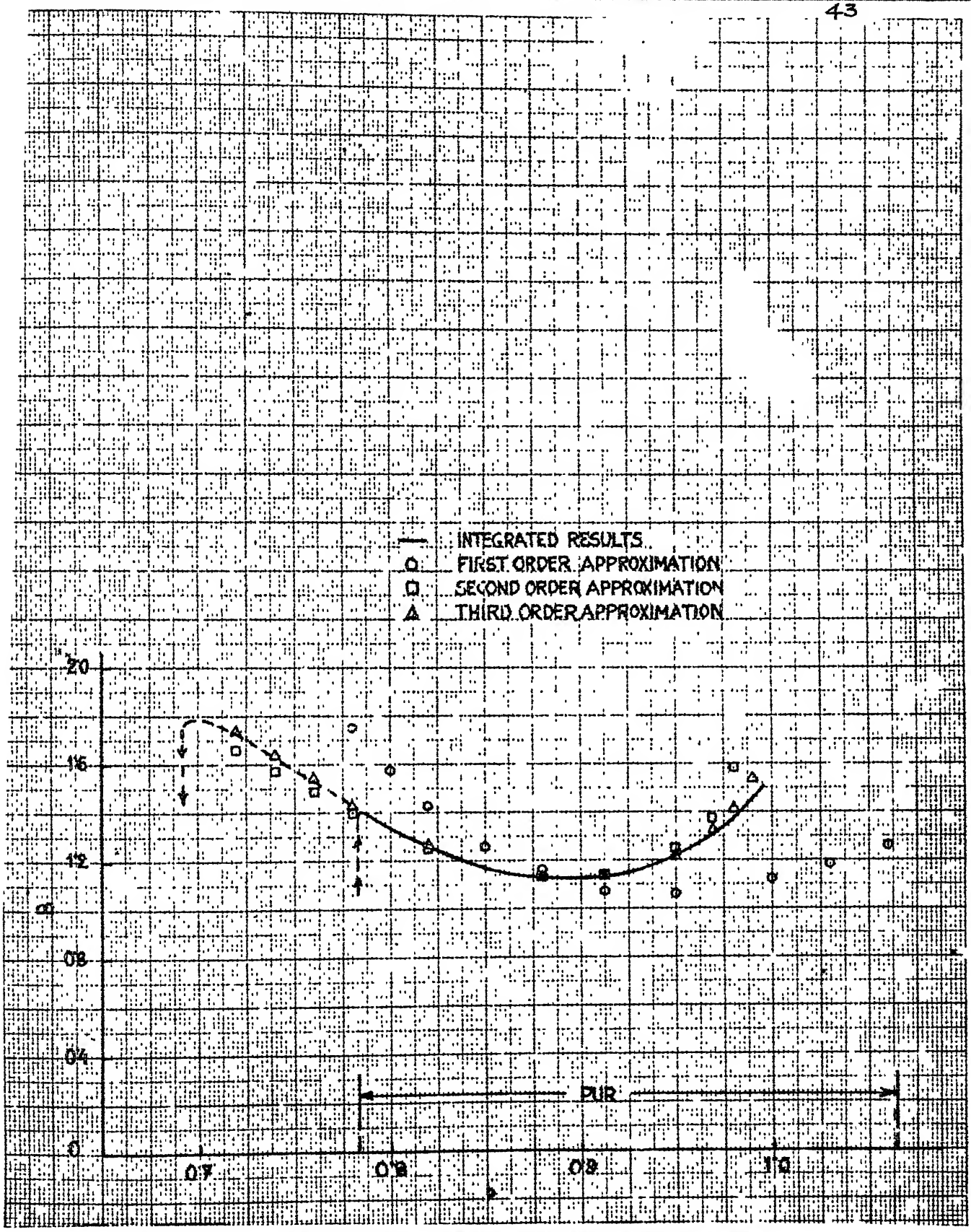

FIG. 2.7 VARIATION OF AMPLITUDE OF PENDULUM WITH EXCITATION FREQUENCY : P = 0.05, $q_1 = 0.5$

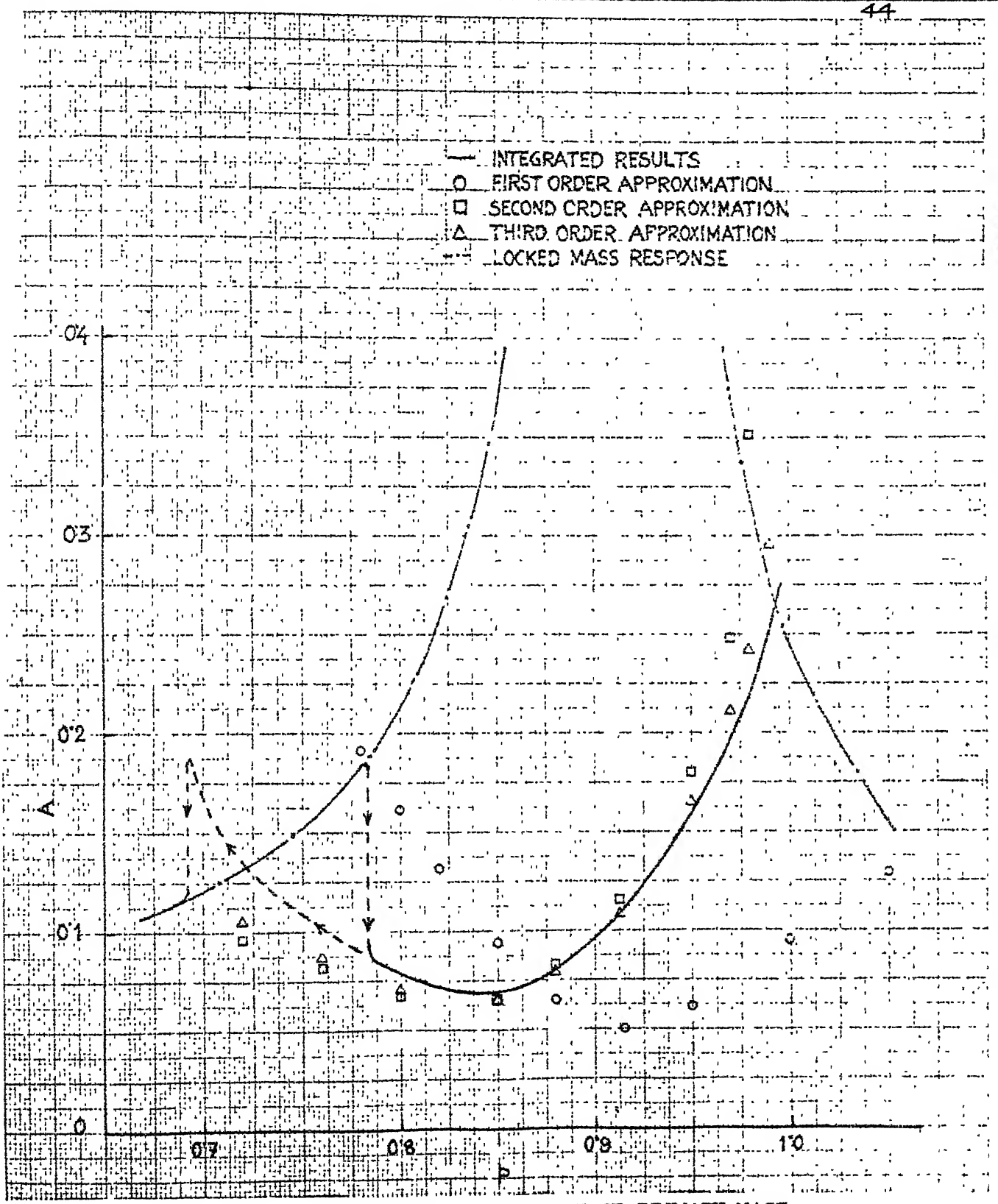

FIG. 2.8 VARIATION OF AMPLITUDE OF PRIMARY MASS WITH EXCITATION FREQUENCY : $P = 0.05$, $q_1 = 0.5$

integrated results. Numerical integrations also reveal that with p near 0.95, when θ is given a slight disturbance (say in the form of an initial condition $\theta(0) = 0.05$) the pendulum makes some revolutions during the transient state and ultimately settles down to a periodic steady state. These number of revolutions are seen to depend strongly on the initial conditions.

As p is increased beyond 0.95 the difference between the results obtained by the second and the third order approximation becomes appreciable, signifying the absence of the dominant first harmonic in the steady state responses. The stability analysis using (2.27) and (2.28) reveals that these solutions are unstable for $p \geq 1.0$ and thus implying that the assumed form of solution may not hold good even for such low values of the excitation parameter, P. In such cases the numerically integrated responses are also found to be nonperiodic. These responses show a complex wave form and are extremely sensitive to the initial conditions. A continuous and irregular transfer of energy between the two modes is apparent from these complex wave forms.

It can be noted here that for $p \geq 1.0$ (upto 1.30) the first order approximation by MTS and harmonic balance yield stable solutions with nonzero value of B. In such

cases the integration of (2.7) and (2.8) yields nonperiodic responses for $1.0 \leq p \leq 1.1$ (after which the zero solution of θ is strongly stable), whereas, that of (2.65) and (2.66) yields periodic responses (with nonzero amplitude of θ) for $1.0 \leq p \leq 1.30$. Further, the first order approximation by harmonic balance shows that the approximate solutions are unstable for $p < 0.78$ which is again verified by integration of (2.65) and (2.66). Hence it may be observed that the first order approximation reveals the behaviour of the approximate equations, (2.65) and (2.66), rather than that of the original equations of motion.

The responses of the system with excitation parameter $P \geq 0.05$, where the responses are nonperiodic over certain frequency range are studied in detail in the following chapters.

(2) Case II: $q_1 = 0, \quad q_2 = \frac{1}{2}$

Figure 2.9 shows the amplitude B for this case with the values of the other parameters kept same as in Fig. 2.7. The approximate results are seen to be quite accurate for the frequencies well inside the primary unstable region (PUR). In the present case, numerically integrated results show periodic steady state responses at all frequencies. It should be noted that, unlike in the previous case, complete revolution of the pendulum is prevented by the

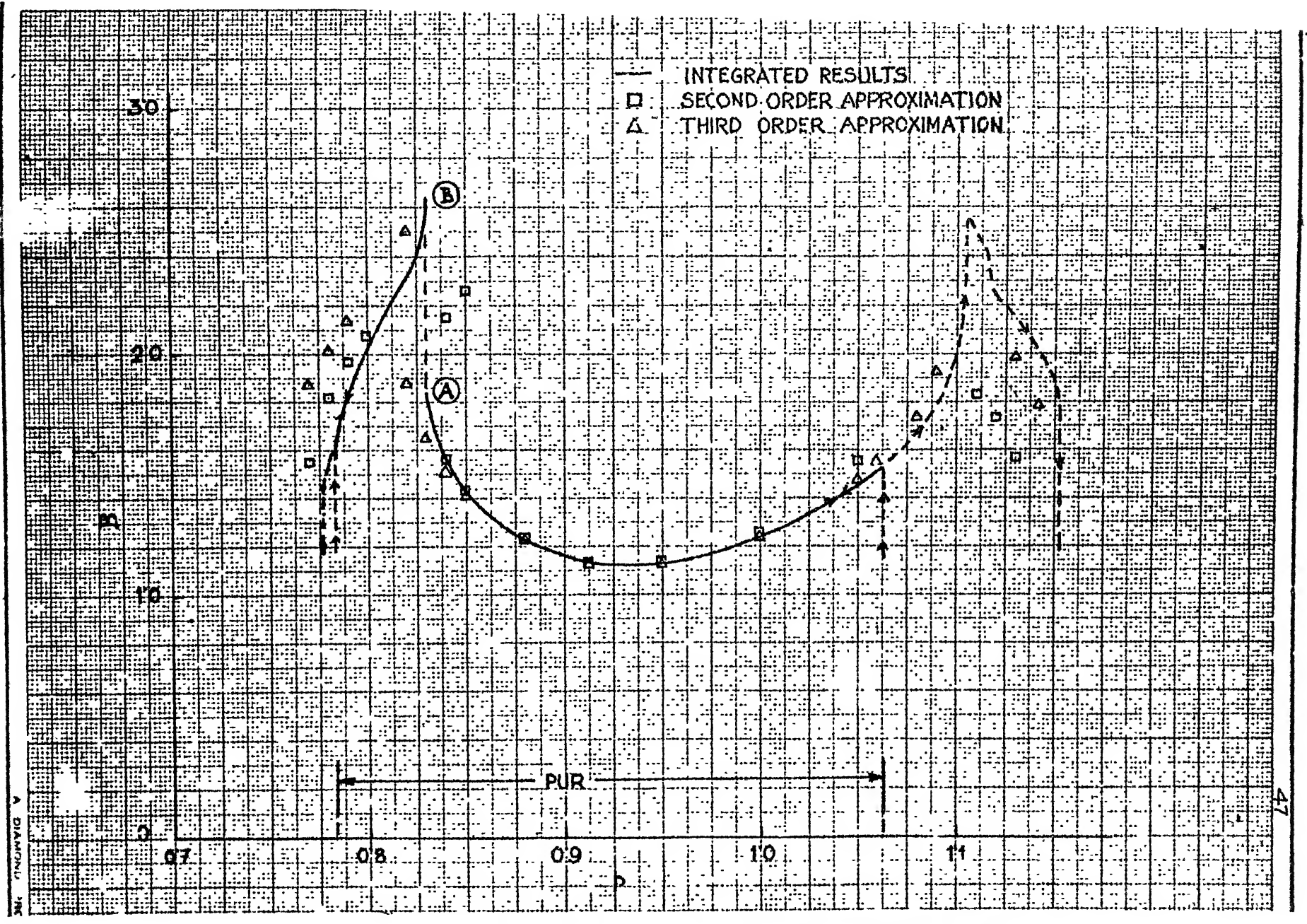

FIG. 2.9 VARIATION OF AMPLITUDE OF PENDULUM WITH EXCITATION FREQUENCY : $P = 0.05$, $q_2 = 0.5$

spring. This in fact renders the steady state solutions to be periodic in the entire frequency range.

The approximate solutions differ from the integrated results near the two peaks. Integration reveals the existence of two steady state solutions at the left peak ($p = 0.83$) — one where the response is almost harmonic (shown by point A in Fig. 2.9) and the other where the response is amplitude modulated (shown by point B). In the latter case (point B), $\bar{x}$ response is found to have small modulation with period 4π and θ - response is found to include some even harmonics as well. At $p = 0.83$, the response time histories for $\bar{x}$ and θ are plotted in Fig. 2.10. Case (a) shows the steady state responses obtained by decreasing p in steps from $p = 0.84$ and case (b) shows those obtained by increasing p from $p = 0.82$. The pendulum response has higher harmonics even when $p < 0.83$.

Near the right peak also integration reveals the amplitude modulated response of $\bar{x}$ and θ - response has other terms present beside the first harmonic. In such cases the amplitude by integration (Fig. 2.9) represents the maximum value during one period of oscillation. Because of higher harmonics, the form of solution, assumed in (2.15) and (2.16), is not correct and this explains the difference between the approximate and the integrated results near the

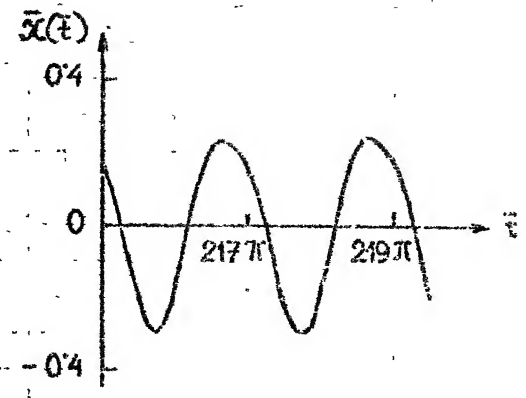
x̄(t̄)
0·4
0
-0·4
217π
219π
t̄

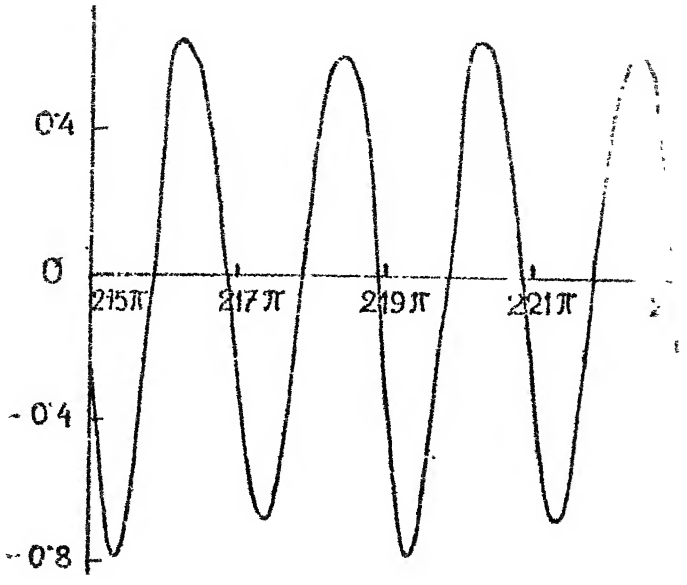
0·4
0
-0·4
-0·8
215π
217π
219π
221π

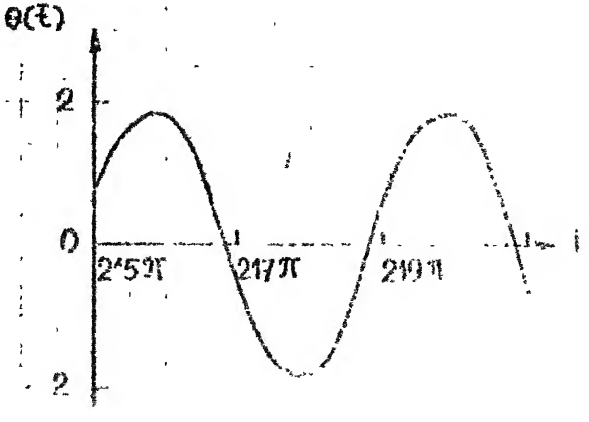
θ(t̄)
2
0
-2
215π
217π
219π

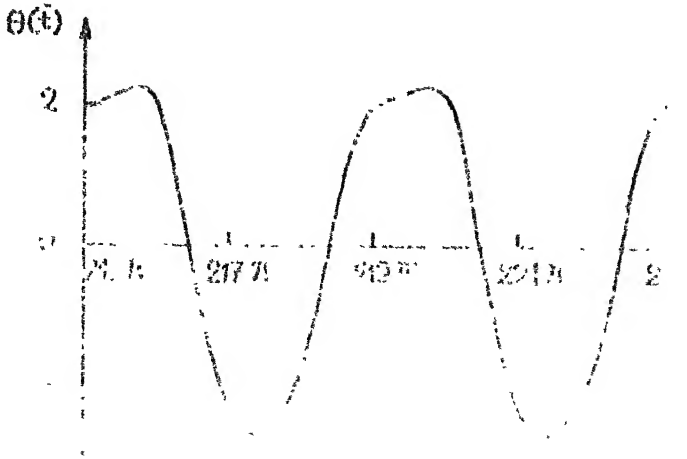
θ(t̄)
2
217π
219π
221π

two peaks. At some frequencies near these peaks (e.g. $p = 0.81$ and 1.10) no stable solution by harmonic balance is obtained. Only the amplitudes of the stable solutions by the approximate method are shown in Fig. 2.9.

Lastly, it may be noted that at $p = 0.83$ (the critical frequency) the bifurcation of the stable harmonic motion to one unstable harmonic motion and another stable amplitude modulated motion is associated with the jumps in the amplitude values, as shown in Figs. 2.9 and 2.10.

CHAPTER 3

RESPONSE WITH LARGE EXCITATION

3.1 INTRODUCTION

In this chapter the behaviour of the system, already considered in Chapter 2, is investigated with large values of the excitation parameter P. The typical range of P studied in this chapter is $0.05 \leq P \leq 0.15$. Here only the case of the gravity controlled pendulum is considered, i.e., $q_2 = 0$ and $q = q_1$ in (2.8). The equations of motion, thus, are same as (2.7) and (2.8) and are reproduced below:

$$(1 + R)\, p^2 \bar{x}'' + 2\, \zeta_1\, p\, \bar{x}' + \bar{x} - p^2 R\, (\theta'' \sin\theta + \theta'^2 \cos\theta) = P \cos \bar{t} \qquad (3.1a)$$

$$p^2 \theta'' + \frac{2\, \zeta_2\, q\, p}{\sqrt{1 + R}}\, \theta' + \left(\frac{q^2}{1 + R} - p^2 \bar{x}''\right) \sin\theta = 0 \qquad (3.1b)$$

The linear natural frequency of the pendulum is taken as half of that of the locked mass system, so that $q = \frac{1}{2}$. All the results in this chapter are for $q = \frac{1}{2}$.

First the boundaries of the unstable regions of the zero solution of (3.1b) are discussed. Inside the primary unstable region, steady state solutions are investigated using the method of harmonic balance. The stability

characteristics of these assumed harmonic solutions are then checked by Floquet's theory. Inside the primary unstable zone two different types of regions are discussed - one where the assumed harmonic solutions are stable and the other, where no stable harmonic solution exists. The boundaries of these regions are also obtained.

These results are then verified by numerical integration of (3.1). First, the steady state amplitudes found by approximate method and numerical integration, are compared for the cases where (3.1) has a steady state with $\bar{x}$ and θ oscillating harmonically. For the regions where the approximate method does not yield any stable harmonic solution, only the numerically integrated results are presented. Such regions are classified in two categories - (i) where there may still be one or more periodic steady states depending on initial conditions, and (ii) where no such periodic state is obtained. For the later case, some physical justifications are given to analyse the results further, even though the integrated results may not converge. Lastly some integrated results are presented briefly for sufficiently large excitation.

3.2 BOUNDARIES OF THE UNSTABLE REGIONS OF THE ZERO SOLUTION OF θ

For studying the boundaries of the unstable regions of the zero solution of θ , $\sin\theta$ is replaced by θ in (3.1 b) rendering it to the following form:

$$p^2\,\theta'' + \frac{2\,\zeta_2\,p\,q}{\sqrt{1+R}}\,\theta' + \left(\frac{q^2}{1+R} - p^2\,\bar{x}_L''\right)\theta = 0 \qquad (3.2)$$

Here $\bar{x}_L$ is the locked mass response and is given by (2.13) and (2.14).

The boundaries of the primary instability of (3.2), with the first order approximation, can be found from (2.19). However, for large values of P, the one term solution assumed in (2.16) does not yield correct bounds and more number of terms in the solution are to be considered, i.e., with $q = \frac{1}{2}$, θ should be assumed as

$$\theta = \sum_{i=1,3,5,..} \left[a_i \cos\left(\frac{i\,\bar{t}}{2}\right) + b_i \sin\left(\frac{i\,\bar{t}}{2}\right)\right] \qquad (3.3)$$

Instead of going through this process, (3.2) is transformed to the standard form of Mathieu equation and the boundaries of instabilities are determined with the help of the standard tables. Substitution of (2.13) in (3.2) yields

$$p^2\theta'' + \frac{2\,\zeta_2\,p\,q}{\sqrt{1+R}}\,\theta' + \left[\frac{q^2}{1+R} + p^2\,A_L\cos\left(\bar{t} - \Phi_o\right)\right]\theta = 0 \qquad (3.4)$$

To convert (3.4) into the standard form of Mathieu equation, the following transformations are used:

$$\bar{t} - \Phi_o = (2u - \pi) \tag{3.5a}$$

and

$$\theta = \psi \exp\left(-\frac{2\zeta_2 q u}{p\sqrt{1+R}}\right) \tag{3.5b}$$

Substitution of (3.5) in (3.4) results in

$$\frac{d^2\psi}{du^2} + (\alpha - 2\beta \cos 2u)\psi = 0, \tag{3.6}$$

where

$$\alpha = \frac{4q^2(1-\zeta_2^2)}{p^2(1+R)}$$

and

$$\beta = 2A_L = \frac{2P}{\sqrt{\left[1 - p^2(1+R)\right]^2 + (2\zeta_1 p)^2}} \tag{3.7}$$

Equation (3.6) is in the standard form of Mathieu equation [1]. The unstable solutions of (3.6) are bounded by the periodic solutions of periods π and 2π alternately. The primary unstable region is bounded by two periodic solutions of period 2π — one of them being odd and the other being even. The odd solution is represented by b_1 (se_1) and is given by a sine series. The even solution is represented by a_1 (ce_1) and is given by a cosine series [1]. Similarly, the secondary unstable region is bounded by two solutions of period π, one of them is odd, represented by

b_2 (se_2) and the other being even, represented by a_2 (ce_2).

The boundaries of instabilities of (3.6) are determined directly from the tables [45] . These tables are given for the following eqiation:

$$\frac{d^2\psi}{d\,u^2} + (\alpha_1 - \beta_1 \cos^2 u) \psi = 0 \qquad (3.8)$$

Therefore, noting the values of α_1 and β_1 from these tables, the boundaries of (3.6) are determined with

$$\beta = \frac{\beta_1}{4}$$

and $$\alpha = \alpha_1 - \frac{\beta_1}{2} \qquad (3.9)$$

From (3.5 b) it is obvious that because of the damping in the pendulum, ζ_2 , the regions of instabilities of θ will be slightly narrower than those of ψ . It was shown in (2.20) that to cause instability with $q = \frac{1}{2}$, P should be greater than $\frac{2\,\zeta_1\,\zeta_2}{/1 + R}$. Since the values of ζ_1 and ζ_2 are quite small, the boundaries for θ and ψ will be almost same, except for very small P.

The boundaries of the primary instability region of (3.6) are shown in Fig. 3.1. The unstable region is bounded by b_1 (se_1) and a_1 (ce_1). For a given excitation parameter, P, and forcing frequency, p, the corresponding values of α and β are calculated from (3.7).

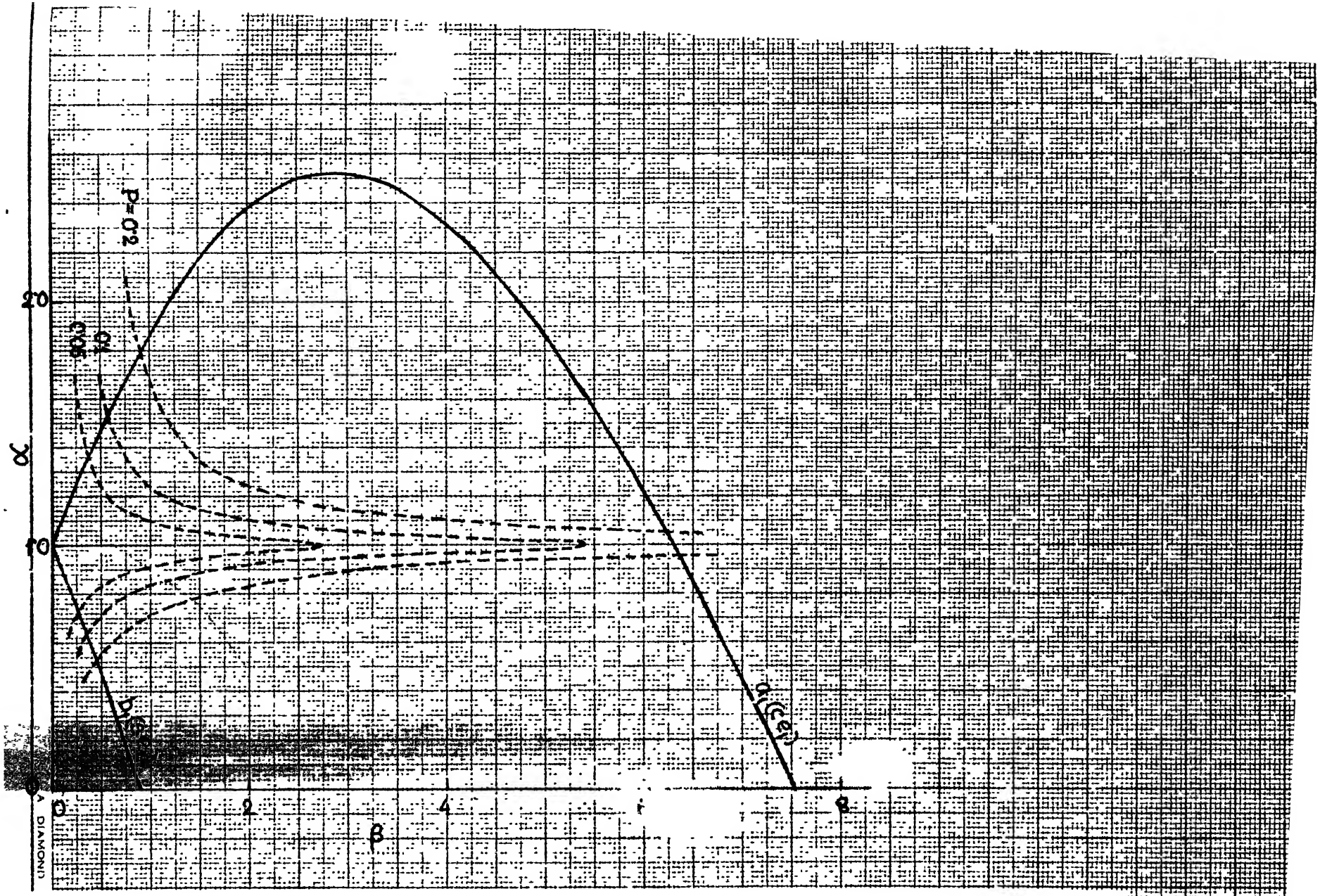

FIG. 3.1 REGION OF PRIMARY INSTABILITY OF MATHIEU EQUATION

For a certain value of P, the range of p over which the zero solution of θ is unstable, is found by plotting the locked mass response curve in the $\alpha - \beta$ plane in Fig. 3.1. The points of intersection of this curve and the instability boundary give the bounds on α. The bounds on p are then determined using the relation

$$p^2 = \frac{4 q^2 (1 - \zeta_2^2)}{\alpha (1 + R)} \qquad (3.10)$$

For easier inspection, it is desirable to plot the boundaries of instabilities in P - p plane. To this end, P is expressed in terms of β as

$$P = \frac{\beta}{2} \sqrt{[1 - p^2 (1 + R)]^2 + (2 \zeta_1 p)^2} \qquad (3.11)$$

For each point (α, β) on b_1 (se_1) etc., the corresponding point in P - p plane is determined using (3.10) and (3.11). These boundaries are plotted in P - p plane shown in Fig. 3.2, where $\bar{b}_1$ (se_1) etc. denote the corresponding boundaries in $\alpha - \beta$ plane. From (3.5a) it is clear that $\bar{b}_1$ (se_1) and $\bar{a}_1$ (ce_1) have period 4π, $\bar{b}_2$ (se_2) and $\bar{a}_2$ (ce_2) having a period 2π.

3.3 APPROXIMATE SOLUTIONS IN THE PRIMARY UNSTABLE REGION AND THEIR STABILITY

The method of harmonic balance, explained in section 2.3, is used to obtain approximate solutions of (3.1) in the primary unstable region. It was observed in

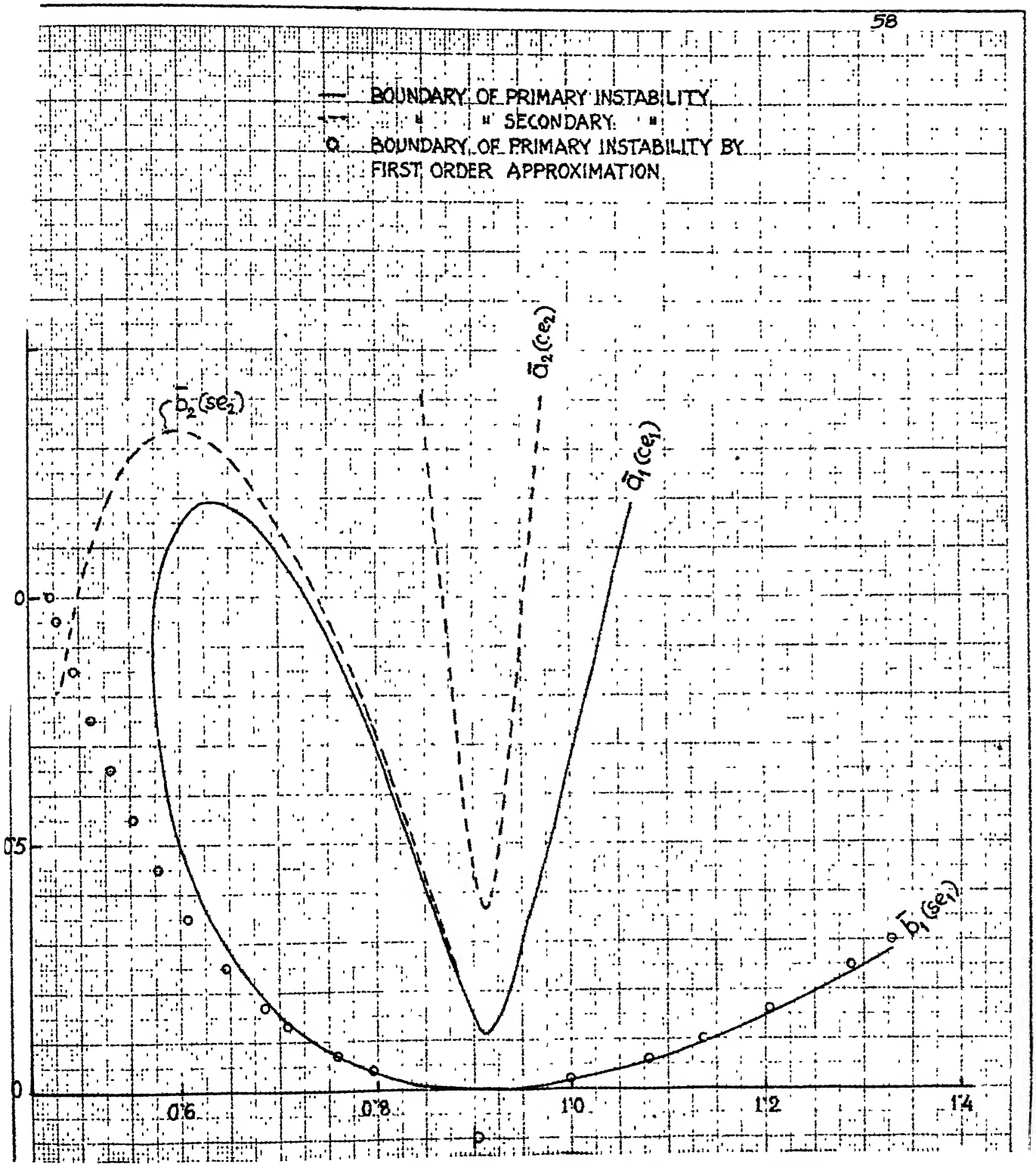

FIG. 3.2 INSTABILITY BOUNDARIES IN P - p PLANE

section 2.5.2 that for $P = 0.05$, the first order approximation does not yield correct results, quantitatively as well as qualitatively. Therefore higher order approximations are considered in this chapter by including higher power terms in the expressions of Bessel's coefficients, $J_n(B)$'s, used in (2.21) to (2.24). Since the amplitude of θ is expected to be quite high for large P, the third and the fourth order approximations are used, i.e., terms upto B^5 and B^7, respectively, are considered in (2.21) to (2.24). The solution, sought for large values of P, is still harmonic and is of the form given by (2.15) and (2.16).

The stability of these solutions is investigated by Floquet's theory after obtaining the perturbed equations (2.30).

3.4 SOLUTIONS THROUGH NUMERICAL INTEGRATIONS

Equations of motion (3.1) are integrated numerically using Gill's modification of Runge-Kutta method [46, 44]. For the cases where the solutions reach periodic steady state, a step size of integration equal to $\frac{\pi}{40}$ is found satisfactory. In some cases the step size is further reduced to $\frac{\pi}{80}$ to check the validity of the results. When the results do not converge with decreasing step sizes, integrations are also performed using Hamming's modified predictor - corrector method [46, 47]. For better accuracies, the double precision

computations are also carried out. The upper error bound in the predictor - corrector scheme is varied from 10^{-3} to 10^{-14}. The initial step size is taken as $\frac{\pi}{40}$. If more than ten bisections of the initial increment are necessary to get satisfactory accuracy, the integration procedure is terminated.

The results presented in this chapter are obtained by Gill's method. Special references are made to the predictor - corrector method wherever used.

3.5 RESULTS AND DISCUSSIONS

The characteristics of the solutions (discussed in this section) depend on the combinations of amplitude, P, and frequency, p, of excitation. These combinations in turn depend on the values of other parameters. All the results presented in this section are for the following values of the parameters: $R = 0.2$, $\zeta_1 = 0.02$, $\zeta_2 = 0.05$, and $q = 0.5$.

3.5.1 Boundaries of Instabilities of the Zero Solution of θ

The primary instability boundaries given by a_1 (ce_1) and b_1 (se_1) are plotted in Fig. 3.1 in $\alpha - \beta$ plane. The locked mass response curves, hereafter referred to as LMRC, are also plotted by dotted lines in the same figure for various values of P. For lower values of P,

(say $P = 0.05$), LMRC intersects the primary boundaries only at two points. These points of intersections determine the bounds on α as $\alpha_{lower} = 0.73$ and $\alpha_{upper} = 1.365$. From these values, the bounds on p are calculated using (3.10) as $p_{lower} = 0.78$ and $p_{upper} = 1.067$.

For a large value of P (e.g. $P = 0.2$), however, it can be seen from Fig. 3.1 that LMRC intersects a_1 (ce_1) at three points. Near $\alpha = 1$, LMRC passes on to the secondary region of instability. This is more clearly seen in Fig. 3.2 where the boundaries are plotted in P - p plane. In this figure b_1 (se_1) and a_1 (ce_1) bound the primary unstable region, and b_2 (se_2) and a_2 (ce_2) are the boundaries of secondary unstable region. For $P > 0.12$, near $p = 0.913$ ($\bar{p} = 1.0$) the secondary unstable region starts appearing and this region expands till $P \approx 0.36$. For $P > 0.37$, the third unstable region appears which is not shown in the figure.

In this figure the boundary of primary instability obtained by the first approximation, i.e., from (2.19), is also shown by the circled points. It is clear that the one term approximation of (2.16) does not give good results for $P > 0.10$.

3.5.2 Results by Approximate Method

The approximate results, presented in this section, are obtained by using the fourth order approximation. These results do not differ much from those obtained by using the third order approximation.

Fig. 3.3 shows the enlarged view of the boundaries of instabilities, already given in Fig. 3.2, for P upto 0.15. Because of dampings ζ_1 and ζ_2, the primary boundary starts from a nonzero value of P (0.0018), as dictated by (2.20). The boundary of the primary instability is shown by the firm line. For sufficiently large P and certain range of p, the approximate solutions are found to be unstable. The zones where the approximate solutions are unstable are found to be seperated by the zone of stable solutions. These zones of stable and unstable solutions are shown in Fig. 3.3. The unstable zones (regions II, III and IV) are shown by hatched areas. The stable zone is indicated as region I. In region IV the nonzero solutions are found to be unstable whereas the zero solution is stable. The areas between the firm line and the chain dotted lines show the overhangs where the zero solution is stable. The nonzero solutions in the overhangs may or may not be stable depending on whether the representative point lies in region I or not. As the entire region IV is quite far away from the primary boundary, the static equilibrium position of the pendulum is strongly stable and the system is expected to behave

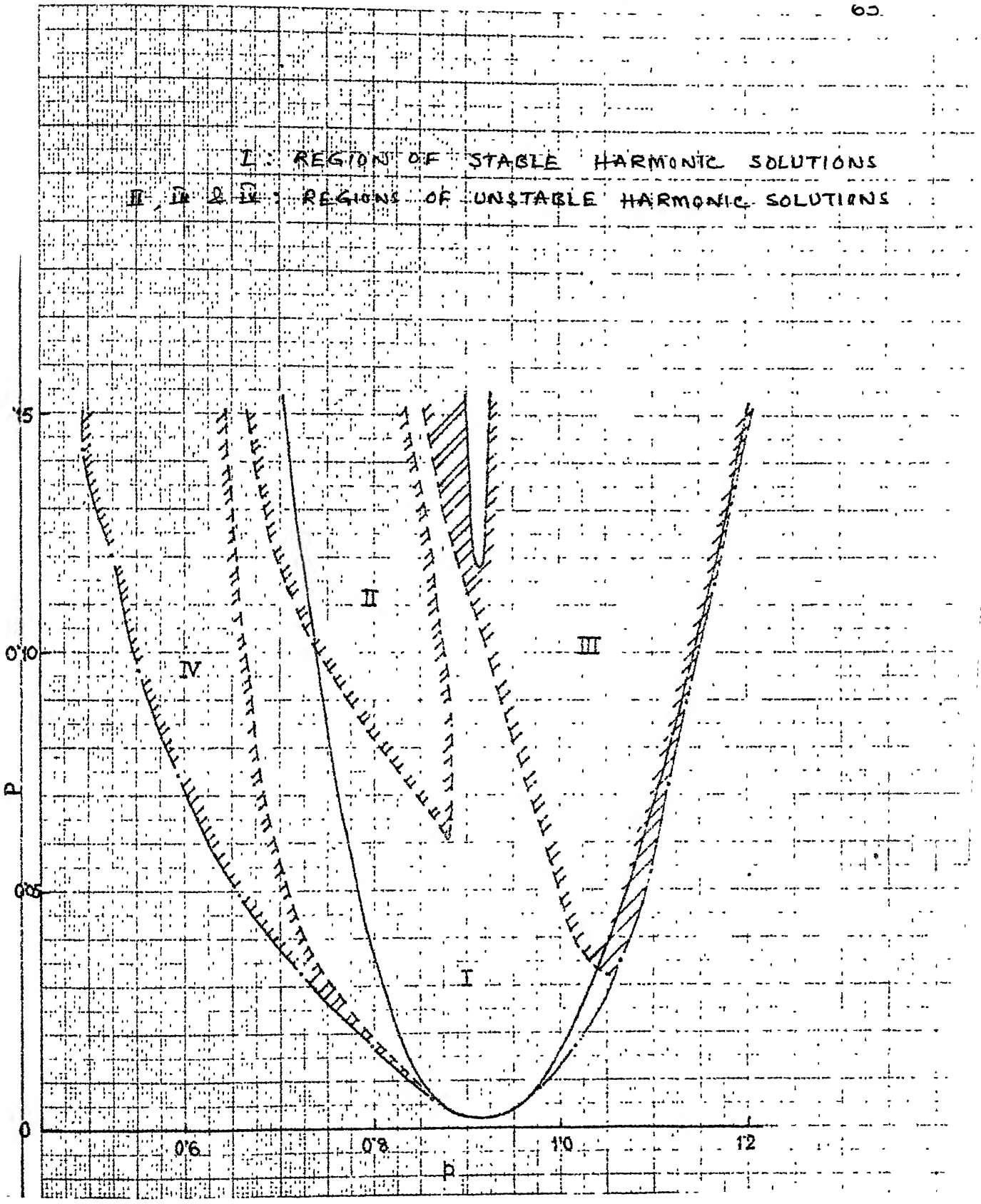

FIG. 3.3 BOUNDARIES OF STABLE AND UNSTABLE HARMONIC SOLUTIONS BY APPROXIMATE METHOD

like a locked mass system. In the discussions to follow, the nature of the solution in region IV is taken as that of the locked mass and is not considered any further.

It is obvious from Fig. 3.3 that as the frequency p, is varied, the representative point passes through various regions depending on the value of P. As an example we consider the behaviour of the solutions for P = 0.07. For $0.685 \leq p \leq 0.84$ the solutions are stable. As the frequency is increased beyond 0.84, region II is entered and the solutions are unstable. After that for a narrow band of frequencies, $0.89 \leq p \leq 0.96$, the representative point is again in region I and the solutions are stable. For further increase in p, region III is encountered rendering the solutions unstable. Another interesting feature to be noted from this figure is that the right hand side overhang diminishes with increasing P and ultimately disappears for $P \geq 0.08$. The left hand side overhang also becomes narrower for large P and in this overhang the solutions are stable only in a narrow range of p.

Finally, with $P > 0.12$, near $p = 0.913$ ($\bar{p} = 1.0$) secondary region of instability starts appearing. Since the secondary region of instability is bounded by the solutions of period 2π, the assumed form of solutions, given by (2.15) and (2.16), is not correct. However, this region of secondary instability is not analysed by the approximate method.

The discussions presented so far dealt with the qualitative aspects of the solutions with special reference to their nature of stability. We now turn our attention towards some quantitative aspects of the responses. To this end, Figs. 3.4 and 3.5 show the amplitudes of the primary and the secondary, respectively, for different values of the excitation parameter. The amplitudes, corresponding to the stable solutions, are joined by firm lines, whereas, those corresponding to the unstable solutions are encircled or squared and are joined by dotted lines. The squared and the circled points refer to the solutions lying in regions II and III of Fig. 3.3, respectively. The overhangs are included in these figures but not indicated specifically. Termination of a response curve with firm line indicates the end of the overhang, after which the zero solution of θ is strongly stable. On the other hand, if a response curve ends with a dotted line then it means that the entire range of p, for which the zero solution of θ is unstable, is not covered in the figures.

It is seen from these figures that for $P \geq 0.05$, the amplitudes sharply increase, at certain frequencies. In fact, these are the frequencies at which region III (Fig. 3.3) is approahced. Moreover, because of the sharp increase in the amplitudes of θ there is an appreciable difference in the successive approximations while solving

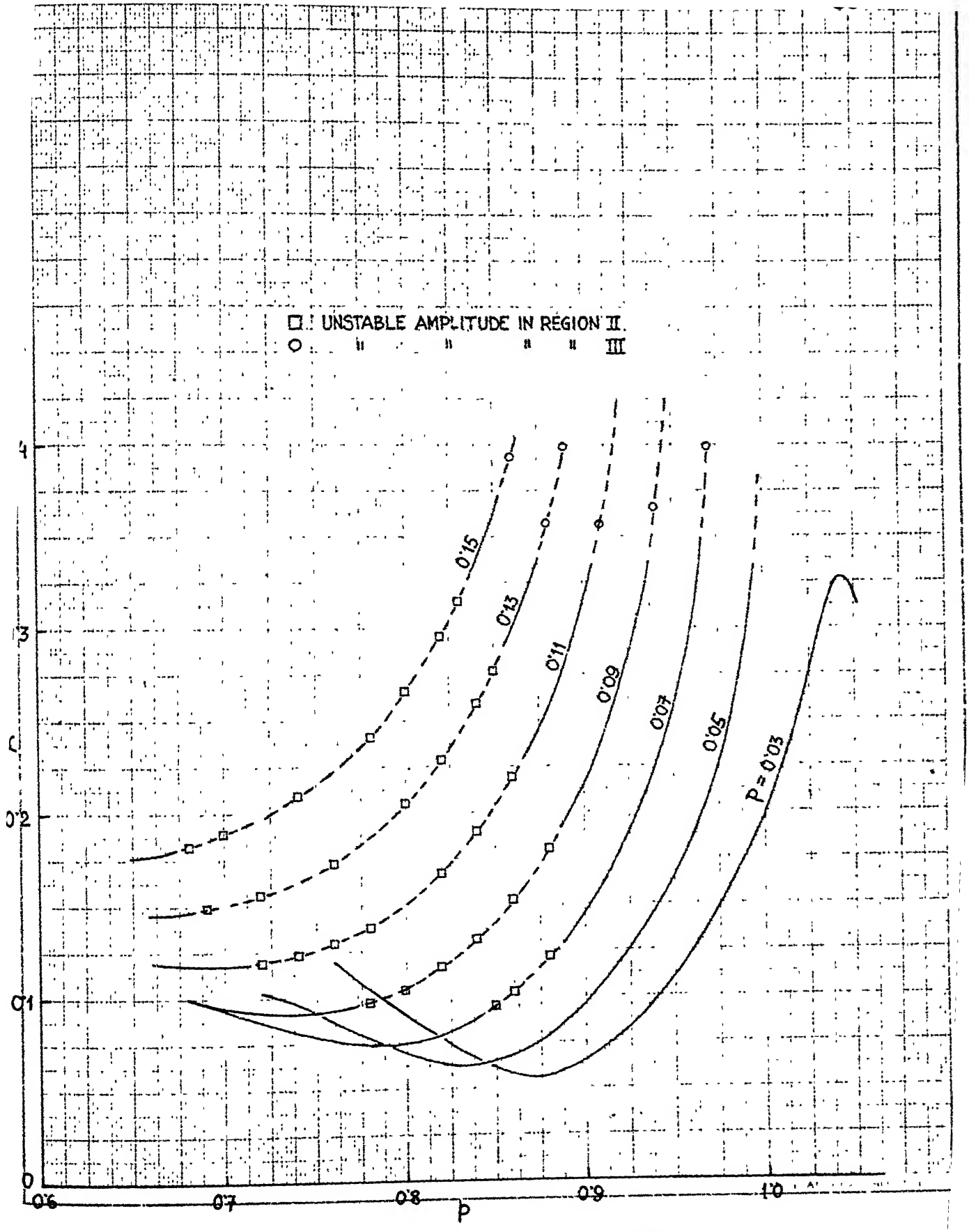

FIG. 3.4 VARIATION OF AMPLITUDE OF PRIMARY MASS WITH EXCITATION FREQUENCY FOR DIFFERENT EXCITATION AMPLITUDES : APPROXIMATE RESULTS

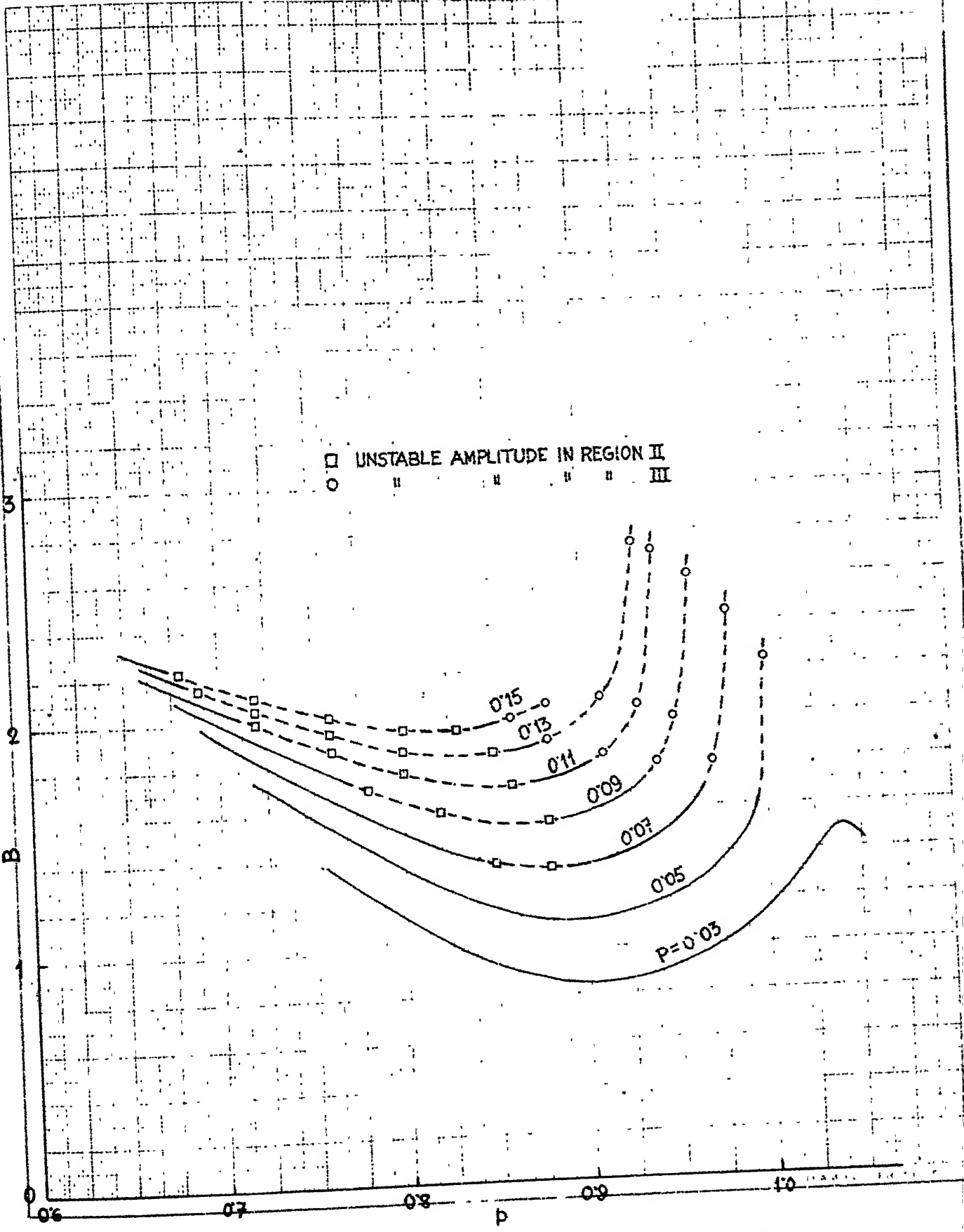

FIG. 3.5 VARIATION OF AMPLITUDE OF PENDULUM WITH EXCITATION FREQUENCY FOR DIFFERENT EXCITATION AMPLITUDES : APPROXIMATE RESULTS

(2.21) It can be remembered that for P = 0.05, this point was discussed in section 2.5.2. Near the frequencies at which region III is approached, there may be more than two solutions of (2.21). As an example, the number of solutions of (2.21) and their stability characteristics with P = 0.07 at frequencies near region III are as follows: (i) for $0.89 \leq p \leq 0.95$ there is only one stable solution, (ii) at p = 0.96 there are three solutions, only one of them being stable, (iii) at p = 0.97 there are three unstable solutions, and (iv) for $p \geq 0.98$ only one unstable solution is obtained. The values of the roots of (2.21) and corresponding values of A for above mentioned cases are given in Table 3.1. For the cases where only unstable solutions are obtained and the number of such solutions exceeds one, that solution which gives a smooth curve for the amplitudes is shown in Figs. 3.4 and 3.5. The amplitudes of these unstable solutions increase sharply and then start decreasing as the frequency p, is further increased. This decreasing trend, however, is not shown in these figures. The complete amplitude curves are shown only for P = 0.03. At this value of excitation the steady state approximate solutions are stable for all values of p. From the amplitude curves for P = 0.03 it can be seen that both A and B increase slowly after p = 0.9, attain a maximum value near p = 1.04 and decrease thereafter.

TABLE 3.1

Some Approximate Solutions

$P = 0.05, \quad R = 0.2, \quad \varsigma_1 = 0.02, \quad \varsigma_2 = 0.05, \quad q_1 = 0.5$

Frequency p	Number of harmonic solutions	θ - amplitude B	$\bar{x}$ - amplitude A	Stability characteristic
0.94	1	1.48	0.23	stable
	1	1.62	0.30	stable
0.96	2	2.33	1.00	unstable
	3	2.53	1.59	unstable
	1	1.79	0.40	unstable
0.97	2	2.06	0.61	unstable
	3	2.50	1.47	unstable
0.98	1	2.45	1.31	unstable

Lastly Fig. 3.5 shows that for all values of P, the solutions become unstable when amplitude of $\bar{x}$, A, reaches a value near 0.35 making it the critical value of A for the combination of parameters selected.

For representative points lying in region II, Fig. 3.3, the amplitudes of the corresponding unstable solutions are not large as they were for region III. In fact, it can be seen from Figs. 3.4 and 3.5 that as region II is entered while decreasing p, the amplitudes, A and B, decrease. Consequently there is not much difference between the results obtained by successive approximations. Only the boundary of region II is slightly dependent on the order of approximations.

Finally typical plots of phase angles, Φ_1 and $2\,\Phi_2$, with P = 0.07 are shown in Fig. 3.6. From this figure it is observed that as region III is approached with increasing p, the phase angles also change very sharply. Similar trends are obtained for other values of P as well.

It may be noted here that for $q = \frac{\sqrt{1+R}}{2}$ (i.e., the linear natural frequency of the pendulum taken as half of that of the primary system) the region III starts at $p \approx 1.05$ with $P = 0.05$, $R = 0.2$, $\zeta_1 = 0.02$ and $\zeta_2 = 0.05$.

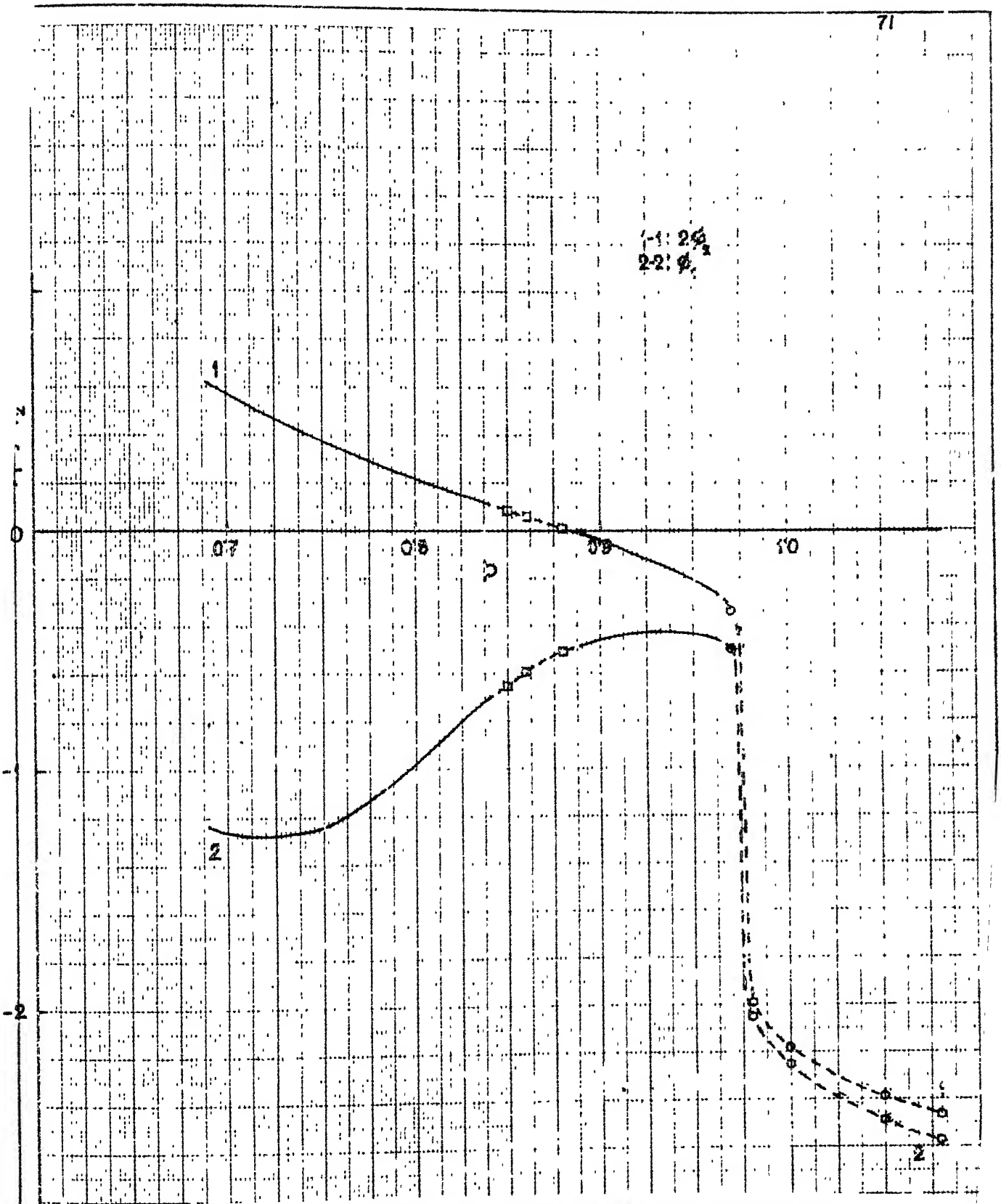

FIG. 3.6 VARIATION OF PHASE ANGLES WITH EXCITATION FREQUENCY : P = 0.07

Another interesting point is that the transition from stable harmonic solution to unstable harmonic solution of region III is associated with sharp increase in the amplitudes, whereas, the transition to region II is smooth.

3.5.3 Numerically Integrated Results

In this section the numerically integrated results are presented. These results are compared with the approximate results discussed in section 3.5.2. First the boundaries of regions of Fig. 3.3 are considered. Then the results for regions I, II and III are presented sequentially.

3.5.3.1 Boundaries of Regions of Stable and Unstable Harmonic Solution

The boundaries of regions of stable and unstable harmonic solutions are obtained by numerically integrating (3.1) and checking whether the solution reaches a harmonic (or near harmonic) steady state or not. For different regions, the boundary points by integrations are found by increasing or decreasing p in steps. This is done because near these points the responses are strongly dependent on initial conditions. Boundaries of these stable and unstable regions are shown in Fig. 3.7. Some results obtained by the approximate method, already shown in Fig. 3.3, are also included. The boundary points from integrated results are indicated by cross marks. This figure reveals

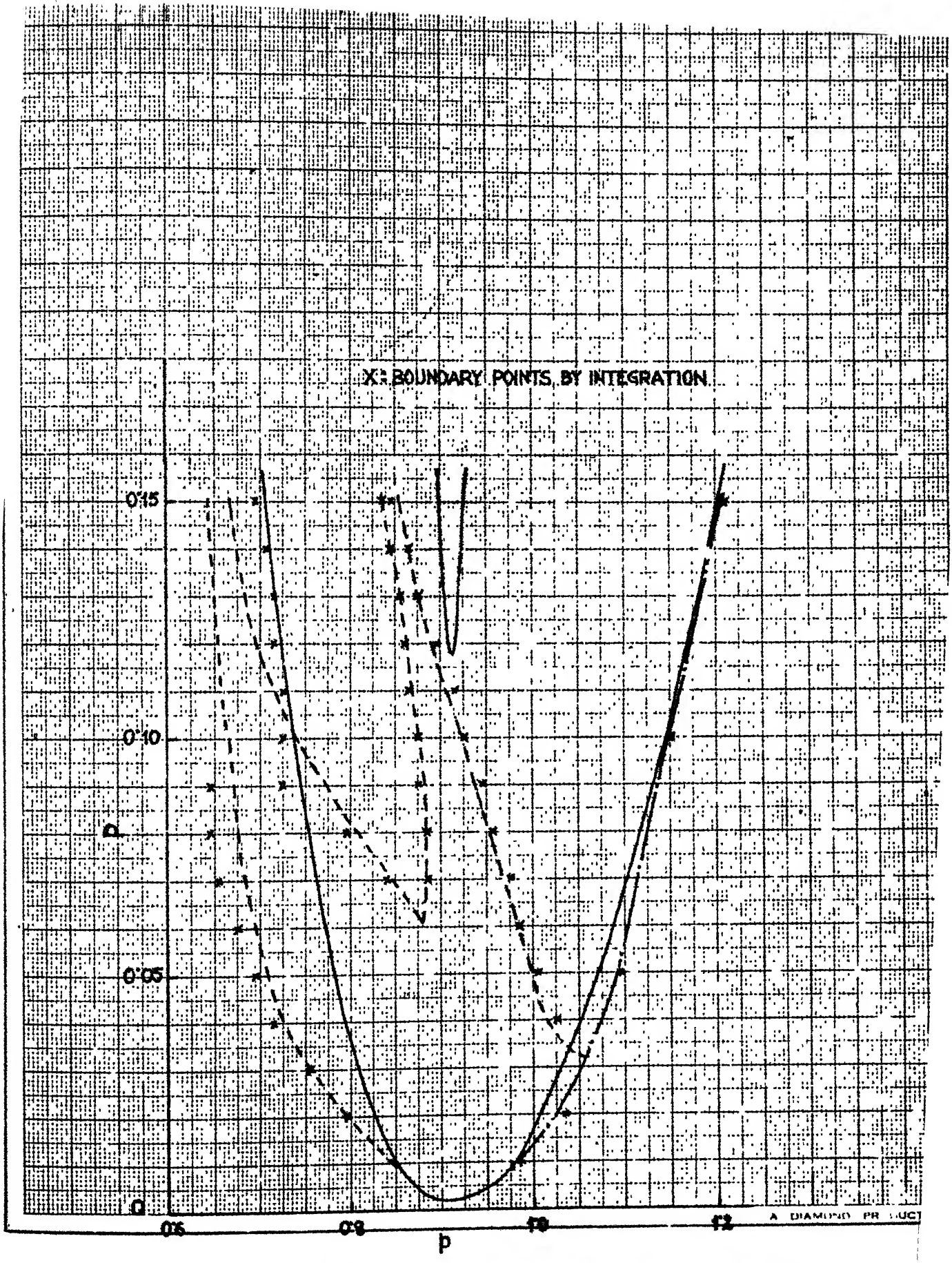

FIG. 3.7 BOUNDARIES OF STABLE AND UNSTABLE HARMONIC SOLUTIONS BY APPROXIMATE METHOD AND INTEGRATIONS

that for $0.04 \leq P \leq 0.09$ the integrated results yield a larger span of the left hand side overhang than that obtained by approximate solutions. For integrated results at $P = 0.09$ region II widens sharply towards left and touches the boundary of the left overhang. After this the left overhang span almost disappears, i.e., with $P \geq 0.10$ the left boundary of region II almost coincides with the boundary of primary instability. It is evident from Fig. 3.7 that, except for the left overhang, the results obtained by integration and approximate method match very well.

3.5.3.2 Numerical Results for Region I

The amplitudes of θ and $\bar{x}$ are shown in Figs. 3.8 and 3.9, respectively, where both the integrated and the approximate results are included. For the integrated results, when the responses are seen to be periodic (with $\bar{x}$ and θ having periods of 2π and 4π respectively), the maximum value in one period of oscillation is taken as the representation of the amplitude. For the cases, where the amplitudes obtained by the approximate method and integration match, the integrated responses are, of course, seen to be completely harmonic. For representative points in region I of Fig. 3.7, the integrated responses reach harmonic or near harmonic steady state. These steady state amplitudes are joined by firm lines in Figs. 3.8 and 3.9. The dotted lines in these figures are for combinations of P and p

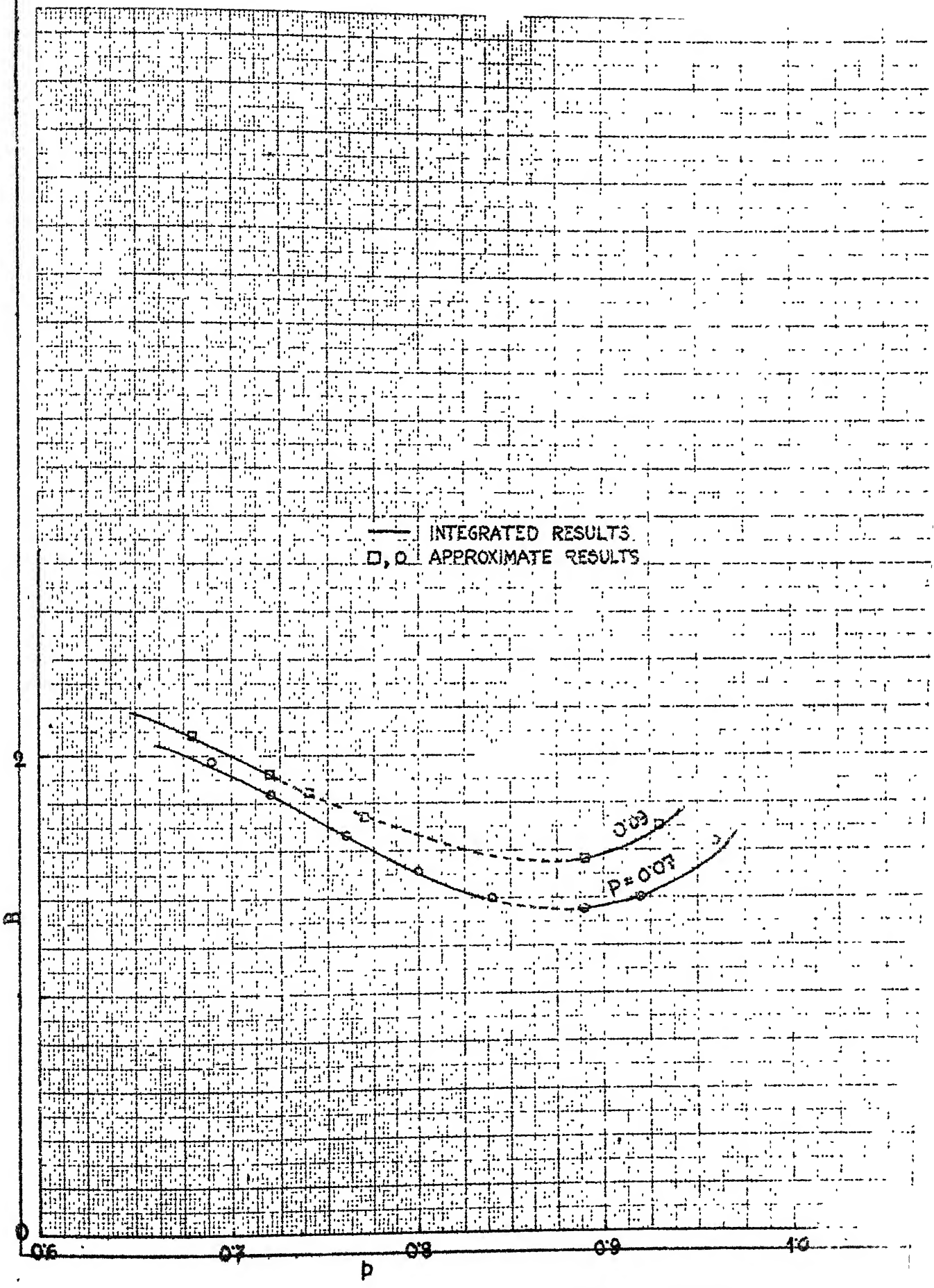

FIG, 3.8 AMPLITUDE OF PENDULUM OBTAINED BY APPROXIMATE METHOD AND INTEGRATION

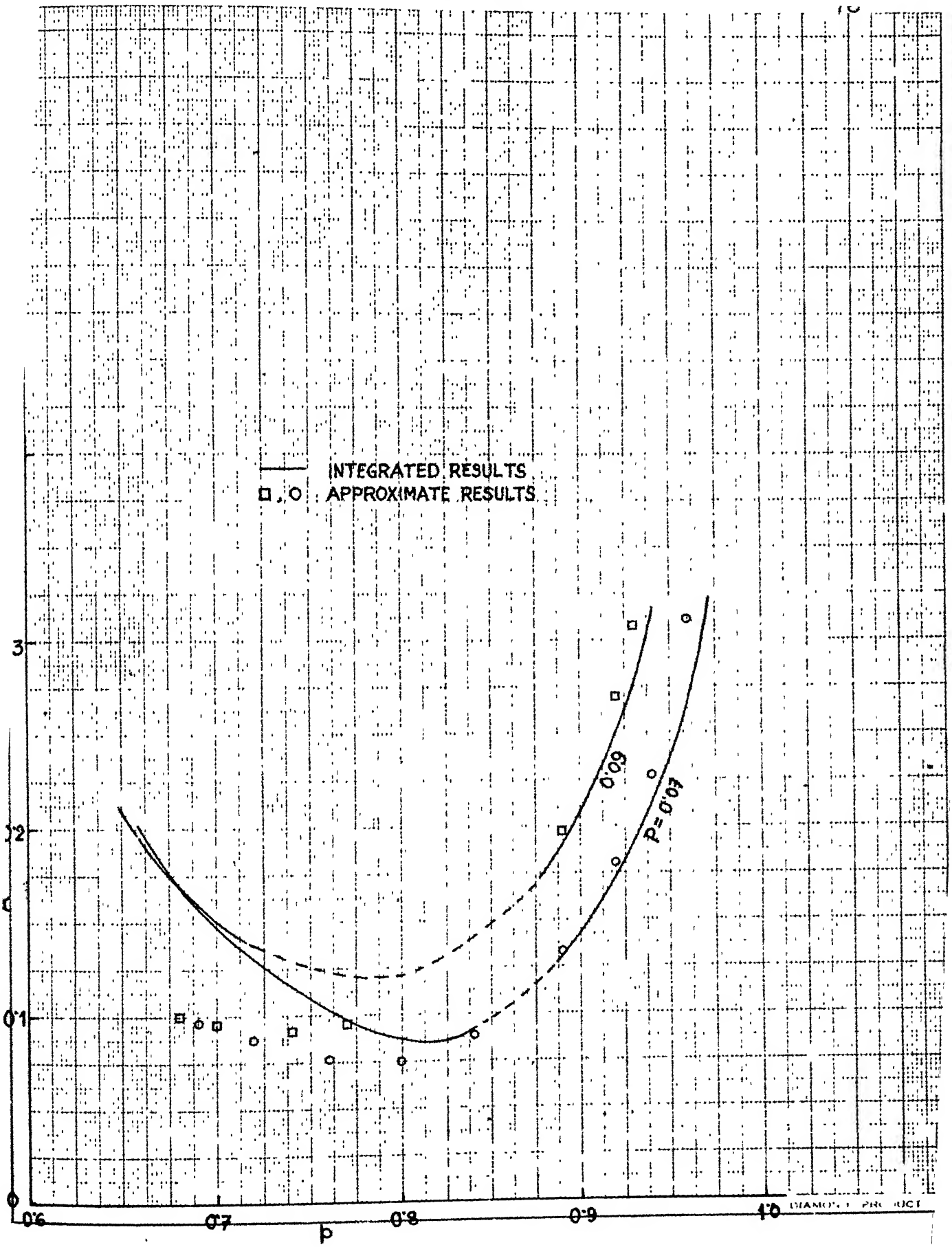

FIG. 3.9 AMPLITUDE OF PRIMARY OBTAINED BY APPROXIMATE METHOD AND INTEGRATION

lying in region II of Fig. 3.7. For these values the integrated responses do not have fundamental period of $\bar{x}$ and θ as 2π and 4π, respectively, and the amplitudes of responses do not have any meaning in ordinary terms. In fact, the dotted lines in Figs. 3.8 and 3.9 are nothing but the extrapolations of the respective firm lines. Figure 3.8 shows that the amplitudes of θ obtained by the approximate method and numerical integration are in very close agreement. At lower values of p, however, these two methods give different values for the amplitude of $\bar{x}$ (Fig. 3.9). The reason for this discrepancy is explained in the following paragraph.

Figures 3.10 and 3.11 show the integrated steady state response time histories of θ and $\bar{x}$, respectively. These responses are for $P = 0.07$ at different values of p. Figure 3.10 shows that the θ - response is harmonic for all values of p. Thus the assumed form, given by (2.16), is correct and so the results obtained by the approximate method are very accurate. Figure 3.11 shows that in the $\bar{x}$ - response, the contributions of the higher harmonics increase with decreasing p. This explains the error in approximate solutions where only the first harmonic was considered. More the contribution of the higher harmonics, greater is the discrepancy between the approximate and the integrated results in Fig. 3.9.

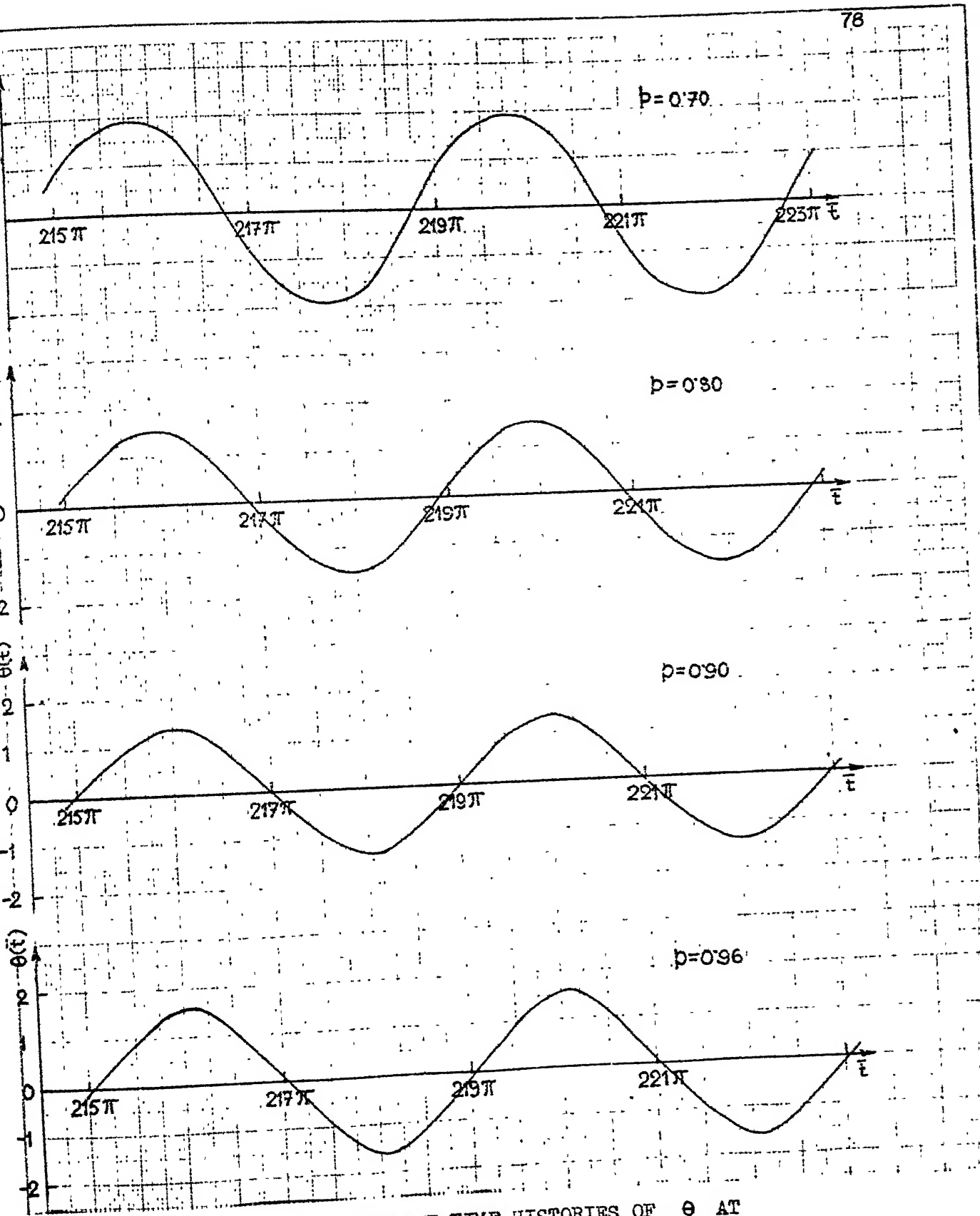

FIG. 3.10 RESPONSE TIME HISTORIES OF θ AT DIFFERENT EXCITATION FREQUENCIES : P = 0.07

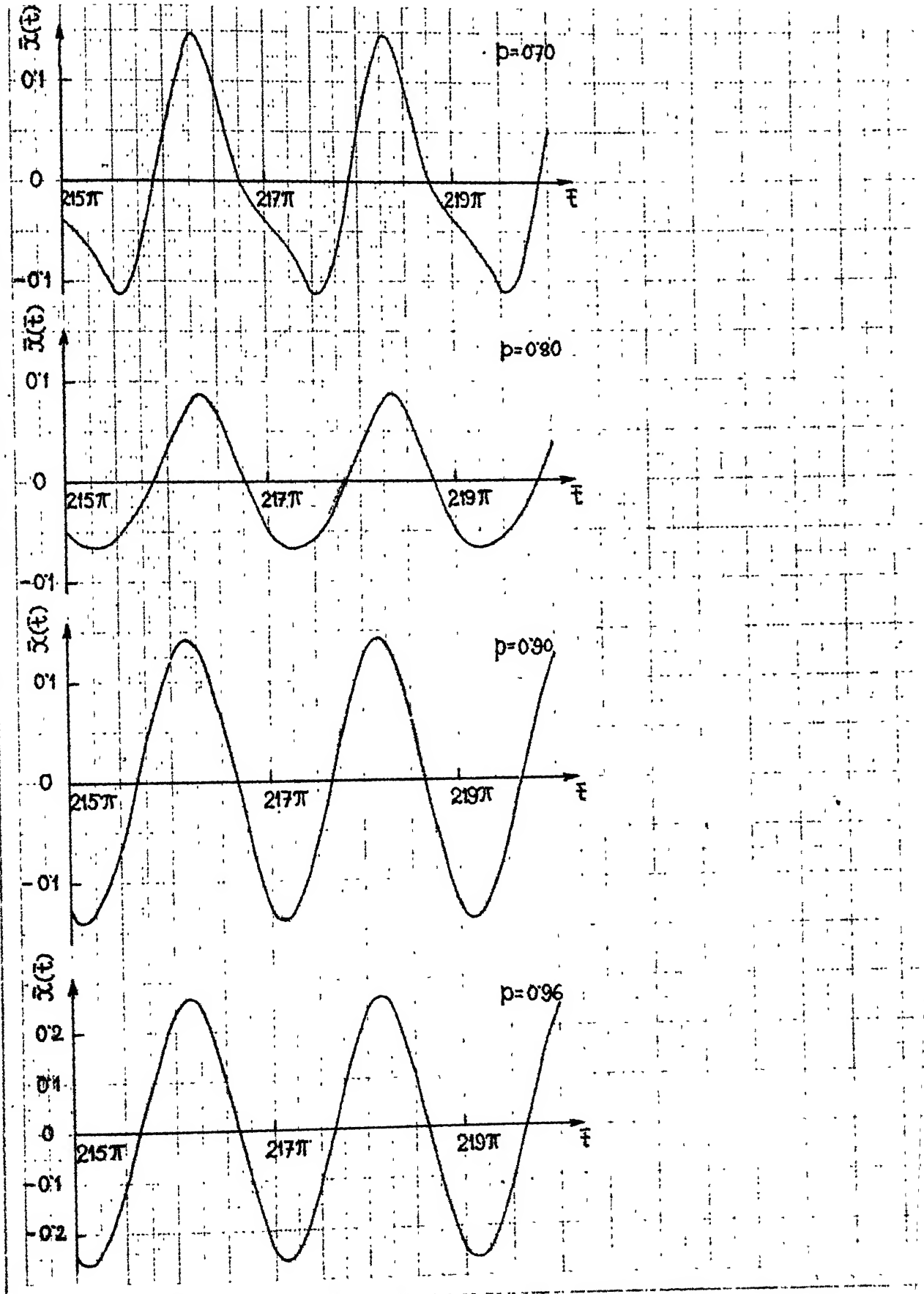

FIG. 3.11 RESPONSE TIME HISTORIES OF $\bar{x}$ AT DIFFERENT EXCITATION FREQUENCIES : P = 0.07

We now discuss some results for $P = 0.15$. In region I, both the approximate method and the integration give stable harmonic or periodic solutions only for two very narrow bands of p — one around $p = 0.84$ and the other around $p = 0.90$. The typical solutions at $p = 0.84$ are: $\bar{x} = 0.34 \cos (\bar{t} - 0.22), \theta = 1.96 \cos (\frac{\bar{t}}{2})$ by approximate method and $\bar{x} = 0.32 \cos (\bar{t} - 0.20)$, $\theta = 1.95 \cos (\frac{\bar{t}}{2} + 0.02)$ by integration. At $p = 0.90$ the approximate method yields a stable harmonic solution: $\bar{x} = 3.81 \cos (\bar{t} - 1.88), \quad \theta = 3.31 \cos (\frac{\bar{t}}{2} + 0.61)$. The integration gives a strongly stable steady state as $\bar{x} = 3.85 \cos (\bar{t} - 1.44), \quad \theta = \pi + 3.64 \cos (\frac{\bar{t}}{2} - 0.76)$. The amplitudes of $\bar{x}$ and θ are seen to be very high with that of θ being $> \pi$.

3.5.3.3 Numerical Results for Region II

For points in region II of Fig. 3.7, the integrated responses of $\bar{x}$ and θ are found <u>not</u> to have the fundamental periods as 2π and 4π, respectively. The responses may or may not be periodic depending on the initial conditions and the values of P and p. Moreover, again depending on initial conditions, more than one periodic steady state may exist. Some idea about the existence of periodic or near-periodic responses can be obtained from the eigenvalues of (2.32) used in the approximate method. This is explained below with some examples.

Table 3.2 gives the eigenvalues of (2.32) for three different cases. In each case, the value of A, B etc. of (2.15) and (2.16) are also given in this table. The approximate solutions of steady states are used to generate the following set of initial conditions by taking $\bar{t} = 0$ in (2.15) and (2.16):

$$\left.\begin{aligned} \bar{x}(0) &= A\cos\Phi_1 \\ \bar{x}'(0) &= -A\sin\Phi_1 \\ \theta(0) &= B\cos\Phi_2 \\ \theta'(0) &= -\frac{B}{2}\sin\Phi_2 \end{aligned}\right\} \quad (3.12)$$

Figures 3.12 to 3.14 show the integrated steady state responses of θ' for the cases cited in Table 3.2. The responses are presented for θ' instead of θ because in some cases, even in the steady states, the pendulum is found to make complete revolutions, periodically or non-periodically.

In case (i) (Table 3.2), P and p combination is in region I but is very close to region II. The maximum eigenvalue is just less than unity. Therefore, the steady state given by the approximate solution is expected to be weakly stable. Figure 3.12 (b) shows that with initial conditions given by (3.12), θ' - response is harmonic with period 4π. However, with slightly different initial conditions, the integration carries the solution to a different

TABLE 3.2

Eigenvalues of (2.32) for Three Different Cases Near Region II

Case	Parameter combination	Amplitudes and phase angles of (2.15) and (2.16)	Eigenvalues of (2.32)			
			λ_1	λ_2	λ_3	λ_4
(i)	P = 0.06 p = 0.88	A = 0.098 B = 1.24 ϕ_1 = - 0.63 ϕ_2 = 0.01	-0.51 + 0.85 i modulus = 0.99	-0.51 - 0.85 i	-0.28 + 0.46 i modulus = 0.54	-0.28 - 0.46 i
(ii)	P = 0.07 p = 0.88	A = 0.12 B = 1.35 ϕ_1 = -0.51 ϕ_2 = 0	-0.70 + 0.78 i modulus = 1.05	-0.70 - 0.78 i	-0.32 + 0.40 i modulus = 0.51	-0.32 - 0.40 i
(iii)	P = 0.08 p = 0.86	A = 0.12 B = 1.46 ϕ_1 = -0.49 ϕ_2 = 0.02	-0.93 + 0.75 i modulus = 1.19	-0.93 - 0.75 i	-0.33 + 0.28 i modulus = 0.43	-0.33 - 0.28 i

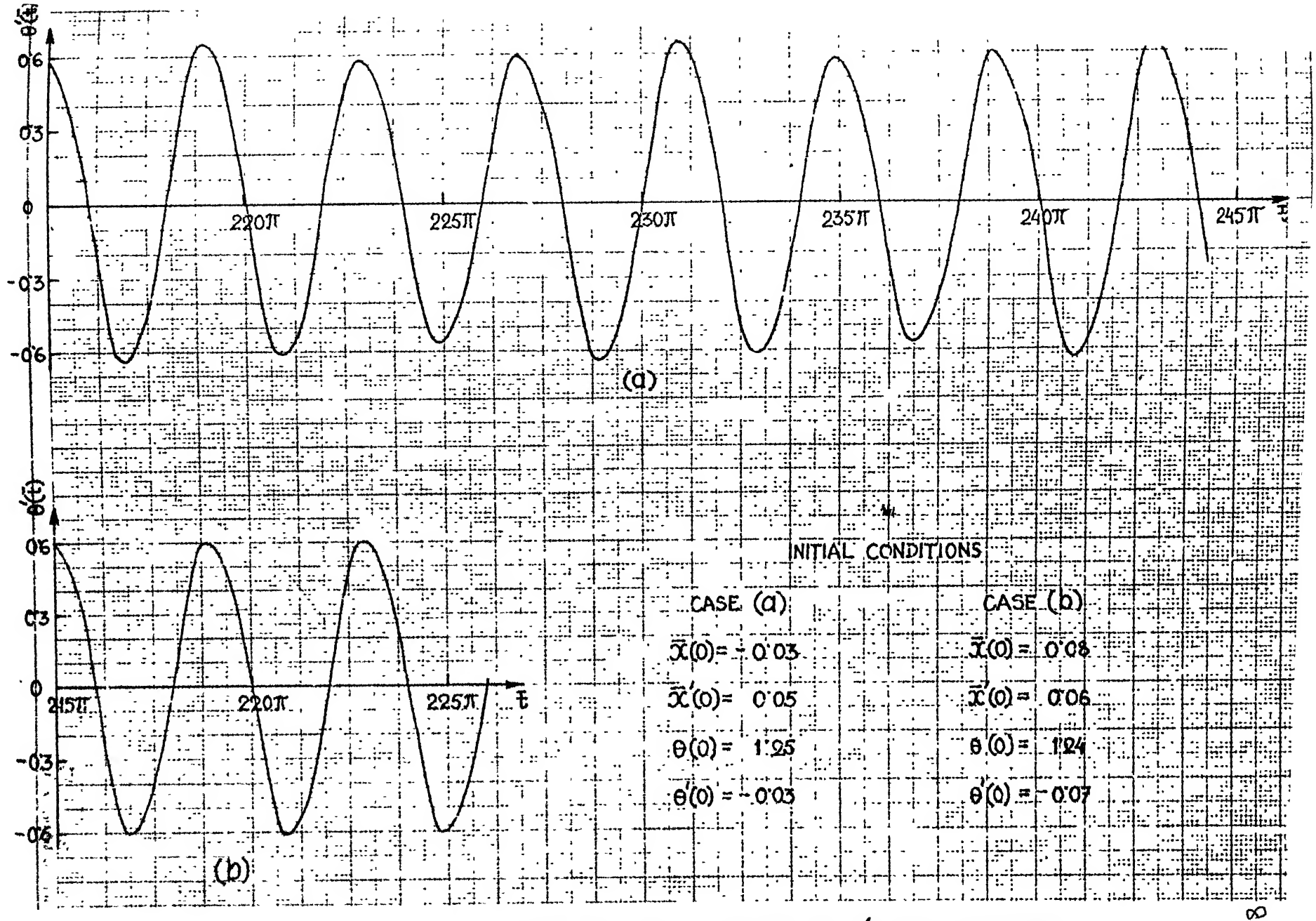

FIG. 3.12 RESPONSE TIME HISTORIES OF θ' WITH DIFFERENT INITIAL CONDITIONS : P = 0.06, p = 0.88

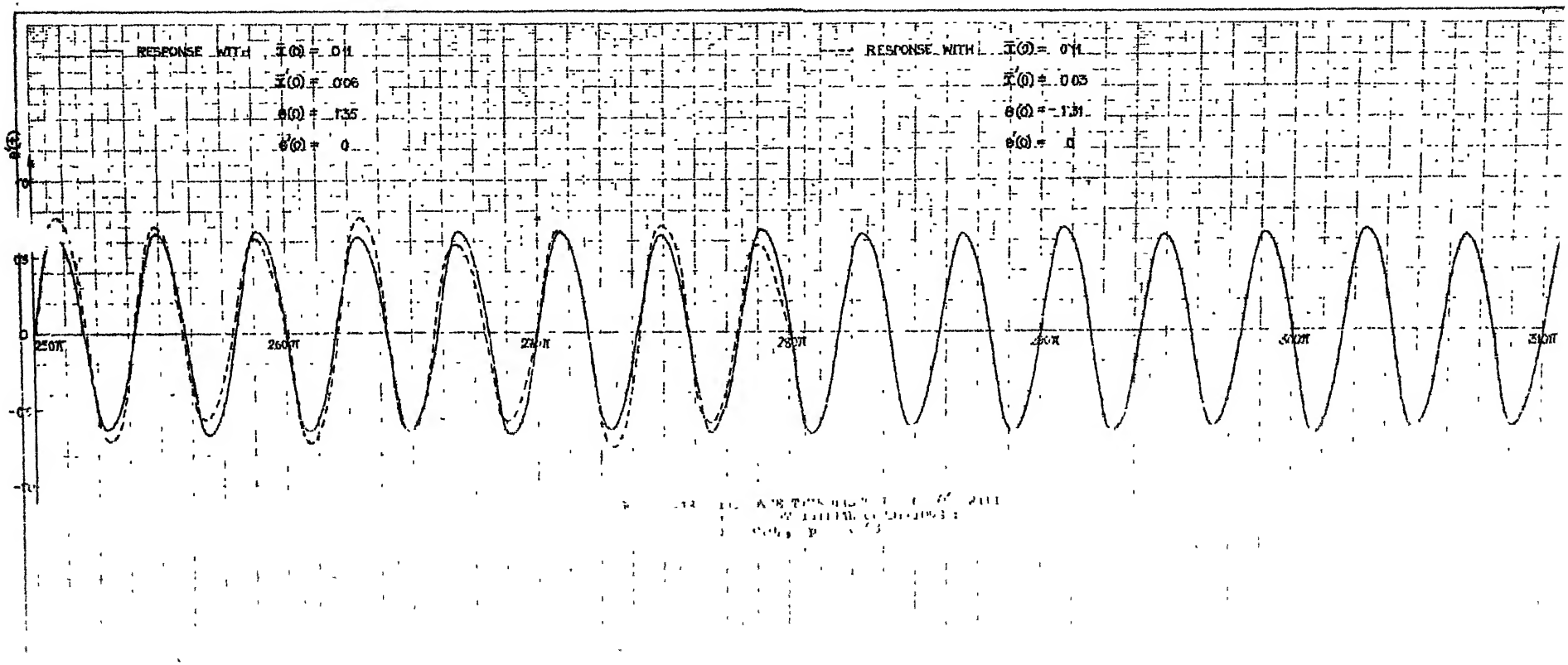
RESPONSE WITH
$\bar{x}(0) = .011$
$\bar{x}'(0) = .006$
$\theta(0) = .135$
$\theta'(0) = 0$
RESPONSE WITH
$\bar{x}(0) = .011$
$\bar{x}'(0) = .005$
$\theta(0) = -.131$
$\theta'(0) = 0$
$\theta(\xi)$
.05
0
250π
260π
270π
280π
290π
300π
310π

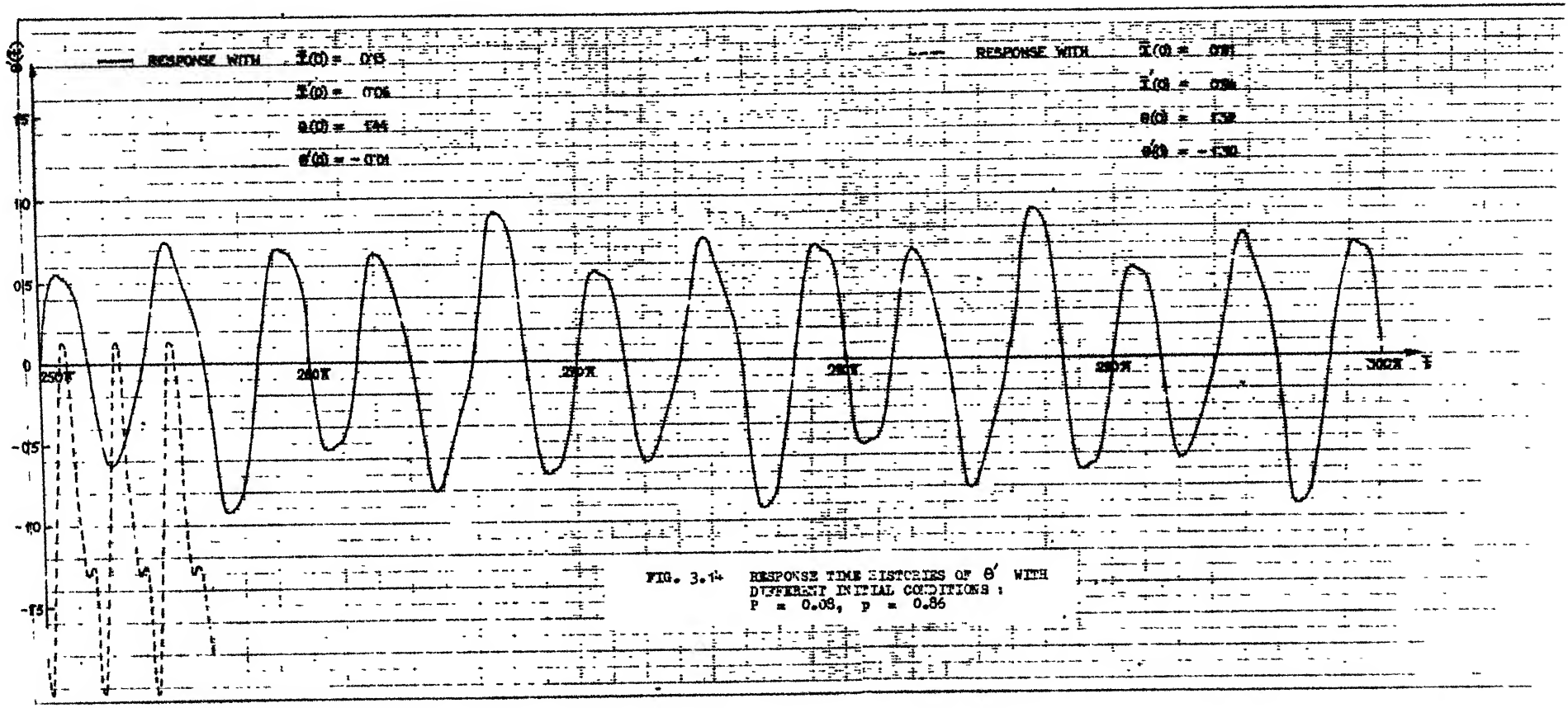

FIG. 3.14 RESPONSE TIME HISTORIES OF θ' WITH DIFFERENT INITIAL CONDITIONS : P = 0.08, p = 0.86

steady state as shown in Fig. 3.12 (a). The response in this case is seen to be amplitude modulated with a time period of 12π .

For cases (ii) and (iii) (Table 3.2) the representative points lie in region II and the maximum eigenvalues are slightly greater than unity. The corresponding steady states, obtained by the approximate solutions, are therefore unstable. For numerical integration also no initial condition is found which takes the solution to a harmonic steady state. As the maximum eigenvalues in these cases are complex and near unity it is expected that the growth of the trivial solution of (2.27) and (2.28) will be slow and oscillatory. Therefore, with the initial conditions (3.12), the numerical integration is expected to give a steady state which will be close to the harmonic steady state given by the approximate solutions. This is confirmed in Figs. 3.13 and 3.14, which show the integrated steady state responses of θ' with two different sets of initial conditions. The firm lines in these figures correspond to initial conditions (3.12). Comparing Figs. 3.13 and 3.14 it is seen that the responses become more irregular as the maximum eigenvalue increases.

The dotted line in Fig. 3.13 shows another steady state θ' - response for case (ii), obtained with a different initial condition. Though the trends are similar, this is seen to differ slightly in magnitude from that represented

by the firm line. It may be noted that both the responses are periodic with time period 44π .

Similarly the dotted line in Fig. 3.14 shows another steady state obtained with an initial condition which is different from that used for firm line. The firm line shows a period of 20 π , whereas, the dotted line response has a period 2 π . Moreover, in the latter case, the mean value of θ' is nonzero. This implies that during the steady state the pendulum keeps on rotating in the same direction, the time for each rotation being 2 π .

The initial conditions, mentioned above, yield periodic steady states in each case considered in Table 3.2. However, if initial conditions are chosen so as to be sufficiently far away from these periodic steady state trajectories, the integrated response becomes irregular and nonperiodic.

With further increase in P than mentioned in Table 3.2 (with the representative point still lying in region II) the maximum eigenvalue also increases and the integrated responses become nonperiodic with any choice of initial conditions.

All the above mentioned results are verified with a smaller step size of integration ($= \frac{\pi}{80}$).

3.5.3.4 Numerical Results for Region III

For points in region III of Fig. 3.7, while checking the stability of the approximate harmonic solution, the maximum eigenvalue of (2.32) is found to be real and much greater than unity. This implies that no harmonic or near harmonic steady state can be obtained in the neighbourhood of the solutions obtained by the approximate method. In such cases the integrated responses are seen to be non-periodic. In other words, even after a long time, when the effects of the transients are expected to die down, the responses do not show any periodicity and are quite irregular. Moreover, the results do not converge by decreasing the step size of integration.

For points in region I, but very close to region III, harmonic steady states are obtained only with the following scheme: The integration is started with points well inside region I and when the steady state is reached, the frequency, p, is increased in small steps. The harmonic steady states, thus obtained, are very weakly stable. As an example, we take $P = 0.05$ and $p = 1.0$, when the approximate method gives an unstable harmonic solution with the maximum eigenvalue being real and much greater than unity. Following the scheme mentioned above, a harmonic steady state, with $\bar{x} = 0.3 \cos(\bar{t} - 0.6)$ and $\theta = 1.52 \cos(\frac{\bar{t}}{2} - 0.2)$ is found by integration. However, this steady

state is very weakly stable so that even a disturbance of 0.1 to the coordinate θ , takes the solution away from this steady state and the responses become nonperiodic. For all other initial conditions, the responses are completely nonperiodic and the results do not converge even with step size equal to $\frac{\pi}{360}$. Figure 3.15 shows typical time histories of θ' for two different step sizes ($\theta(0) = 0.05$, $\theta'(0) = \bar{x}(0) = \bar{x}'(0) = 0$).

For points well within region III no harmonic or periodic steady state can be obtained. For one such point, with $P = 0.05$ and $p = 1.05$, θ' - response is shown in Fig. 3.16. Figure 3.17 shows $\bar{x}$ - responses for $P = 0.05$, $p = 1.0$ and 1.05. Since $\bar{x}$ - coordinate is directly driven by the external harmonic excitation, it is expected that $\bar{x}$ - response will have more regularity as compared to that for θ and this is revealed by Fig. 3.17 as well.

The results, presented in Figs. 3.15 to 3.17, as such do not convey any meaning since these results have not converged with decreasing step sizes of integration. Numerical calculations in double precisions, employing better scheme of integration by predictor-corrector method, also fail to converge. Moreover, a change even in the eighth decimal place, in the initial conditions changes the response completely. These differences in the results for slightly different initial conditions occur because it is found that

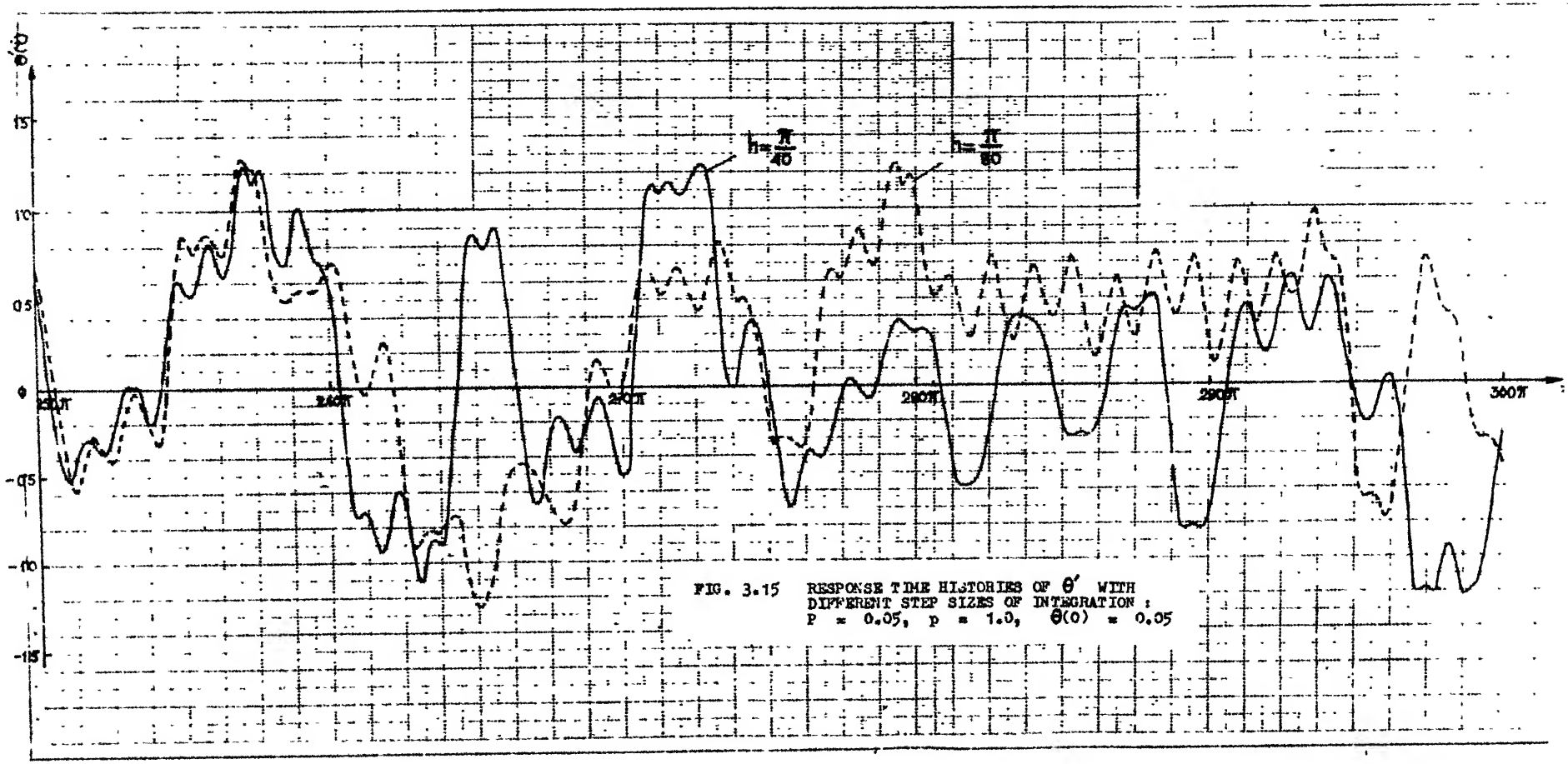

FIG. 3.15 RESPONSE TIME HISTORIES OF θ' WITH DIFFERENT STEP SIZES OF INTEGRATION : P = 0.05, p = 1.0, $\theta(0)$ = 0.05

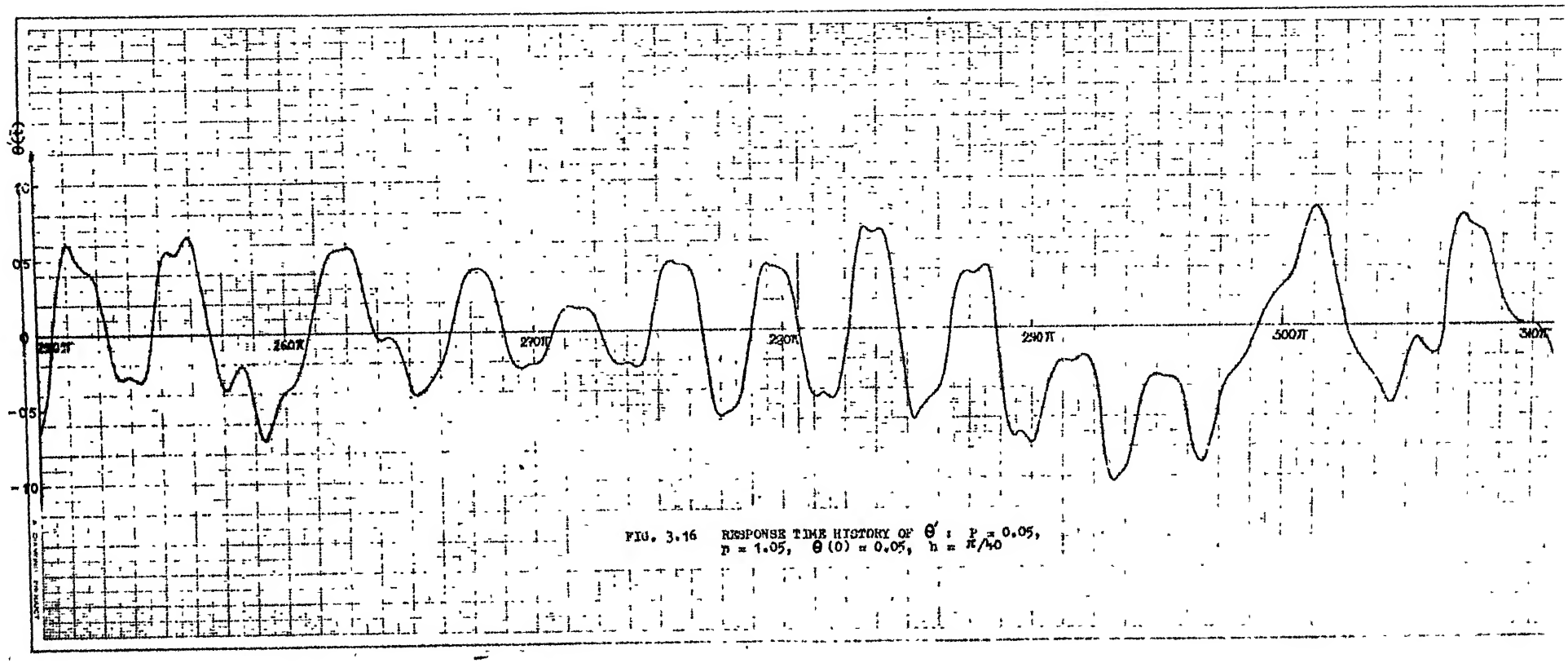

FIG. 3.16 RESPONSE TIME HISTORY OF θ' : $\beta = 0.05$, $p = 1.05$, $\theta(0) = 0.05$, $h = \pi/40$

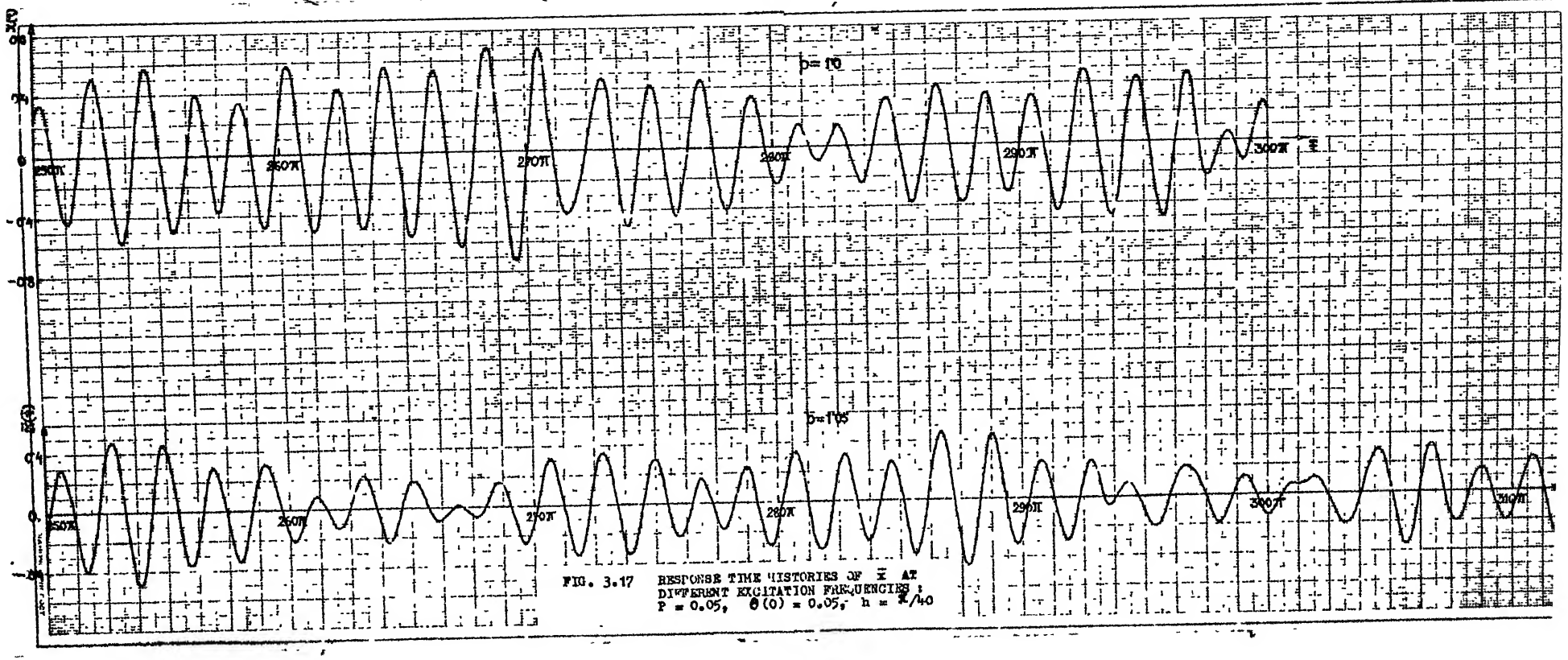

FIG. 3.17 RESPONSE TIME HISTORIES OF $\bar{x}$ AT DIFFERENT EXCITATION FREQUENCIES ; P = 0.05, $\theta(0) = 0.05$, $h = \pi/40$

somewhere in the time history, θ' has a very steep gradient. This makes the subsequent computations very sensitive to the inherent inaccuracies of numerical integrations. In comparison, for region I, where the harmonic steady states are strongly stable, even a coarse step size of integration with any initial condition carries the solution to the same harmonic steady state.

To derive any meaning out of the results obtained for region III, the following argument is put forward. In the actual physical system, if experiments are performed then at every stage there will be some unaccountable external disturbances. It is also not possible to control the parameters to exact values. The numerical integrations can be thought of as a computer simulated experiment. Here, in fact, the control on the parameter values is much better than in the actual physical experiment. The external disturbances in the physical system may be represented by the numerical roundoffs and the inherent errors in the numerical schemes used.

In the light of the above arguments, a strongly stable solution implies consistent and reproducible results from a physical experiment. Likewise, an unstable or a weakly stable solution suggests that the corresponding experimental result can not be reproduced. This is because of the inherent disturbances which, in the latter case, change the

response drastically. These disturbances can only be considered as random. So it is impossible to predict the exact value of the response at a future instant of time. The response time histories can then be treated as sample records of a random process.

"In practical terms, the decision as to whether or not physical data are deterministic or random is usually based upon the ability to reproduce the data by controlled experiments [48]". For parameters lying well inside region I an experiment, producing identical results, can be repeated many times (within the limits of experimental error) and the responses, thus, are deterministic. For region III the experiment can not be designed which will produce identical results when the experiment is repeated and then the data must be considered random in nature. As discussed above, the integrated responses can be considered to represent some physical experiment. Therefore, the only meaningful description of these time histories can be attempted through the statistical analysis, which is presented in Chapter 4.

3.5.3.5 Numerical Results for Sufficiently High Excitation

It is clear from Fig. 3.2 that if P is large then for certain frequencies the representative point lies in the secondary region of instability. For example, with $P = 0.20$ and $p = 0.90$ the numerical results give a periodic

steady state with θ oscillating with period 2π . θ - oscillations with a period of 2π are usually seen to be associated with a shift in mean values of θ from zero. This shift of the dynamic mean position from the static equilibrium position is well known in nonlinear systems and is often called drift or steady - streaming [9].

With sufficiently large P while increasing p the secondary and the primary regions are alternately traversed in Fig. 3.2. As an example, with P = 1.0 the following behaviours of the steady states are observed while increasing frequency: (i) For $p \leq 0.30$ the zero solution of θ is stable. (ii) At $p = 0.40$ the representative point is in the secondary region. θ - oscillation has a period of 2π and a mean value of 0.23. (iii) At $p = 0.55$ the zero solution of θ is a stable solution. (iv) With $p = 0.70$ the point is in the primary unstable region and θ oscillates with a period of 4π . θ and θ' responses are shown in Fig. 3.18(a). (v) Increase in p to 0.80 takes the point to secondary region again and θ oscillates with a period of 2π . Figure 3.18 (b) shows θ and θ' responses and the mean position of θ - oscillation is near $\frac{\pi}{2}$. (vi) At $p = 0.91$ θ oscillation is seen to have a period of 2π and therefore the point, perhaps, lies in the fourth region of instability, the boundaries for which are not computed. (vii) At $p = 1.0$ the point is in the secondary

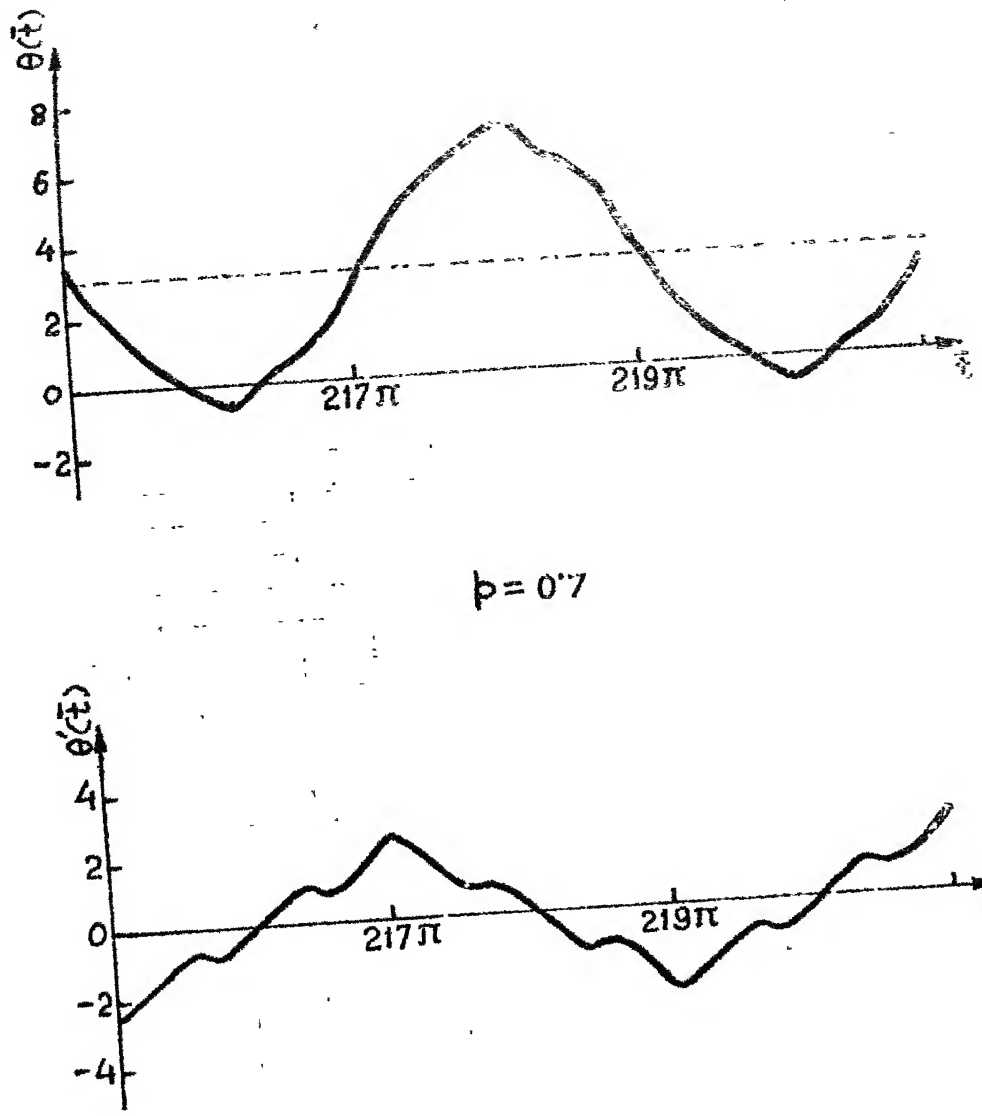

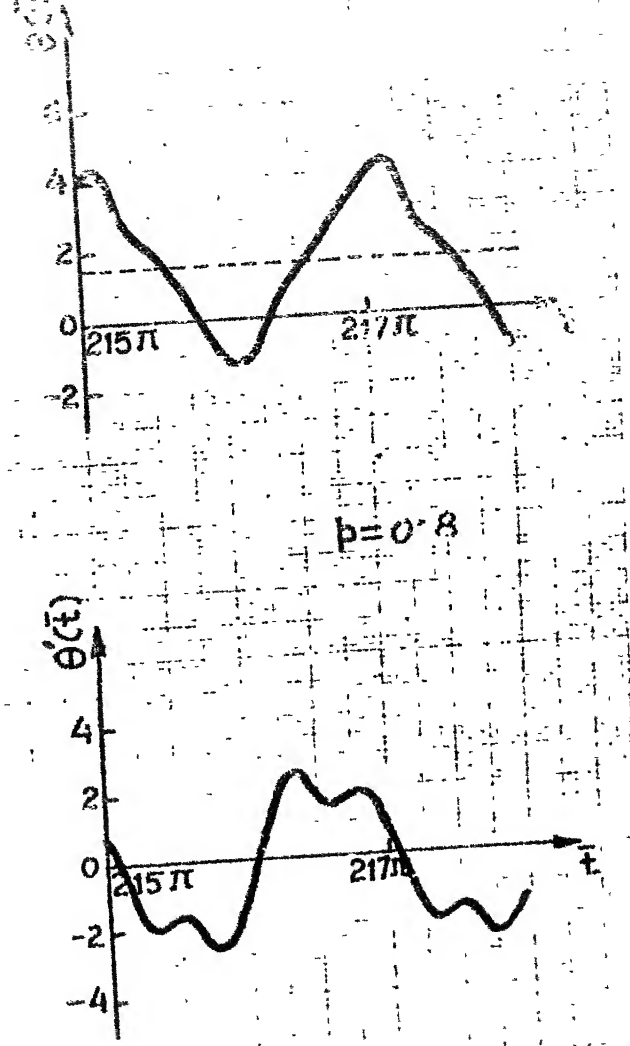

FIG. 3.18 RESPONSE TIME HISTORIES OF θ AND θ' AT DIFFERENT EXCITATION FREQUENCIES : P = 1.0

unstable region and θ oscillates with a period of 2π . (viii) For p greater than 1.20 the pendulum is in the primary region of instability. At $p = 1.20$ and 1.40 the pendulum is found to make continuous rotations with a period 2π , whereas, at $p = 1.80$ it oscillates with a period of 4π . (ix) Finally at $p = 1.90$ the static equilibrium position of the pendulum again becomes stable.

Above are the cases at certain frequencies where $\bar{x}$ and θ oscillate periodically. In between these frequencies there are regions where the integrated responses are non-periodic.

CHAPTER 4

STATISTICAL ANALYSIS OF THE RESPONSE TIME HISTORIES

4.1 INTRODUCTION

In this chapter the nonperiodic responses, obtained by numerical integration, are analysed statistically. Some of these responses were shown in Figs. 3.15 to 3.17. All the relevant standard definitions and formulae used in this chapter are given in appendices A-1 and A-2, respectively. The justification of doing the statistical analysis was given in section 3.5.3.4. It was also mentioned there that the responses for the nonperiodic cases are dependent on the initial conditions and the step sizes of integration. It is assumed now that with other parameters remaining same, the integrated response record, for each combination of the step size and the initial conditions, is a sample record from the same random process. Thus by changing these two parameters different sample records are obtained.

It is further assumed that these sample records are the realizations of a weakly ergodic random process. In other words the sample records are considered to be stationary. The assumption of ergodicity renders the facility of taking time averages over a specific sample record instead of ensemble averages.

First the sample records are tested for the hypothesis of stationarity. This test is done through the run tests on the mean squared values calculated over different intervals from the same sample record. Once this hypothesis is established satisfactorily, different statistical descriptions like autocorrelation functions and power spectral density functions (PSD) are obtained. The near constancy of these quantities over different records (obtained with different combinations of the step size and the initial conditions) justifies the assumption of treating each response history as a sample record.

The statistical analysis is done for the sample records of $\bar{x}$ and θ'. θ' coordinate is selected instead of θ. This is done in order to avoid confusion as in the nonperiodic cases, the pendulum is found to make some complete revolutions in either direction without any fixed pattern.

The statistical quantities are shown to depend on the parameters P and p. In this work no attempt is made to correlate the statistical quantities with P and p.

4.2 PARAMETER ESTIMATORS FOR THE SAMPLE RECORD

For a stationary sample record $\{u_n\}$, taken at N points, with the time interval between the successive points being h_t, the estimators for the basic descriptive

properties (defined in appendix A-2) are given below:

(i) Mean value estimator ($\hat{\mu}$)

$$\hat{\mu}_u = \frac{1}{N} \sum_{i=1}^{N} u_i \qquad (4.1)$$

For ease of calculations, the data points at this stage are transformed as

$$v_n = u_n - \hat{\mu}_u \; ; \quad n = 1, 2, \ldots, N \qquad (4.2)$$

The following estimators are given for the transformed record $\{v_n\}$.

(ii) Variance estimator ($\hat{\sigma}_v^2$)

$$\hat{\sigma}_v^2 = \frac{1}{N-1} \sum_{i=1}^{N} v_i^2 \qquad (4.3)$$

Equation (4.3) gives the unbiased estimator for σ_v^2 . Since the data are transformed, (4.3) also gives the mean square value.

(iii) Autocorrelation function estimator ($\hat{R}_r$)

$$\hat{R}_r = \frac{1}{N-r} \sum_{i=1}^{N-r} v_n \, v_{n+r} \; ; \quad r = 0,1,2,\ldots,s, \qquad (4.4)$$

where s is the maximum lag number. $\hat{R}_r$ is the unbiased estimate of the autocorrelation function at lag r.

The normalized autocorrelation function $\bar{R}_r$ is obtained by dividing $\hat{R}_r$ by $\hat{R}_o$, i.e.,

$$\bar{R}_r = \frac{\hat{R}_r}{\hat{R}_o} \quad ; \quad r = 0,1,2, \ldots, s \tag{4.5}$$

The normalized autocorrelation function for $\bar{x}$ and θ' are represented by $\bar{R}_{\bar{x}}$ and $\bar{R}_{\theta}$, respectively (dropping the subscript r). Variations of these normalised autocorrelation functions with the lag number, r, are shown in the autocorrelograms.

(iv) Power spectral density function estimator ($\hat{G}_k$)

PSD estimator is obtained via the normalized autocorrelation function estimate in two steps. First the raw estimate $\tilde{G}_k$ is obtained as

$$\tilde{G}_k = \tilde{G}_v(f) = 2 h_t \left[1 + 2 \sum_{r=1}^{s-1} \bar{R}_r \cos\left(\frac{\pi r k}{s}\right) + \bar{R}_s \cos k\pi \right] , \tag{4.6}$$

where $\tilde{G}_k$ is calculated at $m + 1$ discrete frequencies

$$f = \frac{k f_c}{s} \quad ; \quad k = 0,1,2, \ldots, s \tag{4.7}$$

with f_c as the cutoff frequency (Nyquist frequency) given by

$$f_c = \frac{1}{2 h_t} \tag{4.8}$$

The smoothened PSD, $\hat{G}_k$, is then calculated as [46]

$$\hat{G}_o = 0.54\ \tilde{G}_o + 0.46\ \tilde{G}_1$$

$$\hat{G}_k = 0.23\ \tilde{G}_{k-1} + 0.54\ \tilde{G}_k + 0.23\ \tilde{G}_{k+1} \quad ; \quad k = 1,2,\ldots,s-1$$

$$\hat{G}_s = 0.46\ \tilde{G}_{s-1} + 0.54\ \tilde{G}_s \qquad (4.9)$$

Dropping the subscript k, the smoothened PSD's for $\bar{x}$ and θ' are represented by $\hat{G}_{\bar{x}}$ and $\hat{G}_{\theta'}$, respectively.

4.3 TEST FOR STATIONARITY [48]

The concept of stationarity, defined in appendix A-1, relates to the ensemble averaged properties of a random process. However, in this chapter the individual sample record, assumed to be from an ergodic process, is referred to as being stationary. By this it is meant that, except for the variations due to normal statistical sampling, the properties computed over short time intervals do not vary significantly from one interval to the next. We assume that the time trends in the mean square value will reveal the nonstationarity of the sample record. Moreover, the sample record is considered to be long compared to that demanded by the lowest frequency component in the data. It is further assumed that the sample records from a nonstationary process will also be nonstationary. With these assumptions the stationarity of the random process is tested by considering a single record and therefrom computing the variances over short time intervals and performing the run test given in appendix A-3.

4.4 RESULTS AND DISCUSSIONS

All the results presented in this section are for the following values of the parameters: $R = 0.2$, $\zeta_1 = 0.02$, $\zeta_2 = 0.05$, $q_2 = 0$ and $q = q_1 = 0.5$. The parameters varied are P and p. Since the nonperiodic responses depend on the initial conditions and the step size of integration, two more parameters are taken into consideration, namely, initial condition of θ, i.e., $\theta(0)$ and the step size of integration h. The initial conditions for other coordinates are taken as zero.

The data points are taken at interval $h_t = \frac{\pi}{10}$. A further decrease in the interval size does not change the results. Moreover, the cutoff frequency, f_c, with $h_t = \frac{\pi}{10}$ is $\frac{5}{\pi}$ (Eqn. 4.8) which is quite large as compared to the highest frequency components of the sample records as shown later. If N data points are taken the total record length is $\frac{N\pi}{10}$.

4.4.1 Mean Values and Variances

Mean values of $\bar{x}$ and θ', for all the sample records considered, are found to be almost zero. The following results are for the transformed data. The variances are calculated with different numbers of data points (i.e., different record lengths) by using (4.9). Tables 4.1 (a) and 4.1 (b) show the variances of $\bar{x}$ and θ', $\hat{\sigma}^2_{\bar{x}}$ and $\hat{\sigma}^2_{\theta'}$,

TABLE 4.1 (a)

Variances with Different Number of Data Points

$P = 0.1$, $p = 1.0$, $\theta(0) = 0.05$, $h = \frac{\pi}{40}$

Numbe of data points N	Record length	Variances	
		$\hat{\sigma}_{\bar{x}}^2$	$\hat{\sigma}_{\theta'}^2$
200	20π	0.077	0.19
400	40π	0.064	0.33
600	60π	0.065	0.31
800	80π	0.084	0.34
1000	100π	0.079	0.35
1200	120π	0.078	0.34
1600	160π	0.079	0.35
2000	200π	0.079	0.36
3000	300π	0.076	0.35
4000	400π	0.074	0.33
8000	800π	0.077	0.34

TABLE 4.1 (b)

Variances with Different Number of Data Points

$P = 0.05, \quad p = 1.05 \quad \theta(0) = 0.05, \quad h = \frac{\pi}{40}$

Number of data points N	Record length	Variances	
		$\hat{\sigma}^2_{\bar{x}}$	$\hat{\sigma}^2_{\theta'}$
200	20 π	0.092	0.29
400	40 π	0.067	0.21
600	60 π	0.065	0.21
800	80 π	0.056	0.18
1000	100 π	0.053	0.20
1200	120 π	0.050	0.20
1600	160 π	0.048	0.19
2000	200 π	0.054	0.19
3000	300 π	0.056	0.20
4000	400 π	0.053	0.20
8000	800 π	0.055	0.20

respectively, for two cases with increasing value of N. It can be seen that the variances do not change significantly for N > 1000.

4.4.2 Run Tests for Checking Stationarity

Following the procedure outlined in appendix A-3, each sample record is divided into 20 equal time intervals with each interval having 200 data points (i.e., time interval = 20π). For each interval the variances are calculated and then these are aligned in time sequence to perform the run test.

Figure 4.1 shows the values of the variances versus the interval number for two combinations of parameters. In each case the median value is shown by the dotted horizontal line. With respect to this median value, the number of runs, r_n , is counted. It is seen that r_n lies between 6 to 15. Thus, from the table in appendix A-4, the hypothesis of stationarity of the sample record is found to be acceptable with 0.05 level of significance.

Similar run tests are performed for other combinations of parameters. Some of these values are given in Table 4.2, where only the median values and the number of runs are indicated. Table 4.3 shows similar results with longer time intervals, each interval now having 1000 data points (i.e., time interval = 100 π). This interval size

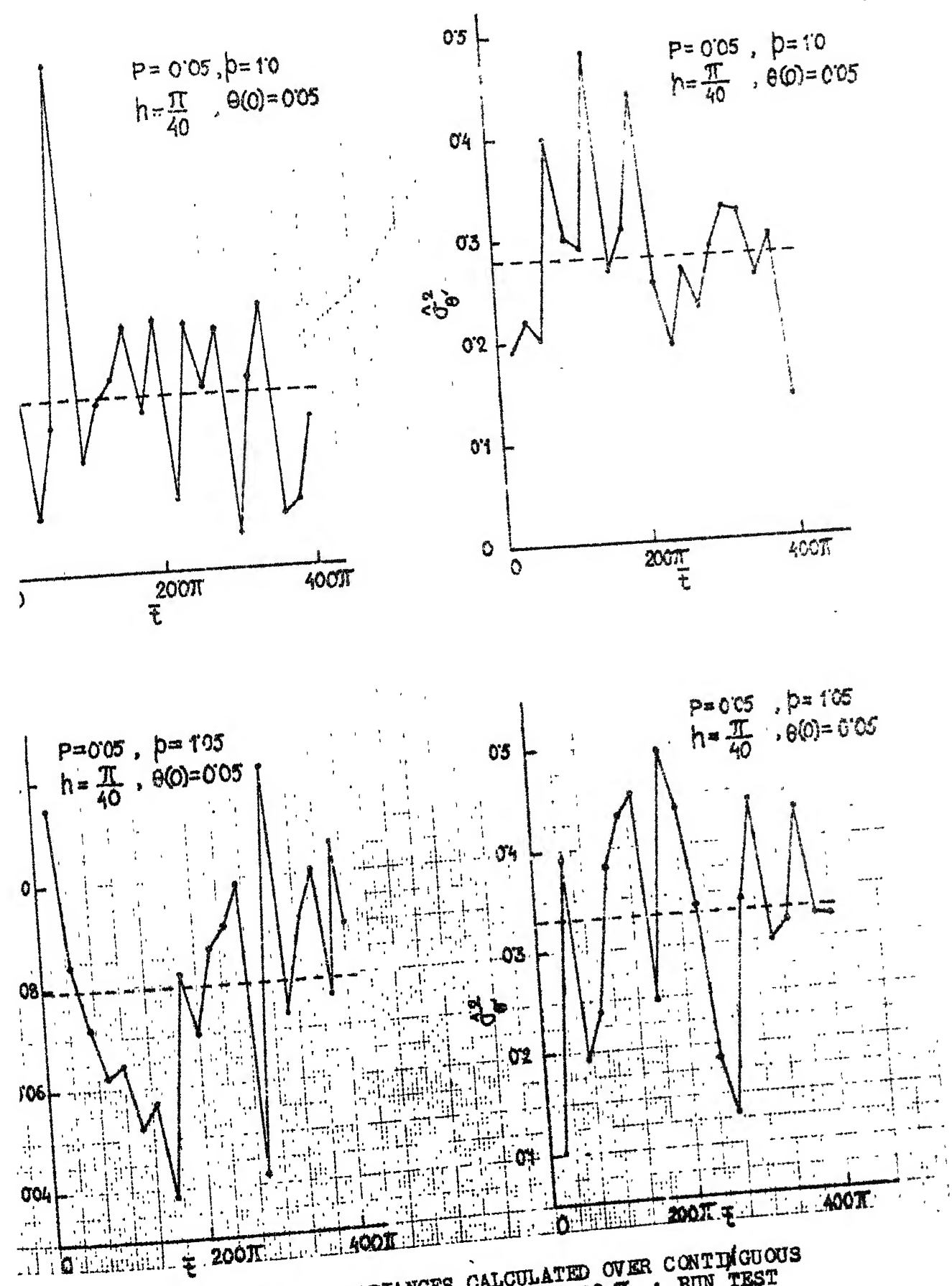

FIG. 4.1 VARIANCES CALCULATED OVER CONTIGUOUS TIME INCREMENTS OF 20 π : RUN TEST

TABLE 4.2

Median Values of Variances and Number of Runs

Number of intervals = 20

Number of data points in each interval = 200

Sl. No.	P	p	θ(0)	h	Median Values of $\hat{\sigma}^2_{\bar{x}}$	Median Values of $\hat{\sigma}^2_{\theta'}$	Number of runs of $\hat{\sigma}^2_{\bar{x}}$	Number of runs of $\hat{\sigma}^2_{\theta'}$
1	0.05	1.0	0.05	$\frac{\pi}{40}$	0.074	0.28	12	9
2	0.05	1.0	0.05	$\frac{\pi}{80}$	0.0825	0.30	7	12
3	0.05	1.0	0.10	$\frac{\pi}{40}$	0.079	0.33	11	11
4	0.05	1.05	0.05	$\frac{\pi}{40}$	0.045	0.165	11	11
5	0.07	1.0	0.05	$\frac{\pi}{40}$	0.0959	0.402	11	10
6	0.07	1.05	0.05	$\frac{\pi}{40}$	0.071	0.223	11	7
7	0.07	1.08	0.05	$\frac{\pi}{40}$	0.063	0.21	12	11

TABLE 4.3

Median Values of Variances and Number of Runs

Number of intervals = 20

Number of data points in each interval = 1000

$h = \frac{\pi}{40}$ for all cases

Sl. No.	P	p	θ(0)	Median values of $\hat{\sigma}^2_{\bar{x}}$	Median values of $\hat{\sigma}^2_{\theta}$	Number of runs of $\hat{\sigma}^2_{\bar{x}}$	Number of runs of $\hat{\sigma}^2_{\theta}$
1	0.05	1.0	0.05	0.076	0.359	14	12
2	0.05	1.0	0.10	0.075	0.342	12	10
3	0.05	1.05	0.05	0.055	0.205	13	11
4	0.07	1.0	0.05	0.095	0.45	13	10
5	0.07	1.05	0.05	0.0817	0.375	11	9
6	0.07	1.08	0.05	0.062	0.228	15	17

is tested because it was seen in Table 4.1 that the variances do not change much for $N > 1000$. It is obvious from these two tables that only in the last case of Table 4.3, the number of runs for $\hat{\sigma}^2_{\theta}$, barely exceeds 15. Several other sample records were also tested. For all the cases, except the one mentioned above, the hypothesis of stationarity of the sample records is found to be acceptable with 0.05 level of significance. Thus with the hypothesis of stationarity having been established, further statistical analysis is undertaken in the following sections.

4.4.3 Autocorrelation Functions and Power Spectral Density Functions

Normalised autocorrelation functions and smoothened power spectral density functions are calculated using (4.5) and (4.9), respectively. With time interval $h_t = \frac{\pi}{10}$ the cutoff frequency

$$f_c = \frac{5}{\pi} \qquad (4.10)$$

From (4.7) the PSD functions are calculated at the following $(s + 1)$ discrete angular frequencies:

$$\bar{\omega}_k = \frac{10\,k}{s} \; ; \quad k = 0,1,2, \ldots, s \qquad (4.11)$$

Figures 4.2 and 4.3 show the typical autocorrelograms for $\bar{x}$ and $\dot{\theta}$, respectively, with $P = 0.05$, $p = 1.0$, $\theta(0) = 0.05$ and $h = \frac{\pi}{40}$. These are obtained by taking

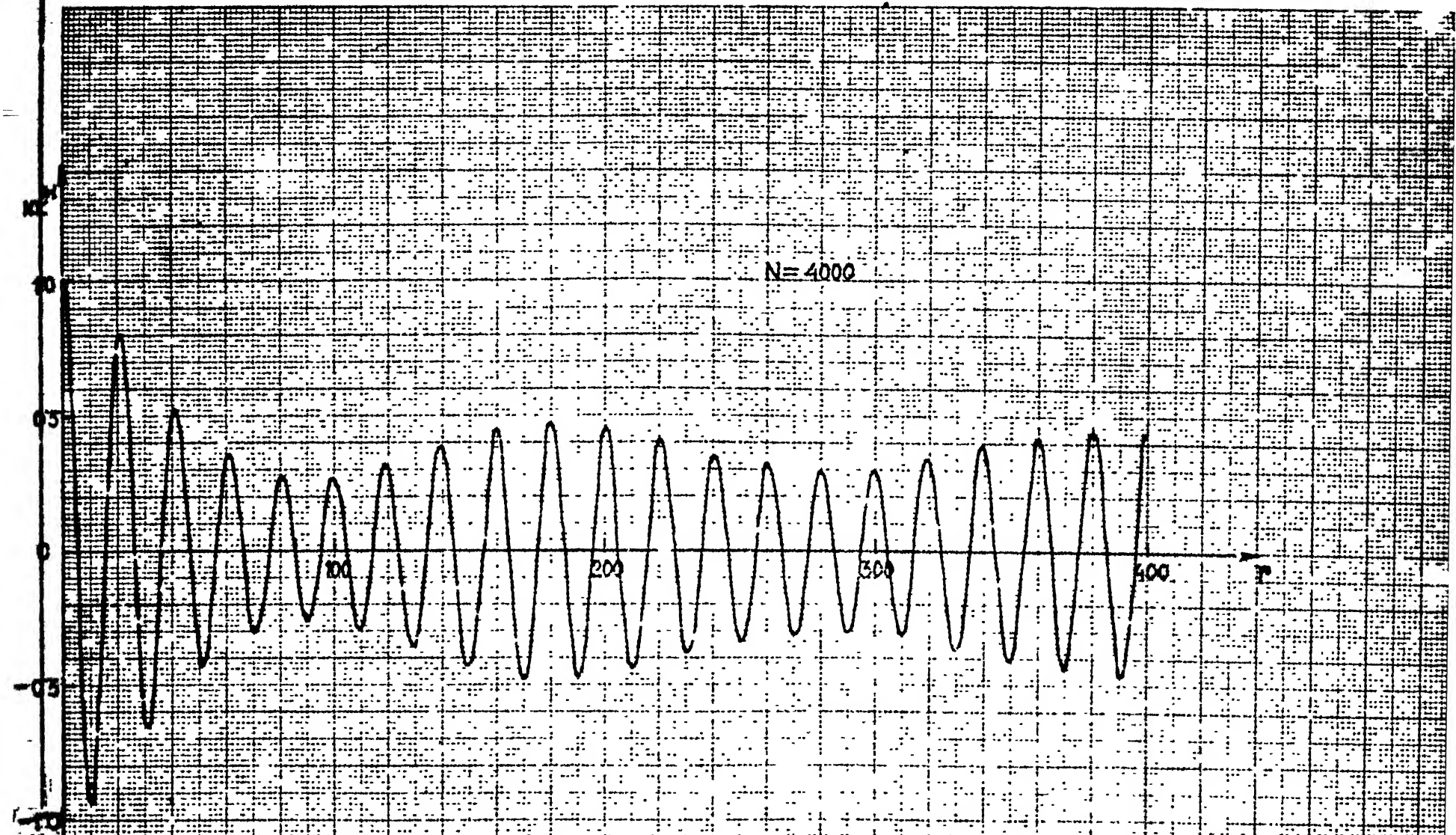

FIG. 4.2 AUTOCORRELATION FUNCTION FOR $\bar{x}$:
P = 0.05, p = 1.0, $\theta(0)$ = 0.05,
h = $\pi/40$

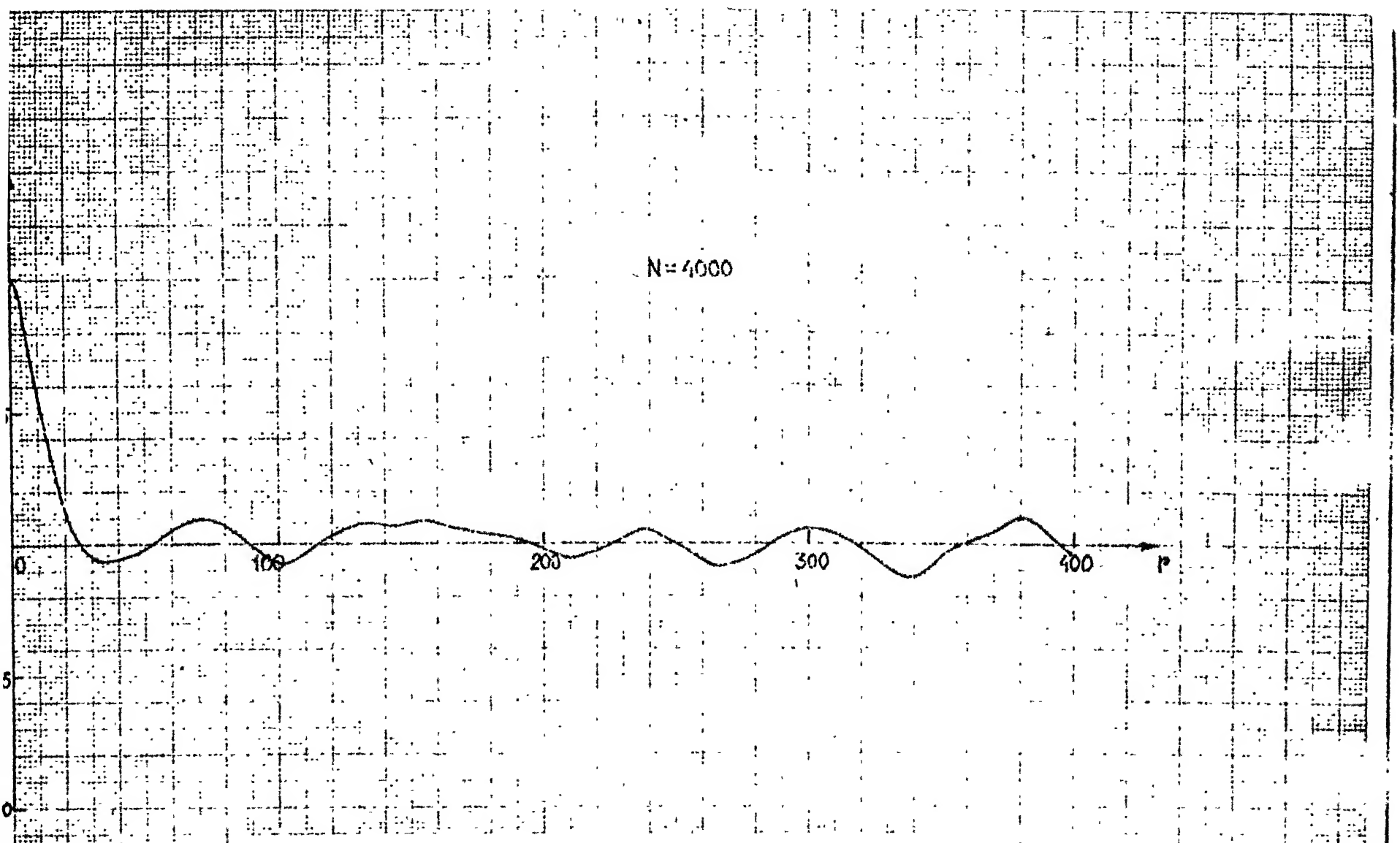

FIG. 4.3 AUTOCORRELATION FUNCTION FOR θ':
P = 0.05; p = 1.0, $\theta(0) = 0.05$,
$h = \pi/40$

4000 data points (i.e.,N = 4000). The maximum lag number, s, is taken to be 10% of N, i.e., s = 400. Almost similar curves are obtained for N = 1000, 2000 and 8000. For the same combination of parameters and with different values of N and s the PSD functions for $\bar{x}$ and θ' are shown in Figs. 4.4 and 4.5. It is seen from these figures that with s = 0.1 N, different values of N (i.e.,different record lengths) give the same trend for PSD's. Some results are also shown with s = 0.2 N and s = 0.05 N. It may be noted that so far as the PSD functions are concerned, sufficiently accurate results are obtained with N = 1000 and s = 100. Further results, unless mentioned otherwise, are obtained with these values of N and s.

For the same values of the parameters used in Figs. 4.2 and 4.3, with the step size only changed to $\frac{\pi}{8C}$, the autocorrelograms for $\bar{x}$ and θ' are shown in Figs. 4.6 and 4.7, respectively. The trends of $\bar{R}_{\bar{x}}$ and $\bar{R}_{\theta}$ in these figures are seen to be similar to those of Figs. 4.2 and 4.3. For the same values of P and p and for five different combinations of $\theta(0)$ and h, $\hat{G}_{\bar{x}}$ and $\hat{G}_{\theta}$, are shown in Figs. 4.8 and 4.9, respectively. It may be concluded from these figures that the different combinations of $\theta(0)$ and h (i.e.,the independent realizations) yield the same trend of PSD's implying that all the realizations are from the same random process.

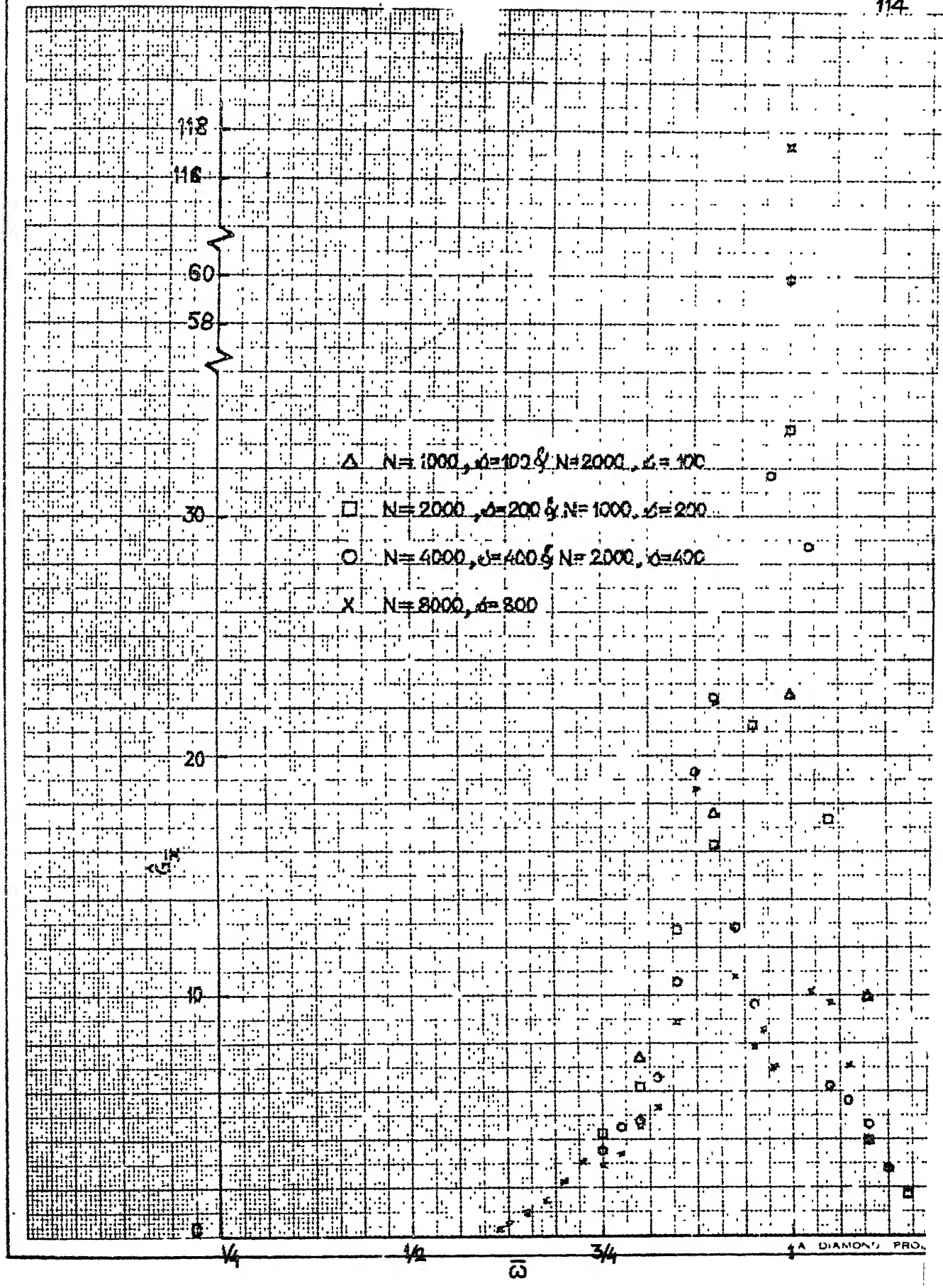

FIG. 4.4 PSD FUNCTION FOR $\bar{x}$ WITH DIFFERENT RECORD LENGTHS : P = 0.05, p = 1.0, $\theta(0) = 0.05$, h = $\pi/40$

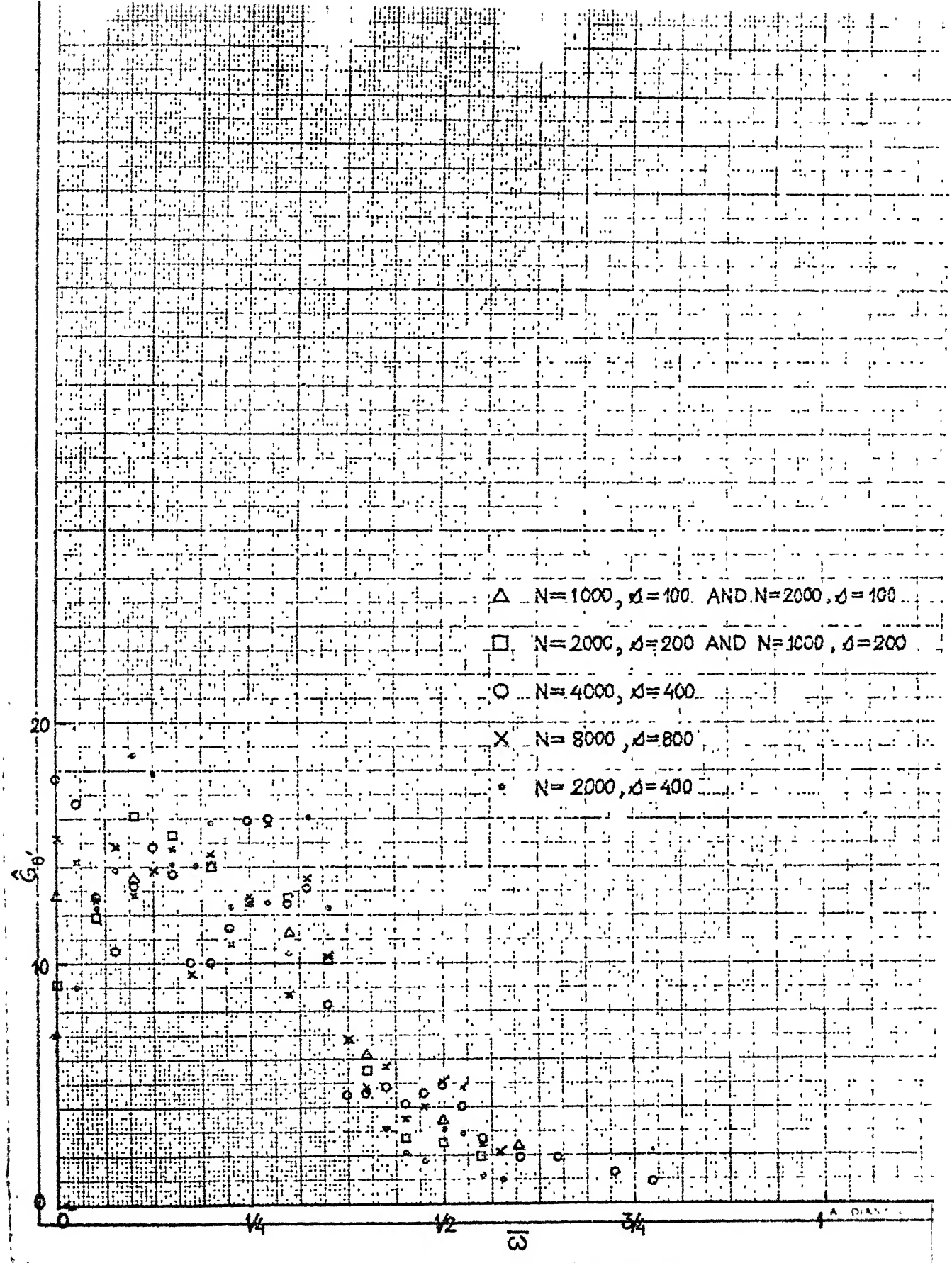

FIG. 4.5 PSD FUNCTION FOR θ' WITH DIFFERENT RECORD LENGTHS : P = 0.05, p = 1.0, $\theta(0) = 0.05$, h = $\pi/40$

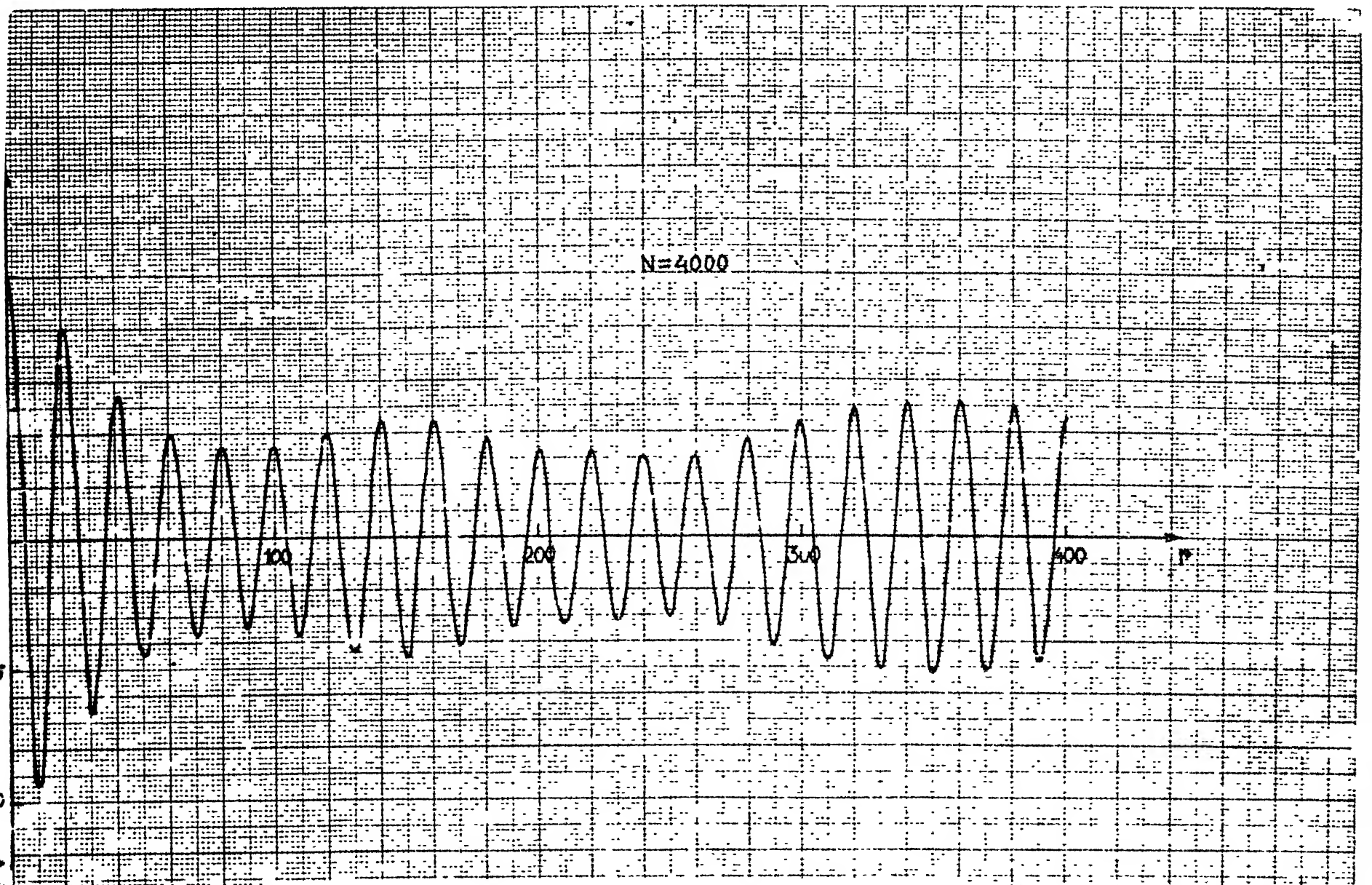

FIG. 4.6 AUTOCORRELATION FUNCTION FOR $\bar{x}$: $P = 0.05$, $p = 1.0$, $\theta(0) = 0.05$, $h = \pi/80$

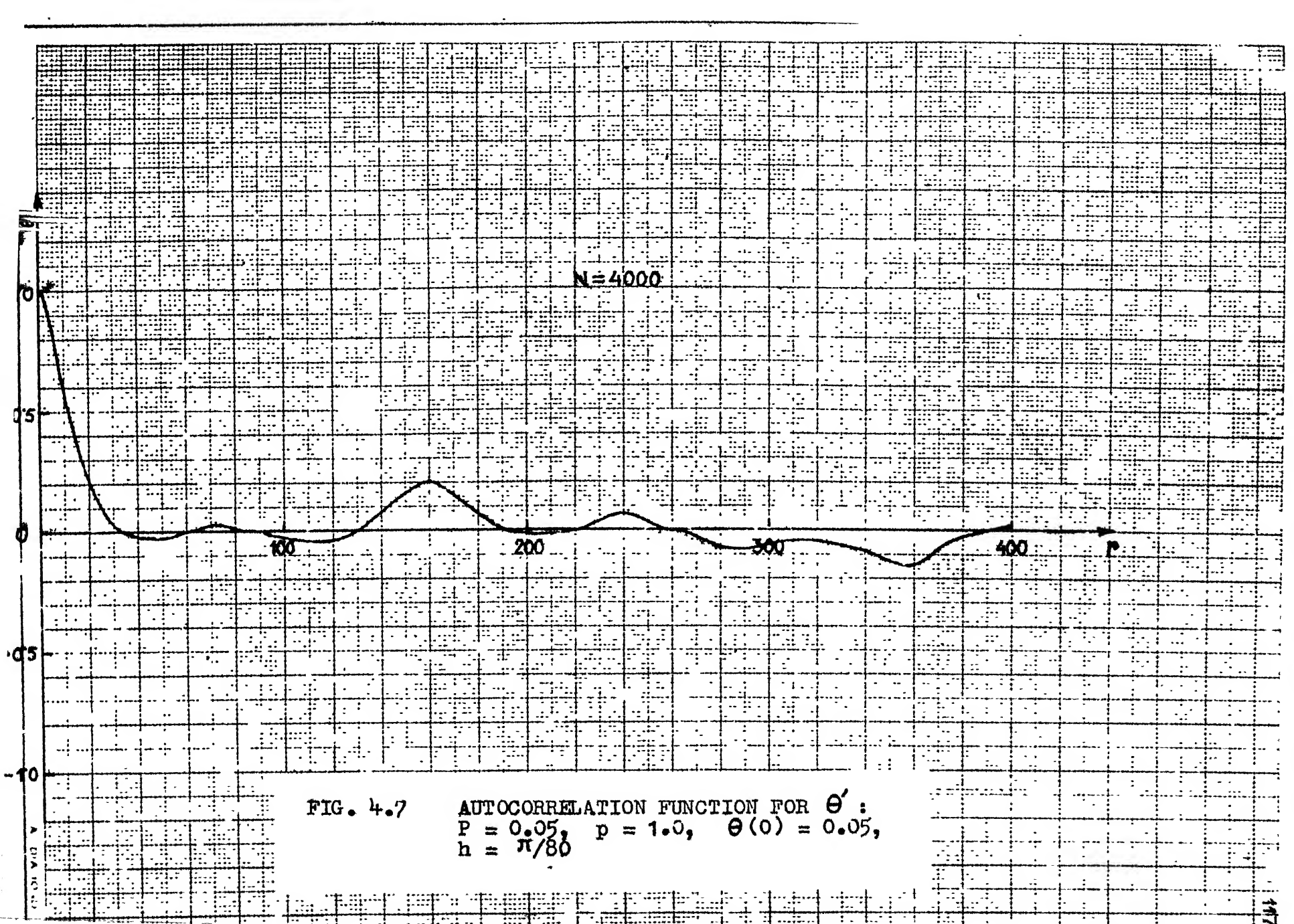

FIG. 4.7 AUTOCORRELATION FUNCTION FOR θ' :
P = 0.05, p = 1.0, $\theta(0)$ = 0.05,
h = $\pi/80$

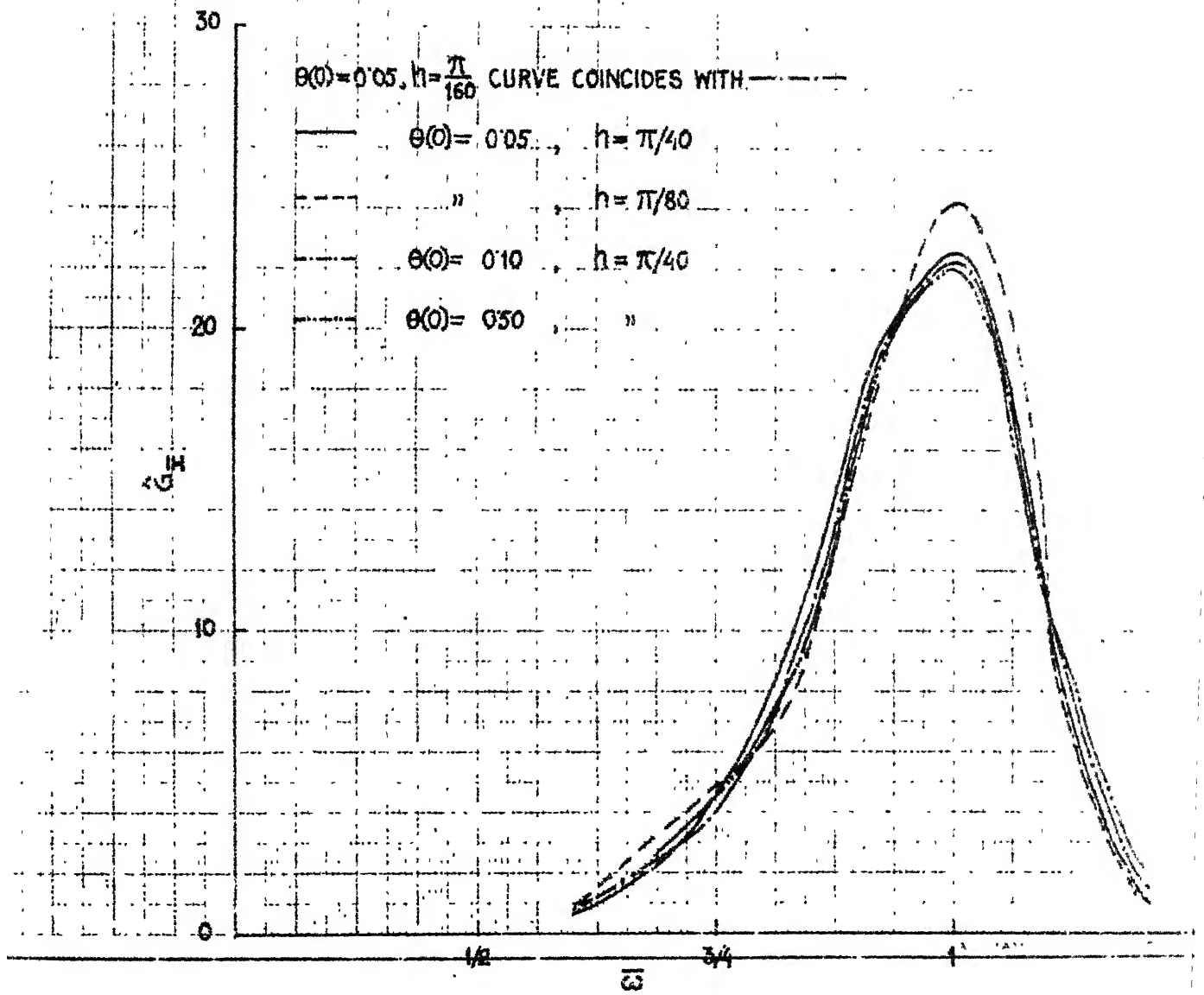

FIG. 4.8 PSD FUNCTION FOR $\bar{x}$ WITH DIFFERENT INITIAL CONDITIONS AND STEP SIZES : P = 0.05, p = 1.0

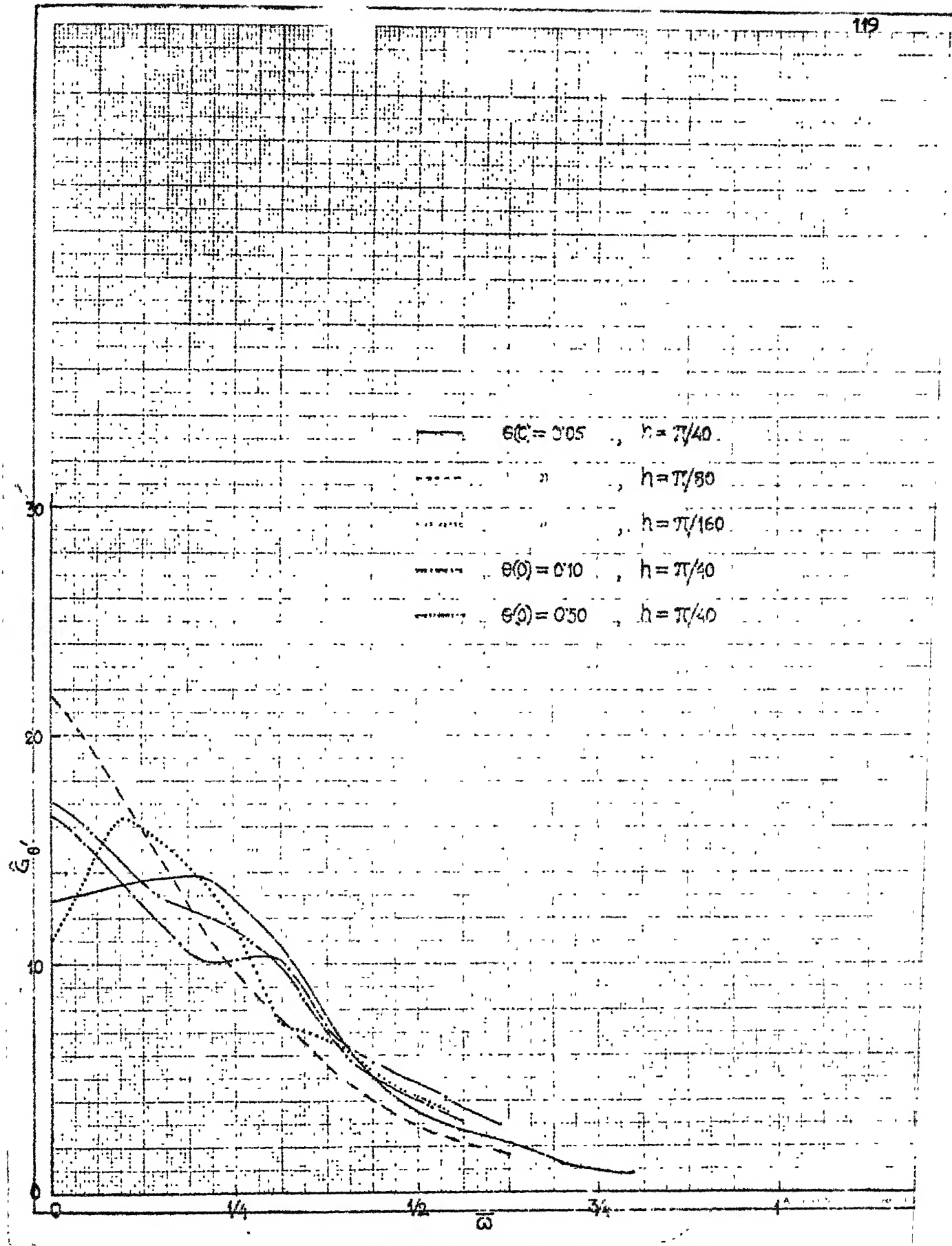

FIG. 4.9 PSD FUNCTION FOR θ' WITH DIFFERENT INITIAL CONDITIONS AND STEP SIZES : P = 0. , p = 1.0

4.4.4 Response Statistics

Now having established that for a given combination of P and p, any value of $\theta(0)$ and a proper value of h yield a correctly representative stationary sample record, some response statistics for different combinations of P and p are discussed below.

(i) P = 0.05, p = 1.0

With this parameter combination the representative point lies near the boundary of regions I and III in Fig. 3.3. It may be recalled that near this point there was a sharp increase in the amplitudes (Figs. 3.4 and 3.5).

Figure 4.3 shows that $\bar{R}_{\theta'}$, almost tends to zero as the lag number, r, increases. This suggests that θ' behaves like a random variable. From the nature of $\bar{R}_{\theta'}$ it may be further observed that the sample record of θ' behaves like that of a wide band random process. On the other hand, Fig. 4.2 shows the presence of a strong periodic trend in the record of $\bar{x}$. However, as $\bar{R}_{\bar{x}}$ falls below 0.5 for $r > 20$, the data can not be considered as deterministic. Rather it can be taken as a random noise superimposed on a periodic signal. The frequency contents of the responses are better seen in Figs. 4.4, 4.5, 4.8 and 4.9.

Figure 4.8 shows a large value of PSD for $\bar{x}$ at the nondimensional angular frequency $\tilde{\omega} = 1.0$ (i.e. at the

forcing frequency). This is further confirmed in Fig. 4.4 where, by increasing the record length, the peak at $\bar{\omega} = 1.0$ increases almost proportionately. The presence of a strongly periodic component in $\bar{x}$ - response at the forcing frequency is also expected because the primary mass is directly driven by the external excitation. The time history records of $\bar{x}$ in Fig. 3.17 also show a predominant periodic component.

Figure 4.9 reveals low frequency contents for θ'- response. No peak is observed at $\bar{\omega} = \frac{1}{2}$. Fig. 4.5 shows that PSD characteristics remain unchanged with increase in record lengths. The corresponding time history was shown in Fig. 3.15.

(ii) $P = 0.05$, $p = 1.05$

For this combination the representative point is in region III (Fig. 3.3) and lies near the boundary of primary instability.

PSD of $\bar{x}$ - response is found to be similar to that of Fig. 4.8 and is not shown. Autocorrelogram of θ' - response is shown in Fig. 4.10. It is seen that the data now have a periodic trend. PSD of θ' - response (Fig. 4.11), besides having a low frequency content, also has a peak at $\bar{\omega} = \frac{1}{2}$. By increasing the record lengths this peak is seen to increase almost proportionately, whereas, the low frequency contents remain almost same. Thus, the sample record of θ'

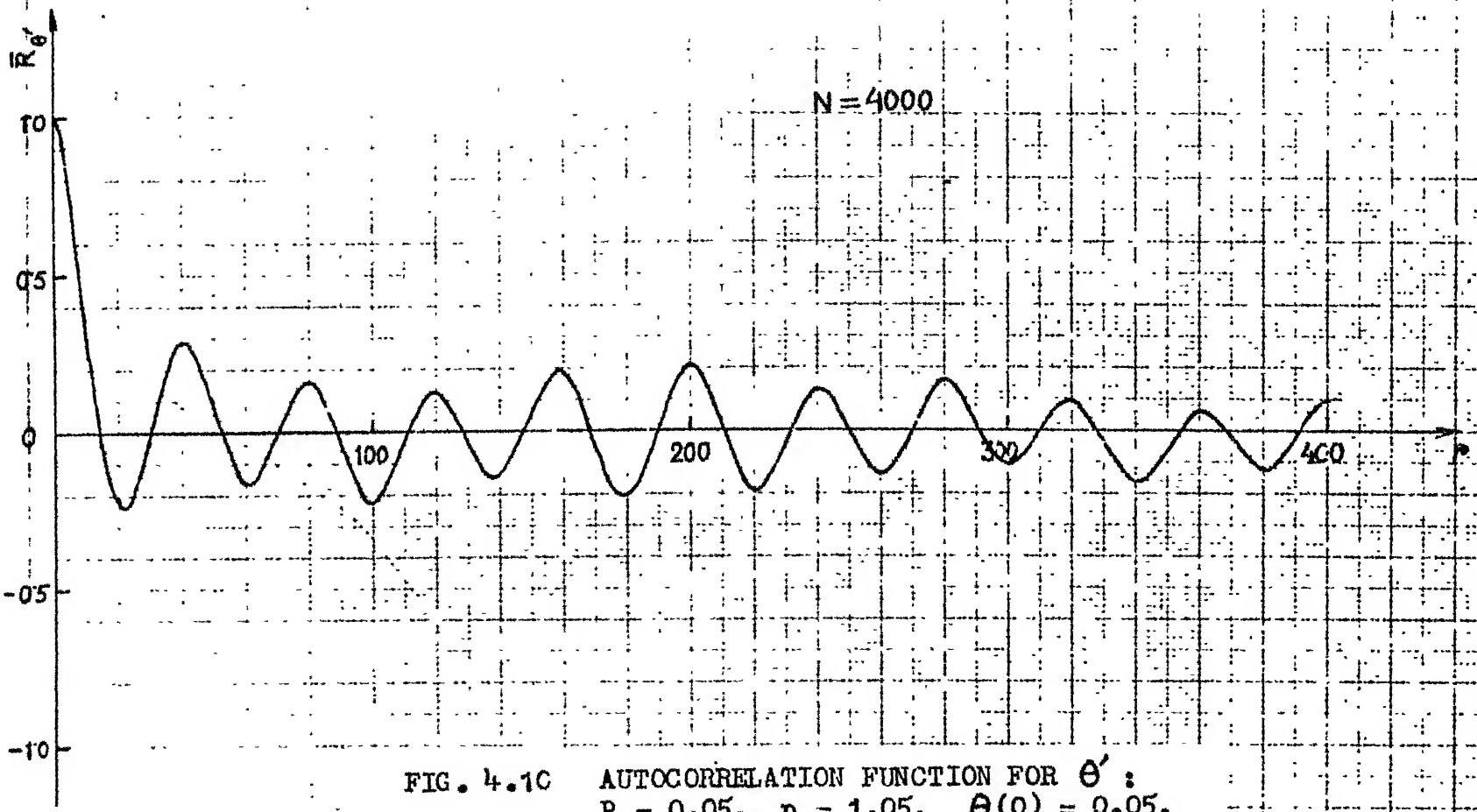

FIG. 4.1C AUTOCORRELATION FUNCTION FOR θ' :
P = 0.05, p = 1.05, $\theta(0) = 0.05$,
h = $\pi/40$

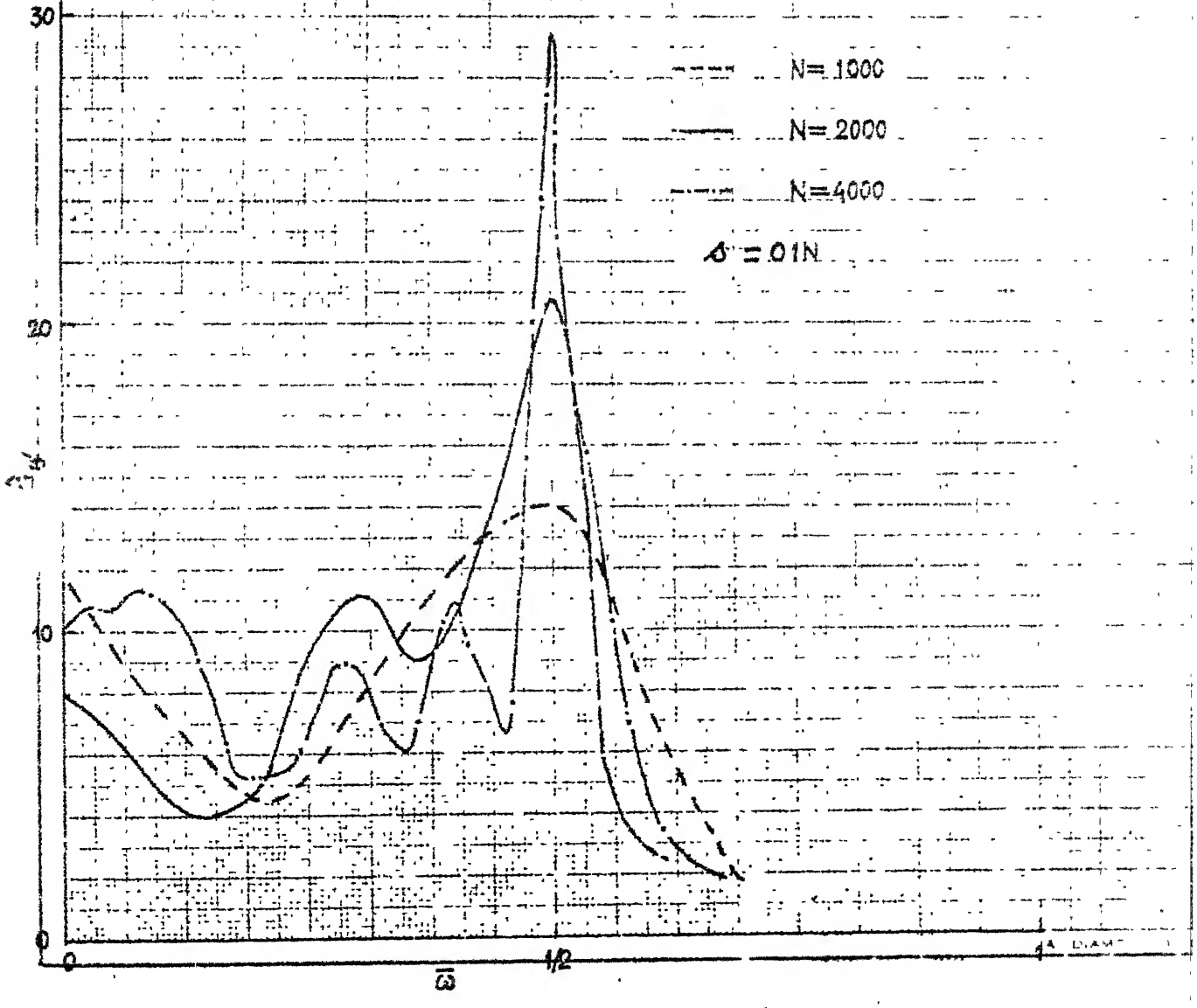

FIG. 4.11 PSD FUNCTION FOR θ' WITH DIFFERENT RECORD LENGTHS : P = 0.05, p = 1.05, $\theta(0)$ = 0.05, h = $\pi/40$

has a periodic component at $\bar{\omega} = \frac{1}{2}$. The corresponding time history was shown in Fig. 3.16 which looks regular compared to that in Fig. 3.15.

(iii) $P = 0.07$, $p = 1.0$, 1.05 and 1.08

For $p = 1.0$ and 1.5 the representative point is well inside the region III in Fig. 3.3. At $p = 1.08$ the point is close to the boundary of primary unstable region.

In each case the sample record is obtained with $h = \frac{\pi}{40}$ and $\theta(0) = 0.05$. PSD's for $\bar{x}$ and θ' are shown in Figs. 4.12 and 4.13, respectively. As in the previous cases, PSD for $\bar{x}$ shows a peak at $\bar{\omega} = 1$. For $p = 1.0$ and 1.05, PSD of θ' has only low frequency contents without any predominant peak. As p is increased to 1.08, a peak is observed at $\bar{\omega} = \frac{1}{2}$.

For all cases discussed in this section, the median values of the variances are given in Table 4.3. For non-periodic responses, the variances together with the PSD's should be used to describe the response statistics.

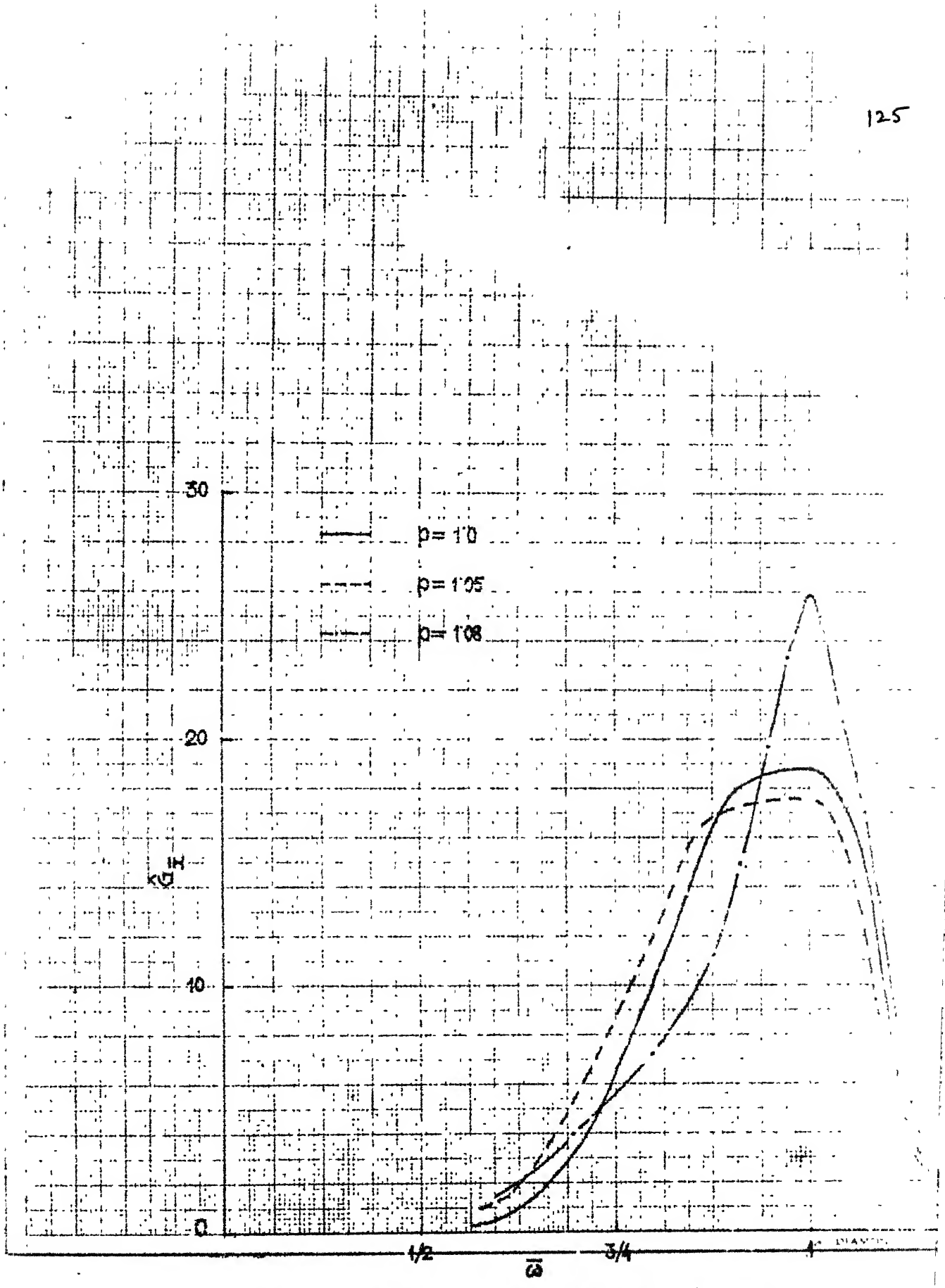

FIG. 4.12 PSD FUNCTION FOR $\bar{x}$ AT DIFFERENT EXCITATION FREQUENCIES ; P = 0.07, $\Theta(0) = 0.05$, $h = \pi/40$

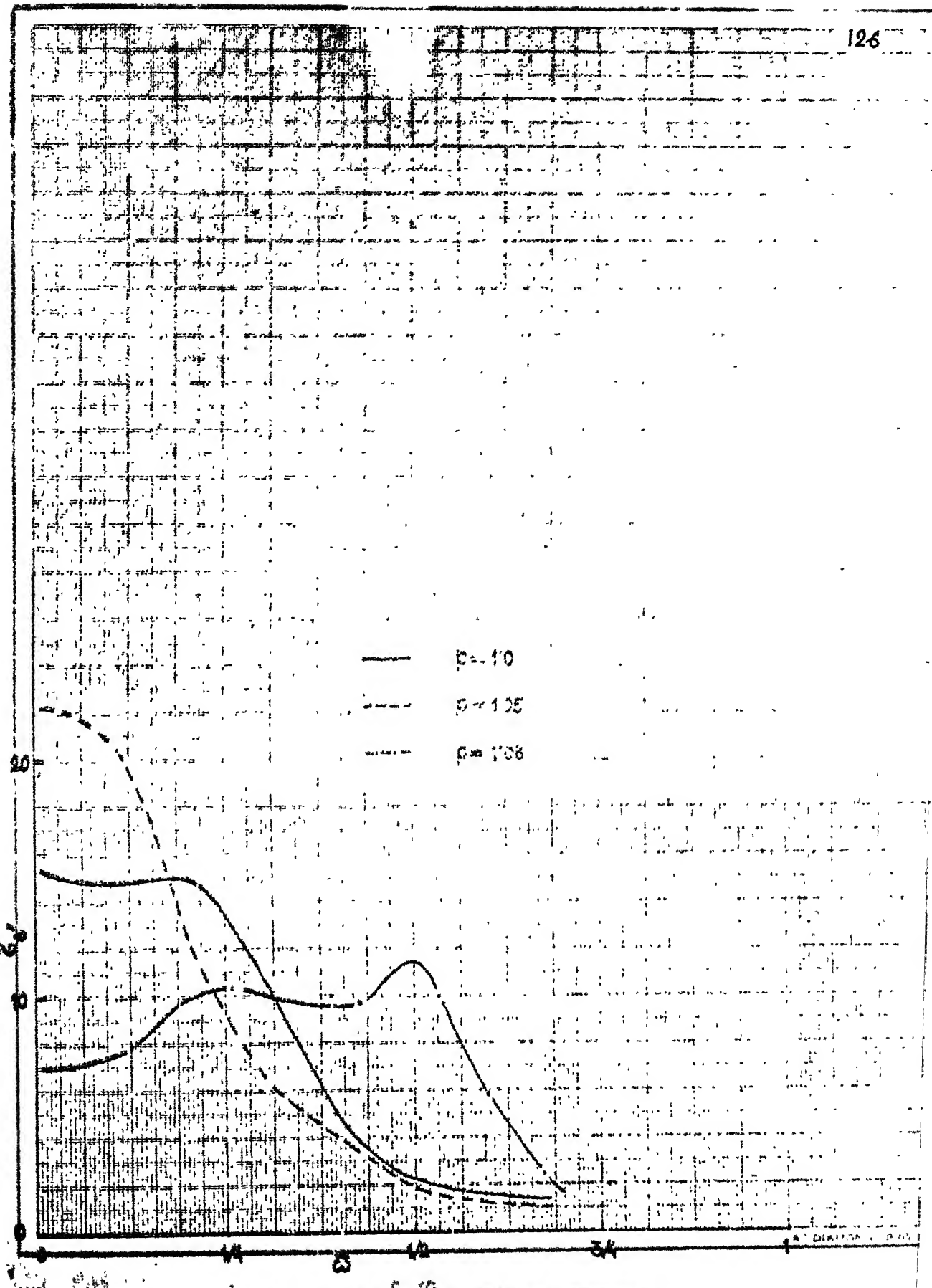

FIG. 4.13 PSD FUNCTION FOR θ' AT DIFFERENT EXCITATION FREQUENCIES : P = 0.07, $\theta(0) = 0.05$, $h = \pi/40$

CHAPTER 5

EXPERIMENTAL INVESTIGATION OF NONPERIODIC RESPONSES

5.1 INTRODUCTION

In this chapter some experimental studies are presented for a harmonically excited two degree-of-freedom autoparametric system. The system, considered in this chapter, is similar to the ones studied in the previous chapters except that the system now is base-excited instead of being force-excited. Though the equations of motion for these two systems are slightly different, the basic characteristics remain same.

It is seen in chapter 3 that for certain combinations of parameters the numerical integrations yield nonperiodic results. In such cases the nonconverging results are later analysed in chapter 4, based on the stipulation that these still represent some physical phenomena where the corresponding physical experiments will also yield nonreproducible results. In this chapter some experimental investigations are undertaken to justify the above mentioned hypothesis qualitatively. The parameters in the experiment are adjusted so as to cause instability of the harmonic steady state motion giving rise to random responses. The statistical analysis of the experimental results is not undertaken.

5.2 MATHEMATICAL MODEL AND EQUATIONS OF MOTION

The mathematical model of the experimental system is shown in Fig. 5.1. The primary mass, M, is connected to the base with a linear spring of stiffness k_1 and a viscous dashpot with damping constant c_1. A compound pendulum of mass m is hinged to the primary mass. The effective length of the pendulum is l and its moment of inertia about the centroidal axis is I. The pendulum rotation is assumed to be damped by a viscous torque for which the damping constant is c_2. The base displacement is represented by y - coordinate and the absolute displacement of the primary mass is shown by x; θ is the angular displacement of the pendulum.

The equations of motion of the system are

$$(M + m)\ddot{x} + c_1(\dot{x} - \dot{y}) + \kappa_1(x - y) - ml(\ddot{\theta}\sin\theta + \dot{\theta}^2\cos\theta) = 0 \qquad (5.1)$$

and

$$(ml^2 + I)\ddot{\theta} + c_2\dot{\theta} + ml(g - \ddot{x})\sin\theta = 0 \qquad (5.2)$$

The base is given a harmonic excitation

$$y = Y\cos\omega t, \qquad (5.3)$$

where Y is the amplitude and ω is the angular frequency of excitation. Using (5.3), (5.1) and (5.2) can be written as

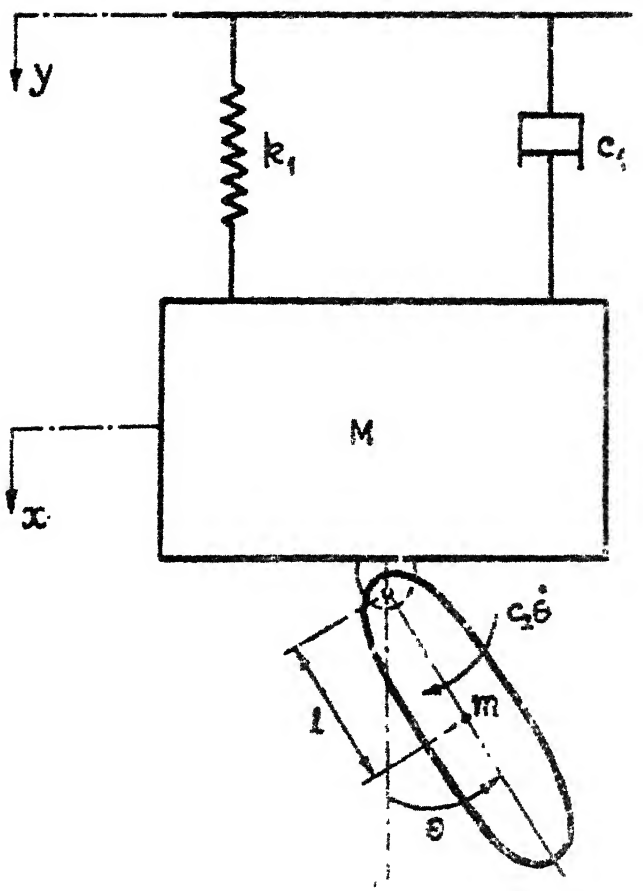

FIG. 5.1 MATHEMATICAL MODEL OF THE EXPERIMENTAL SYSTEM

$$\ddot{x} + 2\,\bar{\zeta}_1\,\omega_1\,\dot{x} + \omega_1^2\,x - \frac{Rl}{1+R}\left(\ddot{\theta}\sin\theta + \dot{\theta}^2\cos\theta\right) = Y\sqrt{\omega_1^4 + (2\,\zeta_1\,\omega_1\,\omega)^2}\,\cos\left[\omega t + \tan^{-1}\left(\frac{2\,\bar{\zeta}_1\,\omega}{\omega_1}\right)\right] \tag{5.4}$$

and

$$\ddot{\theta} + 2\,\zeta_2\,\omega_2\,\dot{\theta} + \left(\omega_2^2 - I_f\,\frac{\ddot{x}}{l}\right)\sin\theta = 0\,, \tag{5.5}$$

respectively, where

$$\left.\begin{aligned}
\omega_1 &= \sqrt{\frac{k_1}{M+m}} \text{ is the natural frequency of the locked mass system,}\\
I_f &= \frac{ml^2}{ml^2 + I} \text{ is the inertia factor,}\\
\omega_2 &= \sqrt{I_f\left(\frac{g}{l}\right)} \text{ is the natural frequency of the compound pendulum,}\\
R &= \frac{m}{M} \text{ is the mass ratio,}\\
\bar{\zeta}_1 &= \frac{c_1}{2\,\omega_1\,(M+m)} \text{ is the damping ratio of the locked mass system}\\
\text{and } \zeta_2 &= \frac{c_2}{2\,\omega_2\,(ml^2 + I)} \text{ is the damping ratio of the compound pendulum.}
\end{aligned}\right\} \tag{5.6}$$

In nondimensional form (5.4) and (5.5) are written as

$$\bar{p}^2\,\hat{x}'' + 2\,\bar{\zeta}_1\,\bar{p}\,\hat{x}' + \hat{x} - \bar{p}^2\,\frac{I_f\,R}{1+R}\left(\theta''\sin\theta + \theta'^2\cos\theta\right) = \bar{Y}\sqrt{1 + (2\,\bar{\zeta}_1\,\bar{p})^2}\,\cos\bar{t} \tag{5.7}$$

and $$\bar{p}^2\,\theta'' + 2\,\zeta_2\,\bar{p}\,q\,\theta' + (q^2 - \bar{p}^2\,\hat{x}'')\sin\theta = 0, \qquad (5.8)$$

respectively, where

$$\bar{p} = \frac{\omega}{\omega_1}, \quad \bar{t} = \omega t + \tan^{-1}(2\,\bar{\zeta}_1\,\bar{p}),$$
$$\hat{x} = I_f\left(\frac{X}{l}\right), \quad \bar{Y} = I_f\left(\frac{Y}{l}\right), \quad q = \frac{\omega_2}{\omega_1} \qquad (5.9)$$

and the prime denotes differentiation with respect to the nondimensional time $\bar{t}$.

Equations (5.7) and (5.8) are same as (2.42) and (2.43) except that the forcing function in (5.7) depends on the frequency and damping as well. For low damping and for forcing frequency near the natural frequency of the locked mass, i.e. $\bar{p} \approx 1$, the quantity under the square root sign on the right hand side of (5.7) is almost unity. Therefore, for these parameter combinations (i.e. $\bar{\zeta}_1 << 1$ and $\bar{p} \approx 1$) the systems, shown in Figs. 2.1 and 5.1, have similar characteristics. Equations (5.7) and (5.8) can be solved approximately by the method outlined in chapter 2.

5.3 DESIGN OF THE EXPERIMENT

5.3.1 Experimental Model

The photograph of the experimental model is shown in Fig. 5.2. Fig. 5.3 shows the sectional views of the model. In this figure (a) is the primary mass, M, supported on the

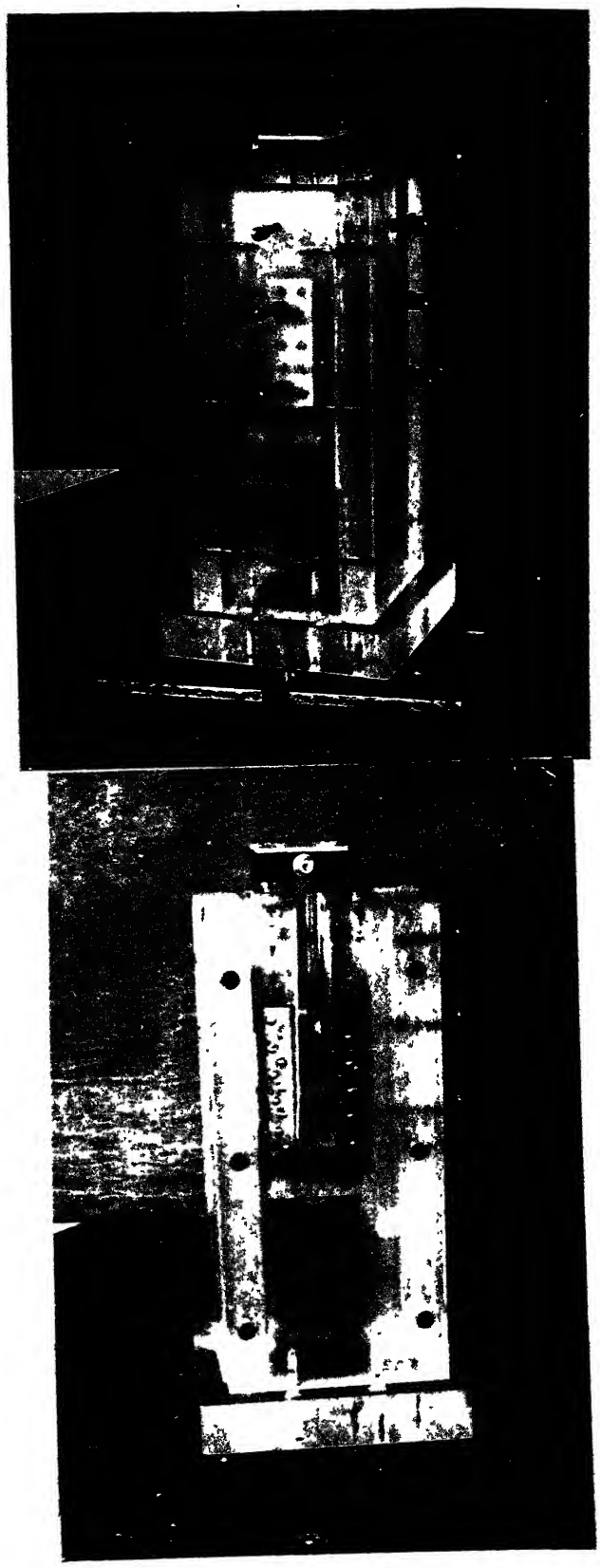

FIG. 5.2 PHOTOGRAPHS OF THE EXPERIMENTAL MODEL

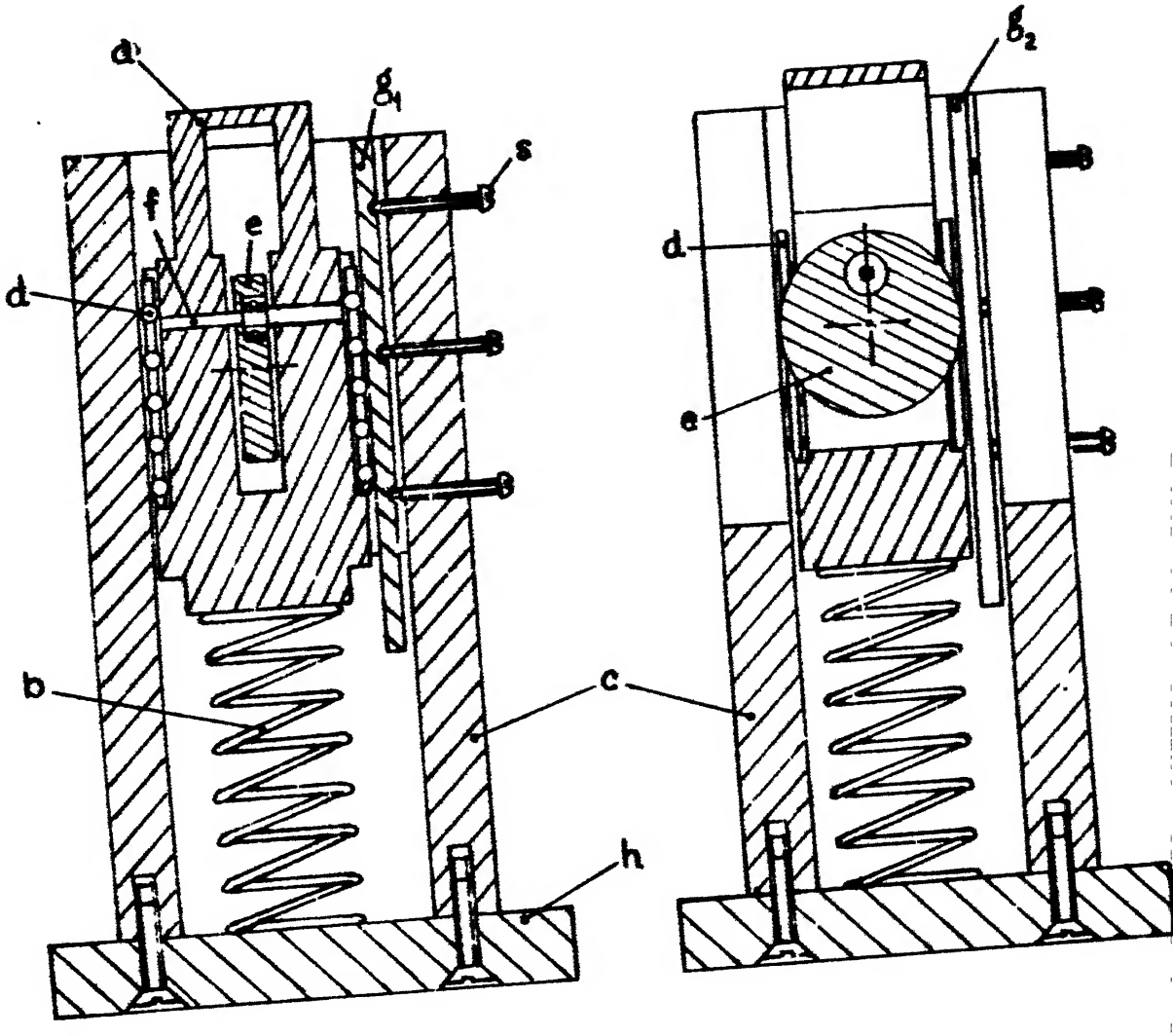

FIG. 5.3 SECTIONAL VIEWS OF THE EXPERIMENTAL MODEL

linear spring (b) of stiffness k_1, One end of the spring is fixed to the primary mass and the other end to the base (h). Fixed to the base is the outside guide block (c). The primary mass oscillates freely within this block on strip ball bearings (d). The strip bearings are free to travel vertically alongside the primary mass and are retained in the grooves as shown in the figure. On two adjacent faces of the primary mass, the strip bearings are pressed from sides by adjusting plates (g_1) & (g_2). The pressure on the bearings can be controlled by moving these plates by the adjusting screws (s). These screws are set with an optimum pressure, obtained by trial and error, to ensure free movement of the primary mass. The compound pendulum (e) is hinged to the shaft (f) which in turn is fixed to the primary mass. The compound pendulum is made of an eccentrically hinged disk. The effective length of the pendulum is

$$l = \frac{D^2}{D^2 - d^2} e \quad , \tag{5.10}$$

where D is the diameter of the disk, d is the hole diameter and e is the eccentricity.

5.3.2 Experimental Set-up and Instrumentation

Figures 5.4 and 5.5 show, respectively, the photograph and the block diagram of the experimental set-up with the associated instrumentation. The experimental model

FIG. 5.4 PHOTOGRAPH OF THE EXPERIMENTAL SETUP

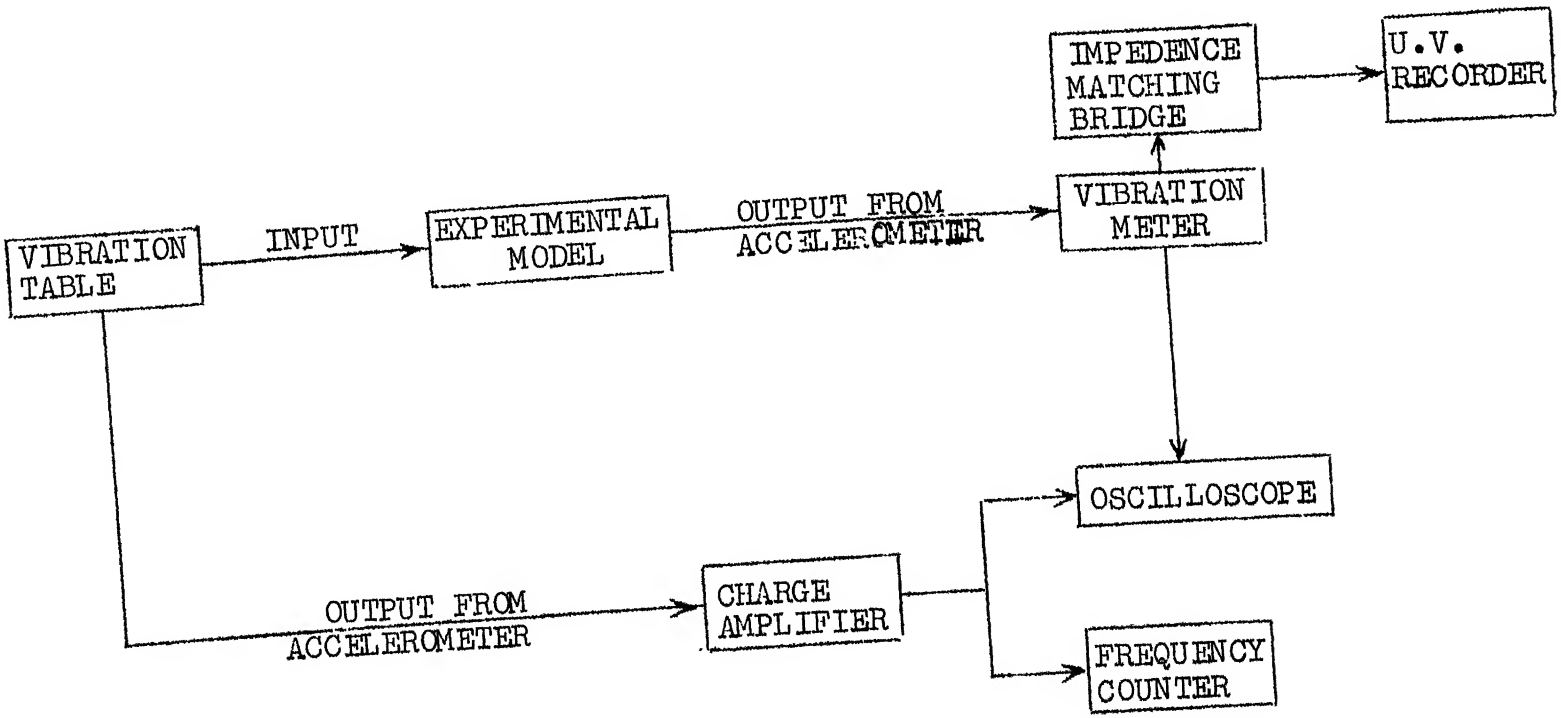

FIG. 5.5 BLOCK DIAGRAM OF THE EXPERIMENTAL SETUP

shown in Fig. 5.2 is rigidly mounted on the table of a mechanical vibrator. The table provides a harmonic displacement which is independent of the load acting on it. Both the amplitude and the frequency of excitation can be varied continuously and independently in the range 0 to 0.15 inches (total displacement) and 5 Hz to 100 Hz, respectively. An accelerometer is rigidly mounted on the top of block (a) shown in Fig. 5.3.

Output from this pickup is fed to the vibration meter which shows the displacement of the primary mass. Output signal of the vibration meter is fed to a u - v recorder for taking permanent records and also to an oscilloscope for visual display of the signal.

The amplitude of the vibration table is set and is measured with the help of a travelling microscope. Another accelerometer is mounted on the vibrating table. Through a charge amplifier the output of the accelerometer is fed to a frequency counter to measure the frequency of excitation. The frequency is measured indirectly by measuring the time periods.

The details of the instruments used are listed in appendix A-5.

5.4 OBJECTIVE AND PROCEDURE OF THE EXPERIMENT

The objective of the experiment is just to verify qualitatively the theoretical results of chapter 3. In other words, experiments are conducted to verify the existence of parameters such that for a given harmonic base excitation the pendulum oscillates harmonically at some frequencies and shows random oscillations at some other frequencies. Accordingly, experiments are conducted at certain discrete frequencies with a fixed base amplitude. The frequencies are chosen so as to reveal different types of motion of the pendulum, namely, (i) steady state harmonic oscillation, (ii) random motion and (iii) strongly stable equilibrium position. Measurement of the pendulum velocity and amplitude is quite complicated. Since the quantitative results are not aimed at, the pendulum motion is not measured. Instead the pendulum motion is observed only visually and the response of the primary is recorded.

The dampings in the primary mass and in the pendulum are idealized as viscous type. The linear natural frequency of the locked mass system, ω_1, and the damping ratio, $\bar{\zeta}_1$, are calculated from the records of free vibration decay. The spring stiffness, k_1, is measured directly from static tests. The effective mass of the locked system, $M + m$, including the contribution of sliding bearings, is calculated from the values of k_1 and ω_1. The linear natural frequency

of the pendulum, ω_2, is obtained from the measurement of its time period. Since ζ_2 is found to be quite low, the number of cycles, n, to bring down the amplitude of oscillation to half of its initial value is counted and ζ_2 is calculated from the relation

$$\exp (- 2 n \pi \zeta_2) = 0.5 \qquad (5.11)$$

By measuring the eccentricity, e, of the compound pendulum, its effective length, l, is calculated from (5.10). Inertia factor, I_f, is obtained from (5.6) as

$$I_f = \omega_2^2 \left(\frac{l}{g} \right) \qquad (5.12)$$

The experimental model is given a base excitation by presetting the amplitude and varying the frequency of the vibration table. Responses of the primary mass and the pendulum are observed for various combinations of the table amplitude and frequency. For the cases of interest, response of the primary mass is recorded.

5.5 RESULTS AND DISCUSSIONS

The measured values of the system parameters are as follows:

spring stiffness $k_1 = 1.2$ kg/cm ,

natural frequency of the locked mass system $f_1 = 6.4$ hz,

locked mass $M + m = 728$ gm,

compound pendulum mass $m = 170$ gm,

natural frequency of the compound pendulum $f_2 = 2.4$ hz,

eccentricity of the pendulum $e = 1.4$ cm,

effective length of the pendulum $l = 1.53$ cm,

inertia factor $I_f = 0.356$,

damping ratio of the locked mass system $\bar{\zeta}_1 = 0.044$

and damping ratio of the pendulum $\zeta_2 = 0.005$. (5.13)

With the above values the nondimensional quantities are calculated as

$$R = \frac{m}{M} = 0.305 , \qquad q = \frac{f_2}{f_1} = 0.375 ,$$

$$\bar{Y} = I_f \frac{Y}{l} = 0.031 \quad \text{and} \quad \bar{p} = \frac{1}{f_1 T} = \frac{1}{6.4 \bar{T}} , \tag{5.14}$$

where T is the time period of the base excitation in seconds.

With $Y = 0.132$ cm ($\bar{Y} = 0.031$), over a certain range of excitation frequency completely nonperiodic responses of the primary and the pendulum are observed. Experimental results for $Y = 0.132$ cm with increasing excitation frequency are presented below. Theoretical responses, obtained by numerical integration of (5.7) and (5.8), with parameter values given by (5.13) and (5.14), are also discussed. Initial conditions used for numerical integrations are

$$\hat{x}(0) = \hat{x}'(0) = \theta'(0) = 0 \text{ and } \theta(0) = 0.05 \tag{5.15}$$

and the step size of integration is taken as $\frac{\pi}{40}$, unless mentioned otherwise.

Theoretical nondimensional response curve for the locked mass system is shown in Fig. 5.6. The circled points show the values obtained from the experiment when the pendulum remains stationary.

The experimentally obtained locked mass response record, x_L (t), for the excitation time period T = 195 msec ($\bar{p} = 0.8$) is shown in Fig. 5.7. In this case the pendulum is not disturbed and stays in its static equilibrium position. The response record is seen to be harmonic and the pk - pk value, as measured by the vibration meter, is 280 mils. This reading is indicated by the point (a) in Fig. 5.6. Now if the pendulum is disturbed slightly from its static equilibrium position, its oscillations start growing until the pendulum and the primary mass reach harmonic steady states. The steady state response record of the primary, x (t), is shown in Fig. 5.8 and the pk - pk value is noted as 185 mils. This gives the nondimensional amplitude of the primary mass as 0.055. The numerical integration yields a stable harmonic steady state as $\hat{x} = 0.076 \cos (\bar{t} - 8.6)$, $\theta = 0.45 \cos (\frac{\bar{t}}{2} - 2.5)$.

It may be noted that when the pendulum oscillates the amplitude of the primary mass is reduced to 185 mils as compared to 280 mils with the pendulum stationary.

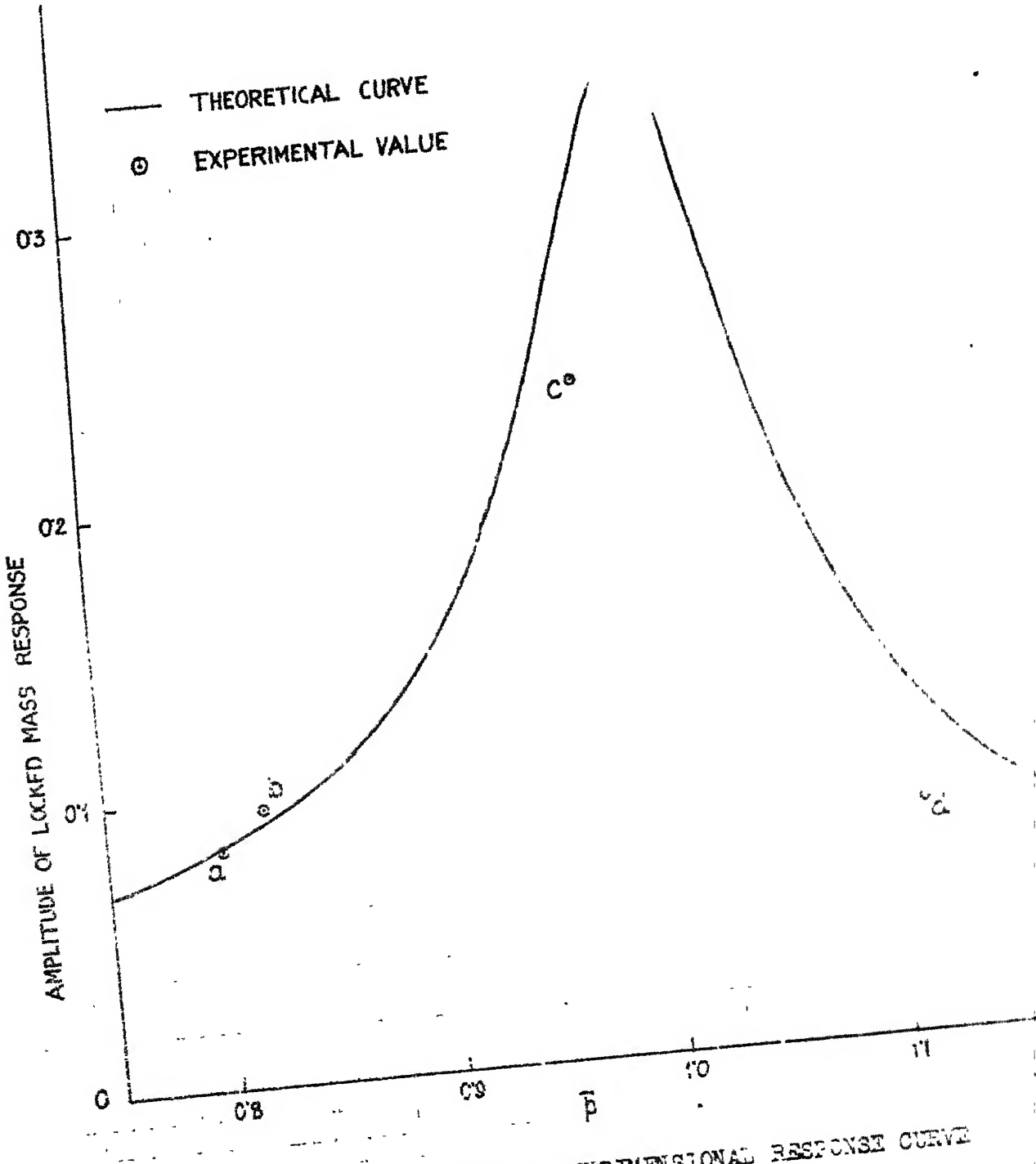

FIG. 5.6 THEORETICAL NONDIMENSIONAL RESPONSE CURVE FOR LOCKED MASS SYSTEM

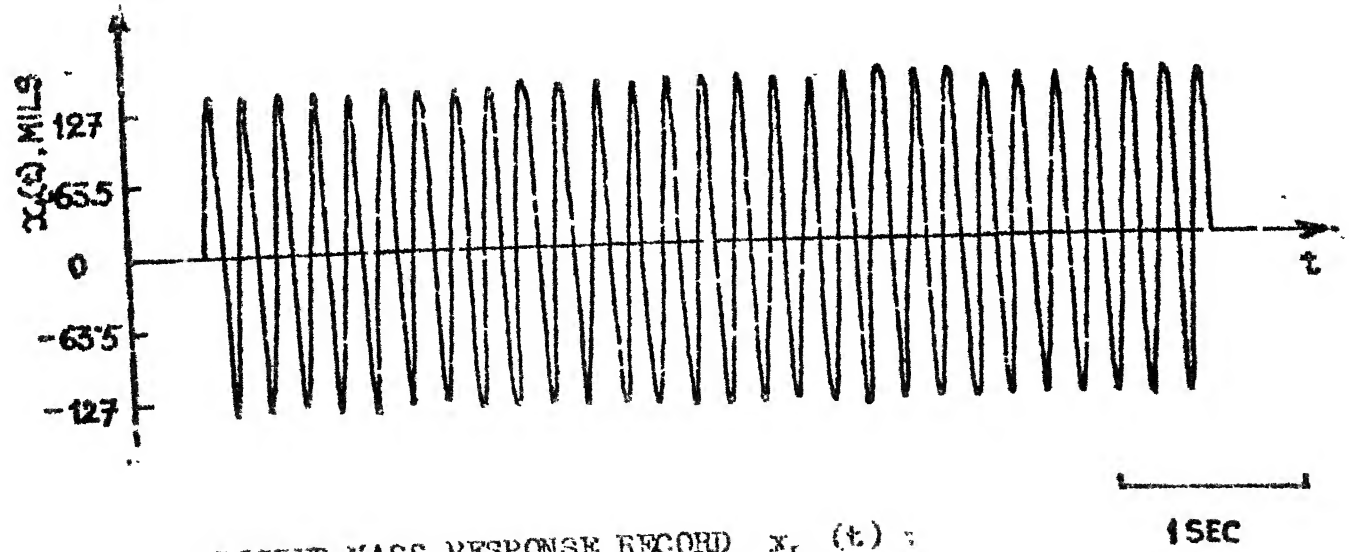

LOCKED MASS RESPONSE RECORD $x_L(t)$;
$\bar{p} = 0.8$

FIG. 5.7

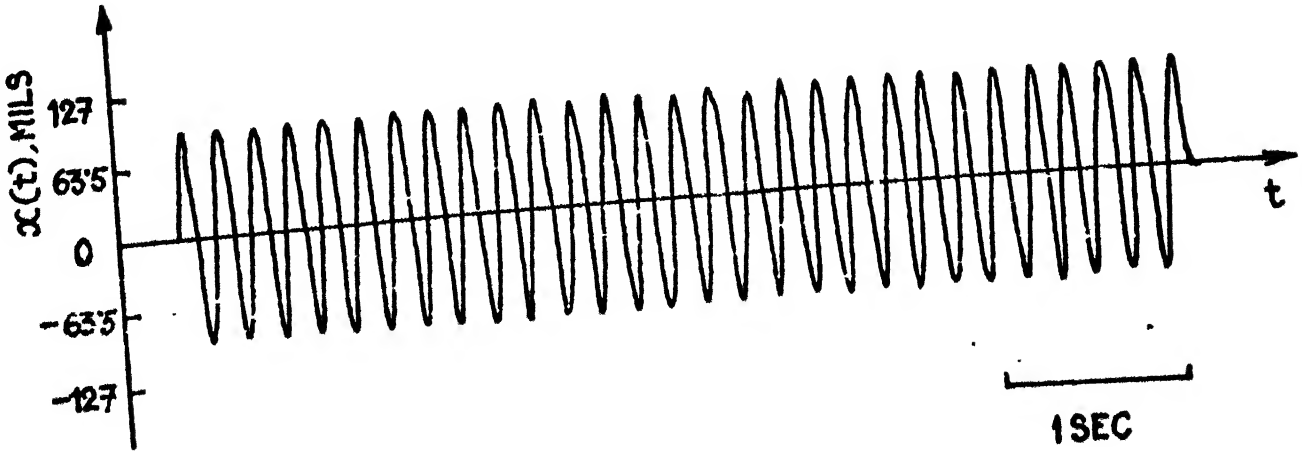

PRIMARY RESPONSE x (t) WITH PENDULUM OSCILLATING HARMONICALLY : $\bar{p} = 0.8$

FIG. 5.8

By increasing the excitation frequency to $\bar{p} = 0.82$ ($T = 190$ msec) similar patterns of the responses are observed. Figure 5.9 shows $x_L(t)$ when the pendulum does not oscillate and Fig. 5.10 shows the primary response, $x(t)$, when the pendulum also oscillates harmonically. Vibration meter shows the pk - pk values for these cases as 330 mils and 285 mils, respectively. For the latter case the nondimensional amplitude is 0.084. Integration also gives a strongly stable steady state as $\hat{x} = 0.09 \cos(\bar{t} - 10.5)$, $\theta = 0.28 \cos(\frac{\bar{t}}{2} - 0.1)$. The reduction in the primary mass amplitude, due to oscillation of the pendulum, may again be observed at this frequency as well. The amplitude of $x_L(t)$ is indicated by the point (b) in Fig. 5.6.

The locked mass response record, $x_L(t)$, for $\bar{p} = 0.97$ ($T = 160$ msec) is shown in Fig. 5.11 and the pk - pk value is measured as 800 mils. The locked mass response is again seen to be harmonic and the corresponding amplitude is shown by the point (c) in Fig. 5.6. Somewhat large discrepancy between the experimental and the theoretical values of the locked mass amplitudes may be attributed to the sharp gradient of the response curve at this frequency range. At this frequency if the pendulum is disturbed slightly from its static equilibrium position, the subsequent pendulum motion does not show any regular pattern even after a long time. It oscillates irregularly for some time and then

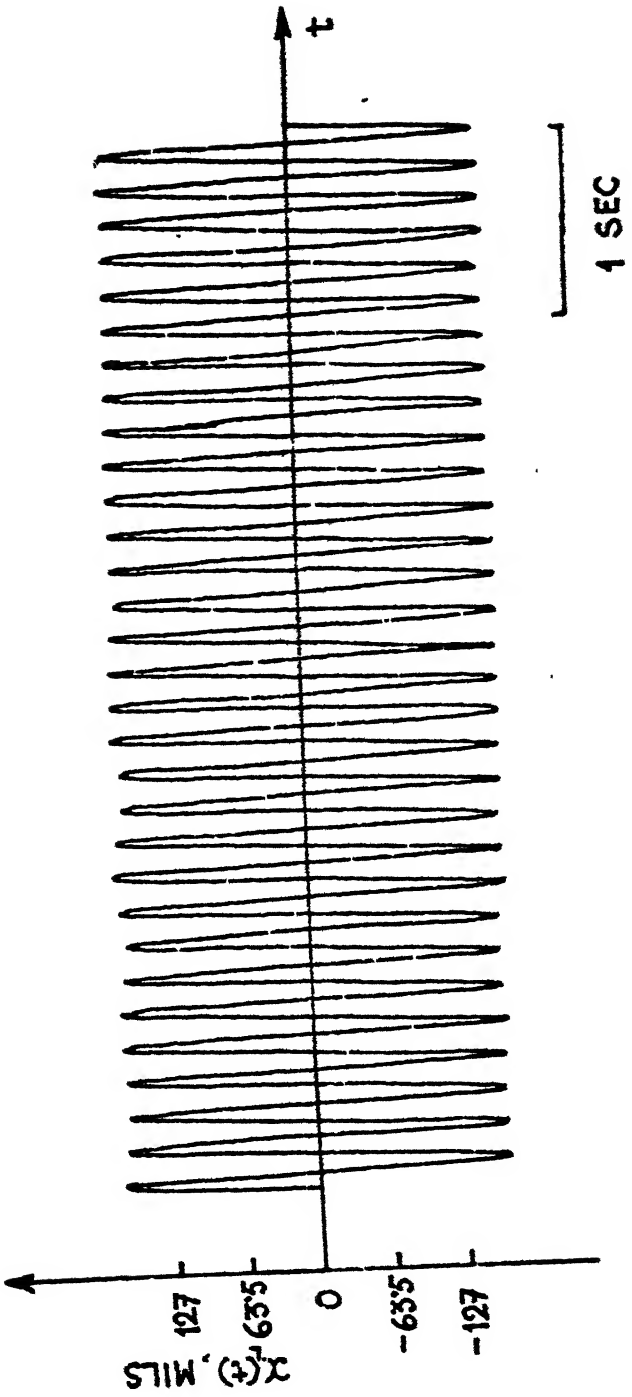

FIG. 5.9 LOCKED MASS RESPONSE $x_L(t)$ AT $\bar{p} = 0.82$

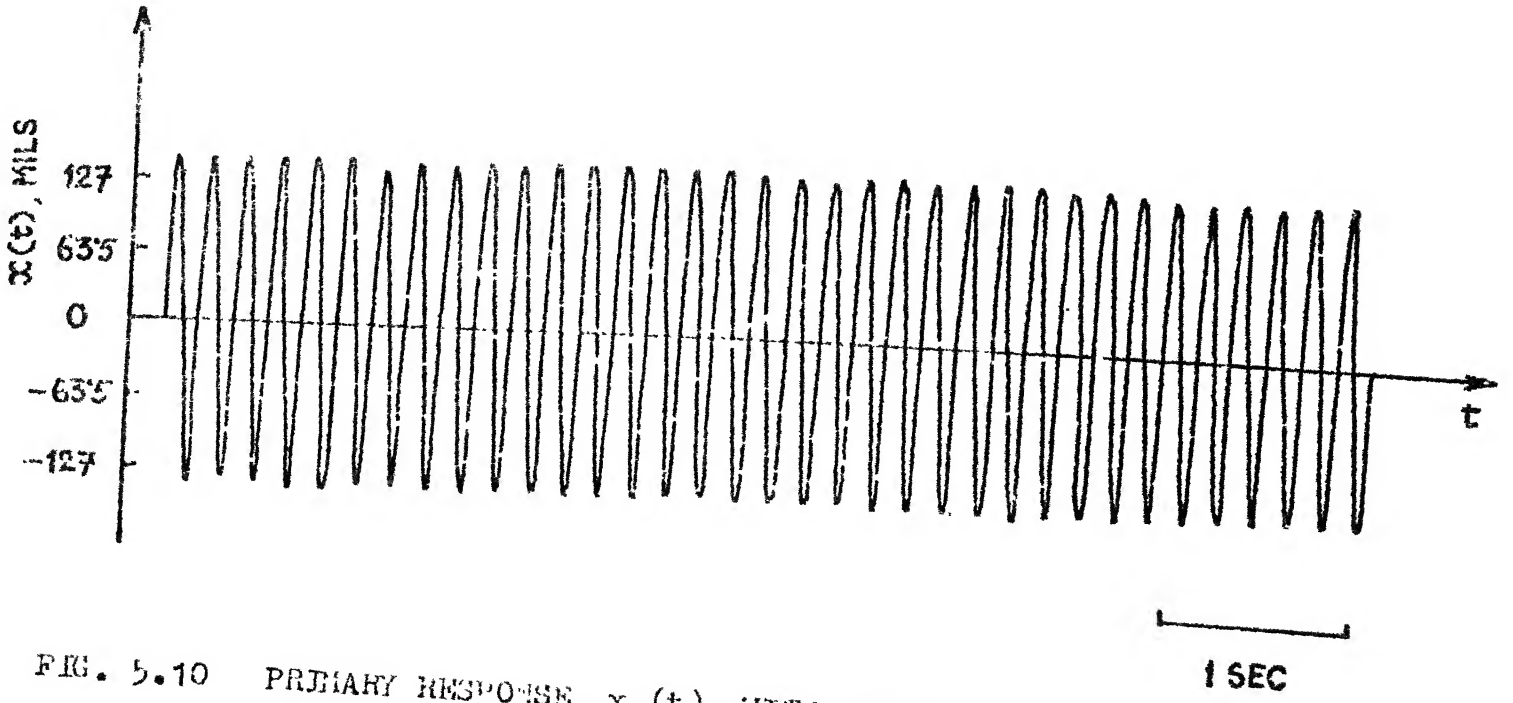

FIG. 5.10 PRIMARY RESPONSE x (t) WITH PENDULUM OSCILLATING HARMONICALLY : $\bar{p} = 0.82$

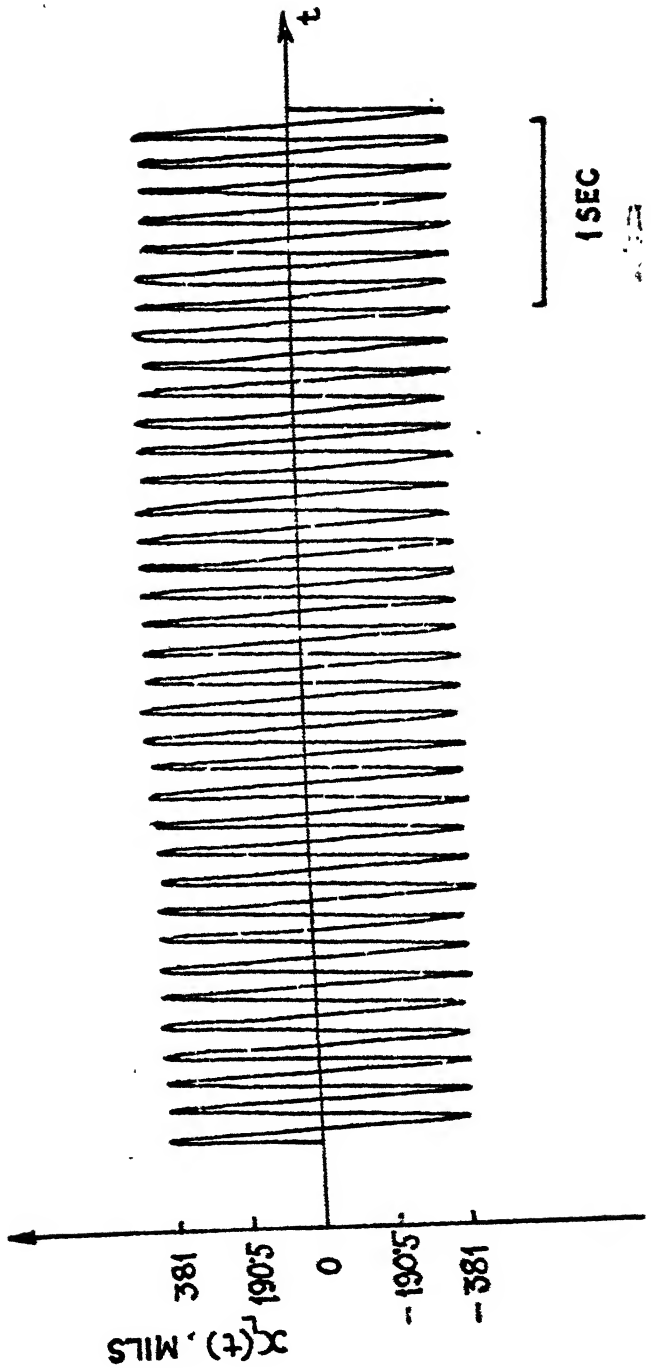

FIG. 5.11 LOCKED MASS RESPONSE $x_L(t)$ AT
$\bar{p} = 0.97$

makes few revolutions. The number and the direction of revolutions also do not show any pattern. Consequently the response of the primary, x (t), ceases to be periodic. The experiment is repeated at the same frequency by stopping the pendulum and then again letting it oscillate. After a lapse of sufficient time, when the transients are expected to die down, the response x (t) is recorded. Some such sample records are shown in Fig. 5.12. It can be seen that the response records appear different. Moreover, the records, though having some regularity, do not look periodic. This regularity in the primary motion is due to the fact that the primary system is directly driven by the base excitation. This was also observed in the theoretical responses as discussed in section 3.5.3.4. The pendulum motion is much more irregular and appears to be random in nature. The randomness in the nature of the pendulum motion is attributed to the inherent external disturbances and the fact that the parameters such as the excitation frequency etc. do not remain exactly at the same value throughout the experiment. Even if there exists a periodic steady state, it is so highly sensitive (for a particular combination of parameters) to these random disturbances and changes in parameter values that the pendulum can not attain this state and hence oscillates randomly. At this excitation frequency the numerical integration, with the initial conditions given by (5.15),

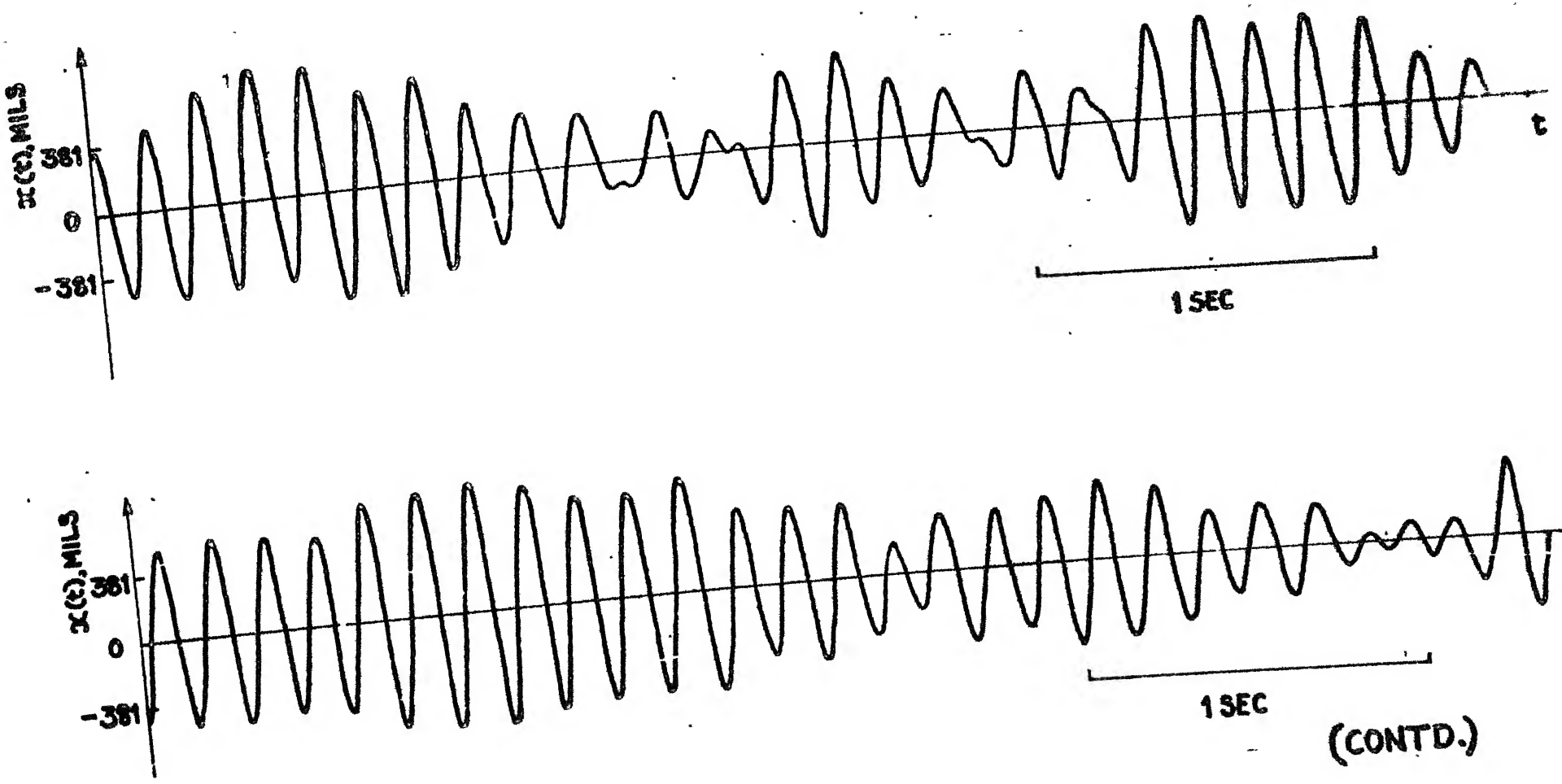
x(t), MILS
381
0
-381
t
1 SEC
x(t), MILS
381
0
-381
1 SEC
(CONTD.)

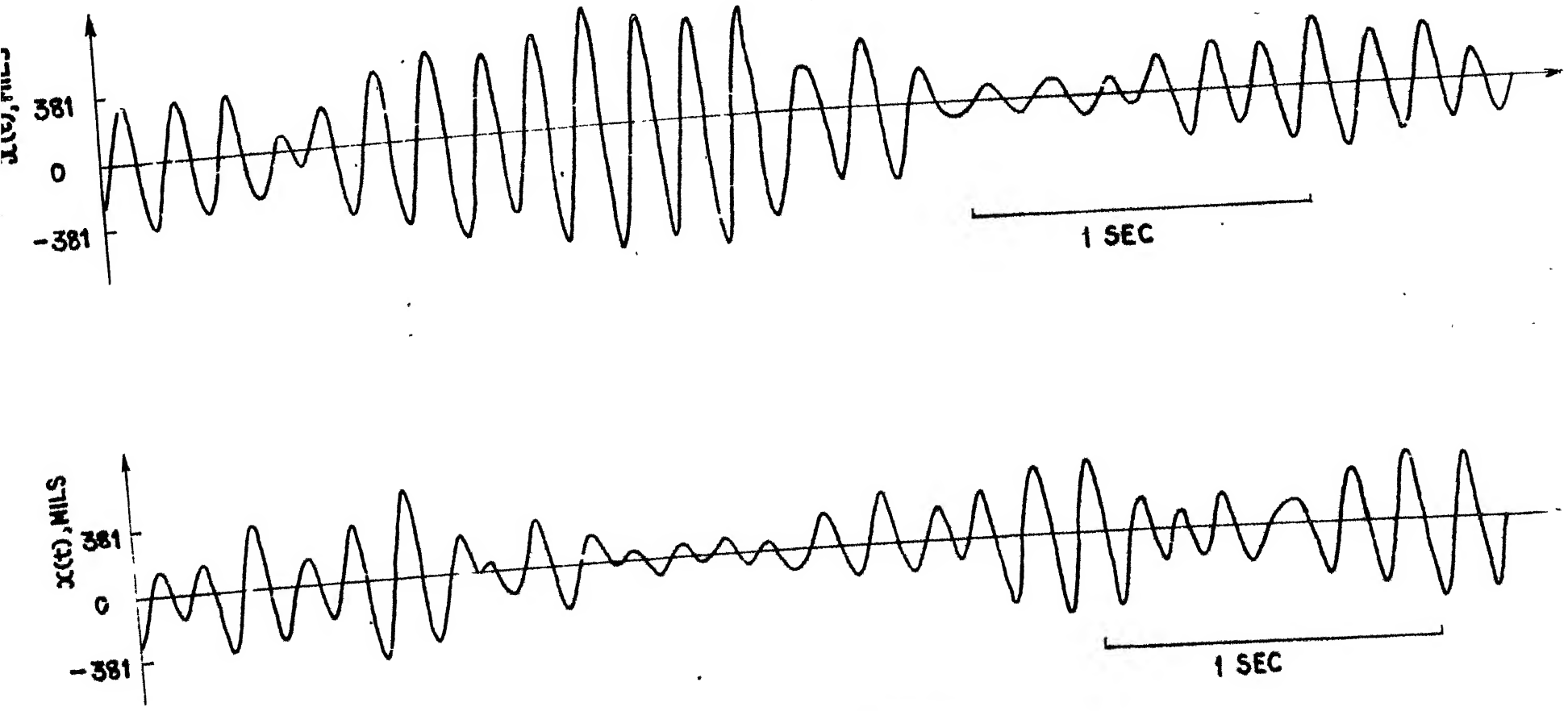

FIG. 5.12 PRIMARY RESPONSE x (t) WITH PENDULUM OSCILLATING RANDOMLY : $\bar{p} = 0.97$

also does not converge for decreasing step sizes $h = \frac{\pi}{40}$, $\frac{\pi}{80}$ and $\frac{\pi}{160}$.

At the excitation frequency $\bar{p} = 1.01$ (T = 155 msec) similar random motion of the pendulum is observed. An increase in the frequency $\bar{p}$ to 1.12 (T = 140 msec) makes the static equilibrium position of the pendulum stable. The disturbances to the pendulum die out and the system oscillates like a locked mass with a pk - pk value as 275 mils. The response is found to be harmonic and the corresponding amplitude is shown by the point (d) in Fig. 5.6.

CHAPTER 6

AUTOPARAMETRIC VIBRATION ABSORBERS

6.1 INTRODUCTION

Haxton and Barr [20] studied the possibility of using an autoparametric vibration absorber where the parametrically excited secondary system neutralizes the vibrations of the primary system. In this chapter some observations are made on the range and scope of the absorber action of the pendulum on the primary mass for the system studied in previous chapters. The conventional auxiliary mass damper is also studied briefly with an additional degree of freedom in rotation provided to the auxiliary system. The natural frequency of this rotational motion is adjusted so as to cause internal resonance.

6.2 AUTOPARAMETRIC VIBRATION ABSORBER (TWO DEGREE - OF - FREEDOM SYSTEM)

In the system considered in chapter 2 (Fig. 2.1) the pendulum is excited parametrically. With a proper selection of parameters the pendulum acts as an absorber for the primary mass as is evident from Fig. 2.6. The parameters which affect the absorber characteristics are the mass ratio R, the damping ratio of the pendulum ζ_2 and the frequency ratio q. The effect of changing q is shown in Fig. 6.1.

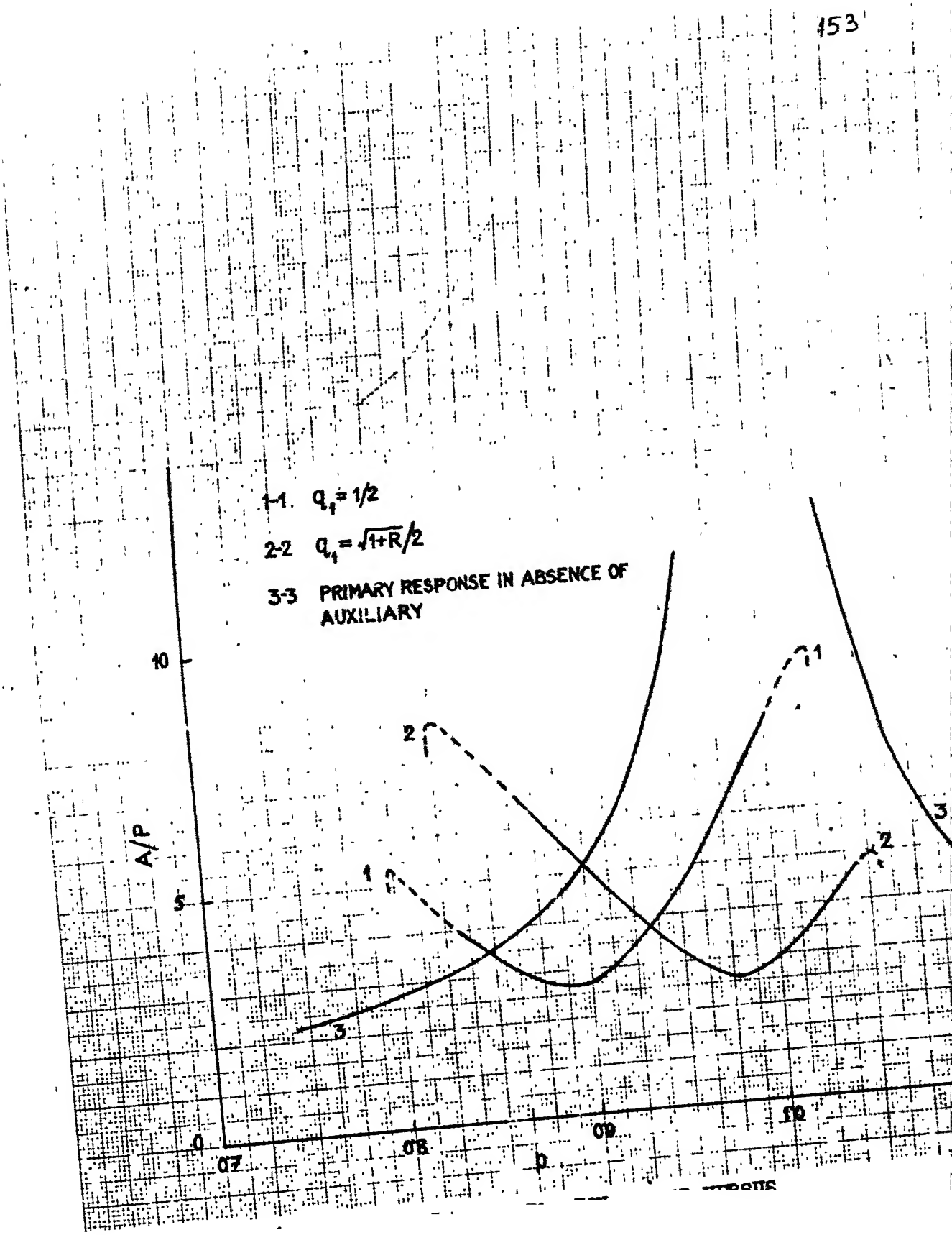
1-1. $q_1 = 1/2$
2-2 $q_1 = \sqrt{1+R}/2$
3-3 PRIMARY RESPONSE IN ABSENCE OF AUXILIARY
A/P
10
5
0
0.7
0.8
0.9
1.0
1
2
3

All the results presented in Figs. 6.1 to 6.4 are obtained by the second order approximation in harmonic balance. These results match well with the integrated results except for small differences in the overhang regions.

In Fig. 6.1 the amplitude of the primary is expressed as the ratio A/P i.e. the dynamic magnification factor. Curve 1 - 1 is obtained with $q_1 = \frac{1}{2}$, $q_2 = 0$ i.e. the linear natural frequency of the pendulum (ω_2) is taken as half of that of the locked mass. Curve 2 - 2 is with $q_1 = \frac{\sqrt{1+R}}{2}$, $q_2 = 0$ i.e. ω_2 is half of the natural frequency of the primary mass. The location and the magnitude of the peak are seen to change with change in q. Curve 3 - 3 shows the response of the primary system, with the same excitation, in absence of the auxiliary system.

Figure 6.2 shows the dynamic magnification factor for different values of ζ_2. The response in the overhang region are indicated by dotted lines. It can be seen that (with the combination of parameters as noted in the figure) the optimum absorber action is obtained with $\zeta_2 = 0.10$.

It was shown in chapter 2 that with $\zeta_2 = 0.05$ ($R = 0.2$, $\zeta_1 = 0.02$, $q_1 = 0.5$), over a certain frequency range, the responses become nonperiodic with $P = 0.05$. In this case if the damping in the pendulum, ζ_2, is increased to 0.15 the responses are again harmonic and are shown in Fig. 6.3.

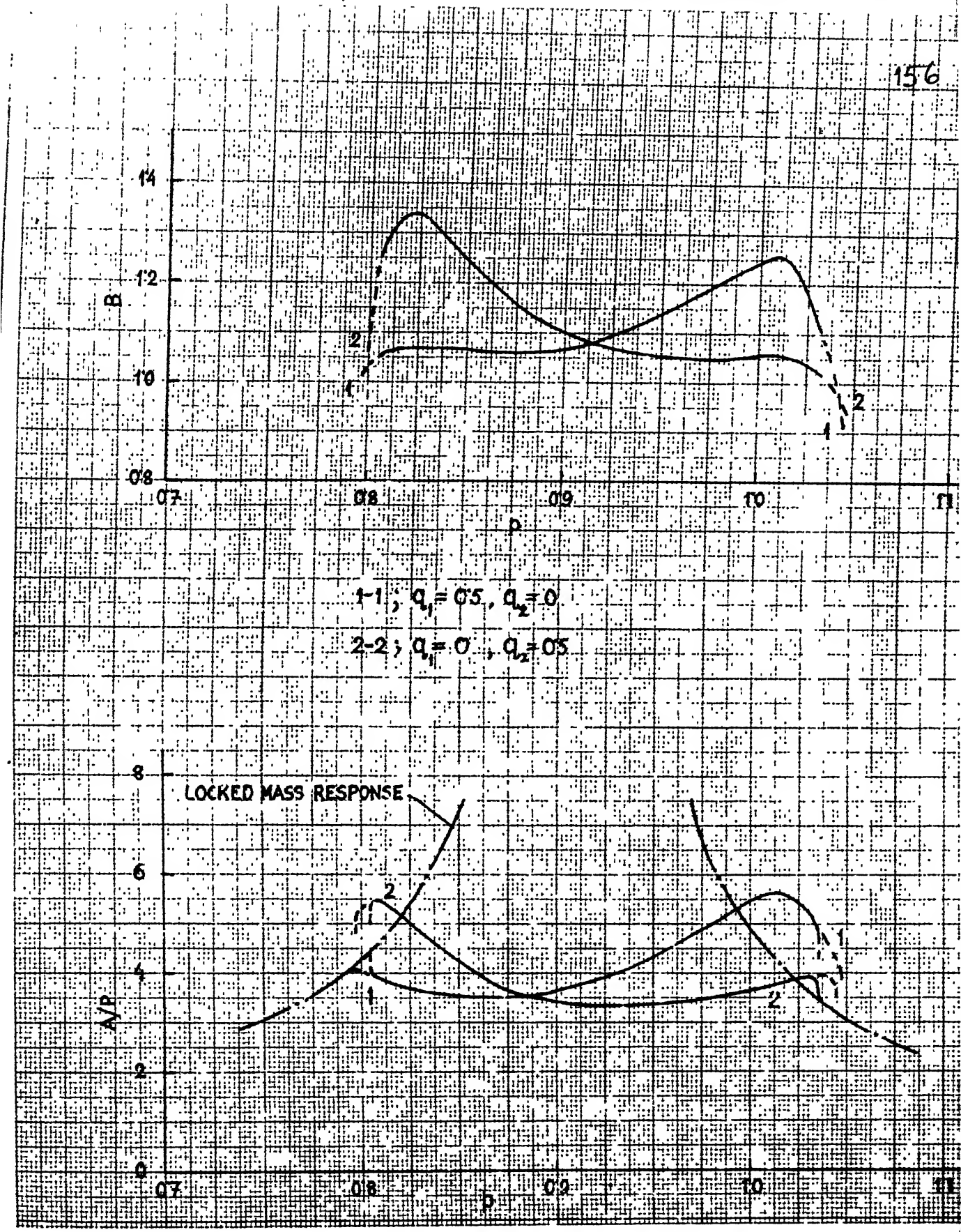

FIG. 6.3 AMPLITUDE OF THE PENDULUM AND DYNAMIC MAGNIFICATION FACTOR VERSUS FREQUENCY : $P = 0.05$, $\zeta_2 = 0.15$

The locked mass response is also included in Figs. 6.2 and 6.3. Comparison of these figures ($\zeta_2 = 0.15$) reveals that the dynamic magnification factor is not independent of P (i.e. the response of the primary is not linearly dependent on P) and the range over which the pendulum affects the primary response is also different for different values of P. Dependence of A on P not being linear was also observed in Fig. 2.4.

It can be seen from Fig. 2.4 that for $P < 0.0018$ the internal resonance does not take place and the system responds like a locked mass. For $0.0018 < P < 0.005$ the primary response is almost independent of P. But for these small values of P the primary unstable region is also quite narrow ($0.875 < p < 0.96$ for $P = 0.005$ and $\zeta_2 = 0.05$ vide Fig. 3.3) and only near the resonant frequency of the locked mass system (i.e. near $p = 0.913$) the pendulum reduces the amplitude of the primary. As P is increased beyond 0.005 only the initial change in A is somewhat linear (Fig. 2.4). Moreover, variation of A with P is obviously dependent on p which is clear from Fig. 6.4. In this figure changes of A with P are shown at two different frequencies. The chain dotted lines show the locked mass response amplitudes over the range of P where the static equilibrium position of the pendulum is stable. The dotted lines show the

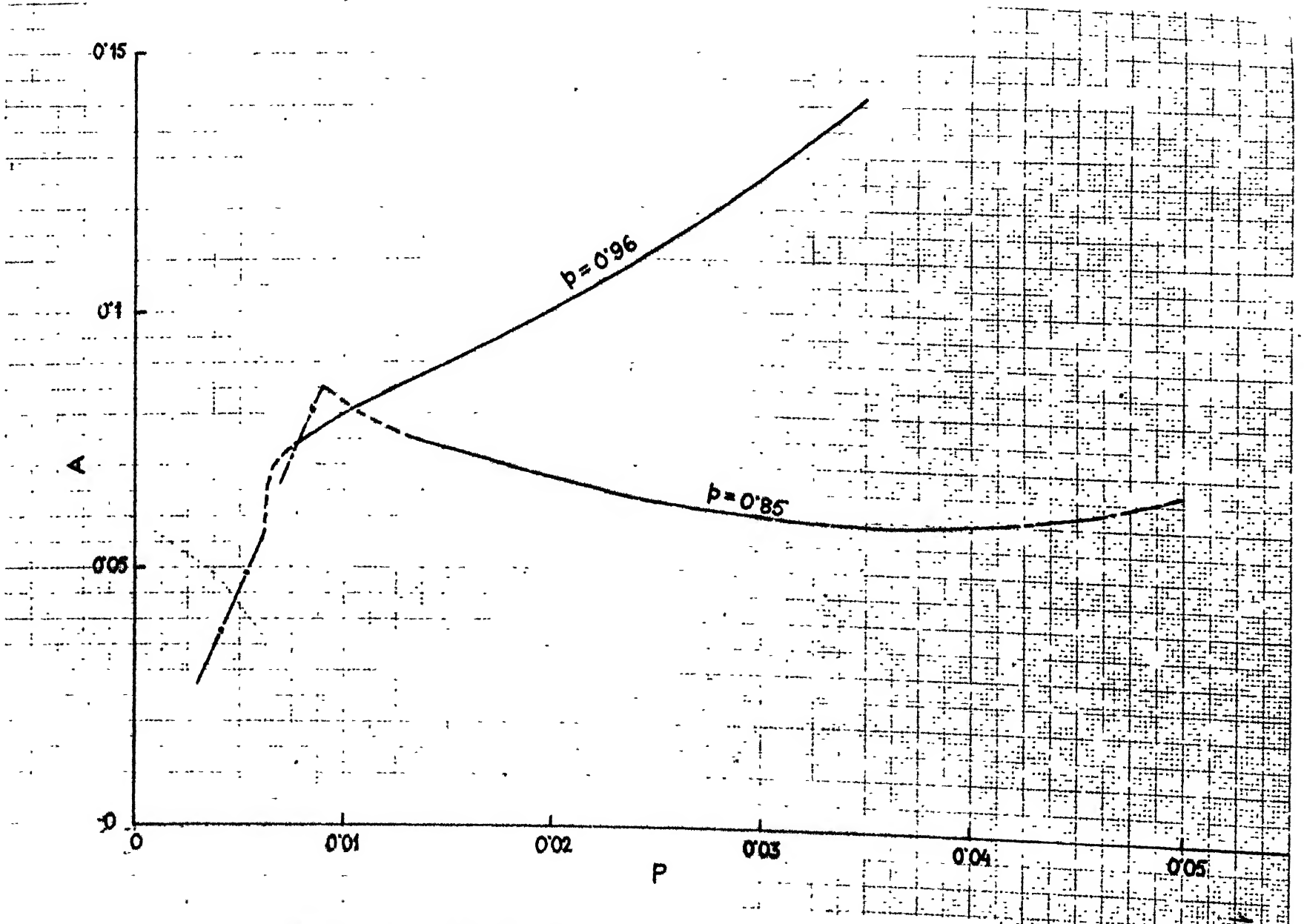

FIG. 6.4 VARIATION OF AMPLITUDE OF PRIMARY MASS WITH EXCITATION AMPLITUDE AT DIFFERENT EXCITATION FREQUENCIES : $\zeta_2 = 0.05$

amplitudes in the overhang regions and the firm lines show the amplitudes when θ also oscillates harmonically. Considering also the fact that the responses become nonperiodic over a certain frequency range for values of P beyond a certain critical value (which obviously depends on ζ_2) it is clear that for different ranges of P different values of ζ_2 will provide the optimum absorber action.

6.3 AUTOPARAMETRIC VIBRATION ABSORBER (THREE DEGREE - OF - FREEDOM SYSTEM)

6.3.1 Equations of Motion

Figure 6.5 shows a three-degree-of-freedom system which is similar to that shown in Fig. 2.1 except that the pendulum (under gravity field) is now considered to be elastic. The stiffness of the elastic pendulum is represented by k_3, c_3 being the damping coefficient. The length of the pendulum under static equilibrium is l and z represents the relative displacement between M and m.

The equations of motion are

$$(M + m)\ddot{x} + k_1 x + c_1 \dot{x} + m\ddot{z}\cos\theta - 2m\dot{z}\dot{\theta}\sin\theta - m(l + r)(\ddot{\theta}\sin\theta + \dot{\theta}^2\cos\theta) = F\cos\omega t, \quad (6.1)$$

$$m\ddot{z} + k_3 z + c_3 \dot{z} + m\ddot{x}\cos\theta - m(l + z)\dot{\theta}^2 + mg(1 - \cos\theta) = 0, \quad (6.2)$$

$$m(l + z)^2\ddot{\theta} + c_2\dot{\theta} + 2m(l + z)\dot{z}\dot{\theta} + (l + z)(mg - m\ddot{x})\sin\theta = 0 \quad (6.3)$$

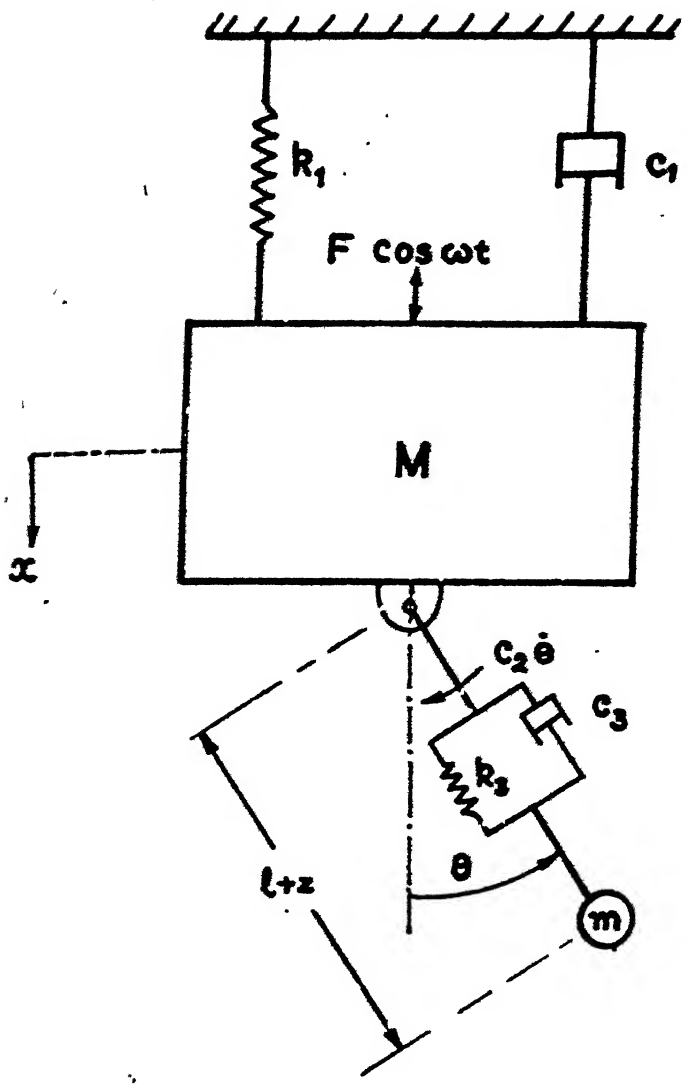

FIG. 6.5 THREE-DEGREE-OF-FREEDOM AUTOPARAMETRIC SYSTEM

In nondimensional form these equation are written as

$$p^2 (1 + R) \bar{x}'' + 2 \zeta_1 p \bar{x}' + \bar{x} + R p^2 [\bar{z}'' \cos\theta - 2 \bar{z}' \theta' \sin\theta - (1 + \bar{z}) (\theta'' \sin\theta + \theta'^2 \cos\theta)] = P \cos \bar{t} , \quad (6.4)$$

$$p^2 \bar{z}'' + \delta^2 \bar{z} + 2 \mu p \bar{z}' + p^2 \bar{x}'' \cos\theta - (1 + \bar{z}) p^2 \theta'^2 + \bar{q}^2 (1 - \cos\theta) = 0 , \quad (6.5)$$

$$(1 + \bar{z})^2 p^2 \theta'' + 2 \zeta_2 \bar{q} p \theta' + 2 (1 + \bar{z}) p^2 \bar{z}' \theta' + (1 + \bar{z}) (\bar{q}^2 - p^2 \bar{x}'') \sin\theta = 0 , \quad (6.6)$$

respectively. The various nondimensional parameters are defined as follows:

$$\bar{x} = \frac{x}{l} , \quad \bar{z} = \frac{z}{l} , \quad \bar{t} = \omega t , \quad \Omega_1 = \sqrt{\frac{k_1}{M}} , \quad \omega_2 = \sqrt{\frac{g}{l}} ,$$

$$\Omega_4 = \sqrt{\frac{k_3}{m}} , \quad p = \frac{\omega}{\Omega_1} , \quad \delta = \frac{\Omega_4}{\Omega_1} , \quad \bar{q} = \frac{\omega_2}{\Omega_1} ,$$

$$\zeta_1 = \frac{c_1}{2 M \Omega_1} , \quad \zeta_2 = \frac{c_2}{2 \omega_2 m l^2} , \quad \mu = \frac{c_3}{2 m \Omega_1} \text{ and}$$

$$P = \frac{F}{k_1 l} . \quad (6.7)$$

With high values of δ and μ the pendulum behaves like a rigid one ($\bar{z} = 0$) and (6.4) and (6.6) are same as (2.7) and (2.8). If the rotational motion of the mass m is locked ($\theta(\bar{t}) = 0 \; \forall \; \bar{t}$) the system behaves like an ordinary auxiliary mass damper and the equations of motion become

$$p^2 (1 + R) \bar{x}'' + 2 \zeta_1 p \bar{x}' + \bar{x} + R p^2 \bar{z}'' = P \cos \bar{t} \quad (6.8)$$

and $p^2 \bar{z}'' + \delta^2 \bar{z} + 2 \mu p \bar{z}' + p^2 \bar{x}'' = 0$ (6.9)

The responses for the primary and the auxiliary masses are obtained from (6.8) and (6.9) as

$$\bar{x} = A \cos (\bar{t} + \varphi_1)$$
$$\text{and } \bar{z} = Z \cos (\bar{t} + \varphi_3) , \quad (6.10)$$

$$\text{where } A = \sqrt{s_1^2 + s_2^2} , \quad \varphi_1 = \tan^{-1} (- \frac{s_2}{s_1}) ,$$
$$Z = \sqrt{s_3^2 + s_4^2} , \quad \varphi_3 = \tan^{-1} (- \frac{s_4}{s_3}) , \quad (6.11)$$

s_i (i = 1, 2, 3, 4) being given by

$$s_1 = \frac{(\delta^2 - p^2) s_5 + (2 \mu p) s_6}{s_5^2 + s_6^2} P ,$$

$$s_2 = \frac{(\delta^2 - p^2) s_6 - (2 \mu p) s_5}{s_5^2 + s_6^2} P ,$$

$$s_3 = \frac{P s_5 p^2}{s_5^2 + s_6^2}$$

$$\text{and } s_4 = \frac{P s_6 p^2}{s_5^2 + s_6^2} ,$$

with $s_5 = (1 - p^2) (\delta^2 - p^2) - (2 \zeta_1 p) (2 \mu p) - R \delta^2 p^2$

and $s_6 = (1 - p^2) \; 2 \mu p + (\delta^2 - p^2) 2 \zeta_1 p - p^2 R (2 \mu p).$ (6.12)

For $\zeta_1 = 0$ the optimum values of δ and μ are [49]

$$\delta = \frac{1}{1 + R}$$

and

$$\mu = \sqrt{\frac{3R}{8\ (1 + R)^3}} \qquad (6.13)$$

6.3.2 RESULTS AND DISCUSSIONS

Equations (6.4) to (6.6) are integrated numerically with $R = 0.2$, $P = 0.02$, $\zeta_1 = 0.02$ and $\zeta_2 = 0.12$. Initial conditions $\theta(0) = \theta'(0) = 0$ yield the results for the conventional auxiliary-mass-damper, which can be obtained directly from (6.10) to (6.12). For this case the optimum values of δ and μ (with $R = 0.2$, $\zeta_1 = 0$) are obtained from (6.13) as 0.833 and 0.208, respectively. With these values of δ and μ the dynamic magnification factor of the primary mass is shown in Fig. 6.6 (b) by the chain dotted line.

It is well known that for the values of δ and μ different from the optimum values, the locations and the magnitudes of maxima and minima in the primary response curve change. For example, the dotted lines in Fig. 6.6 (b) shows the dynamic magnification factor for the primary mass with $\delta = 1$ and $\mu = 0.1$ ($\theta(\bar{t}) = 0 \; \forall \; \bar{t}$). With this change the amplitude decreases near $p = 1$ but the peak at $p = 0.8$ becomes quite large. It is obvious that if the auxiliary

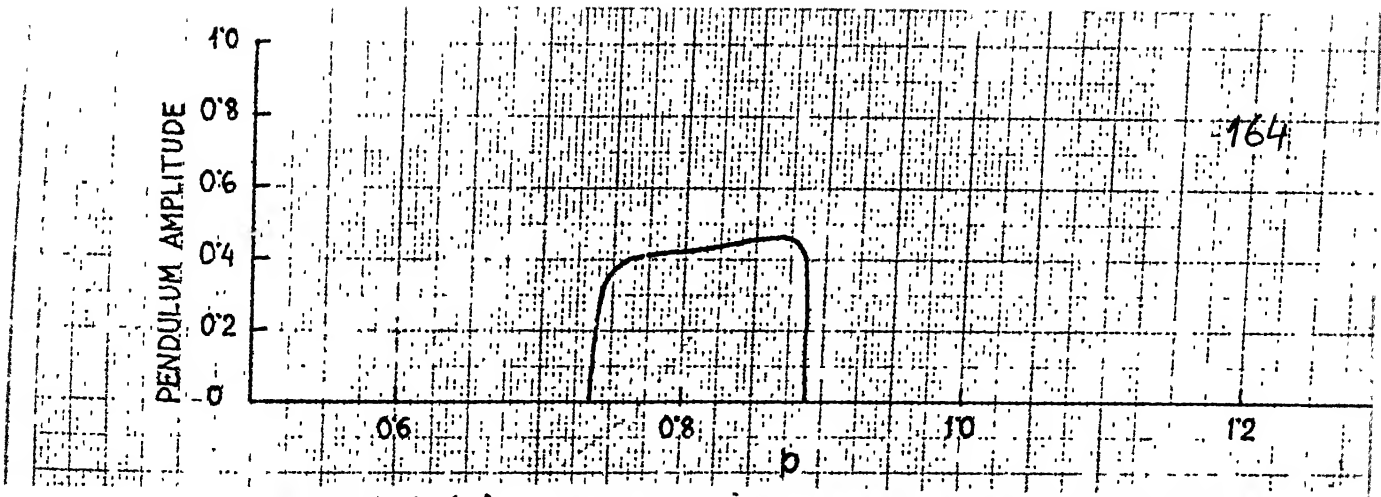

FIG. 6.6 (a) AMPLITUDE OF PENDULUM VERSUS EXCITATION FREQUENCY : P = 0.02

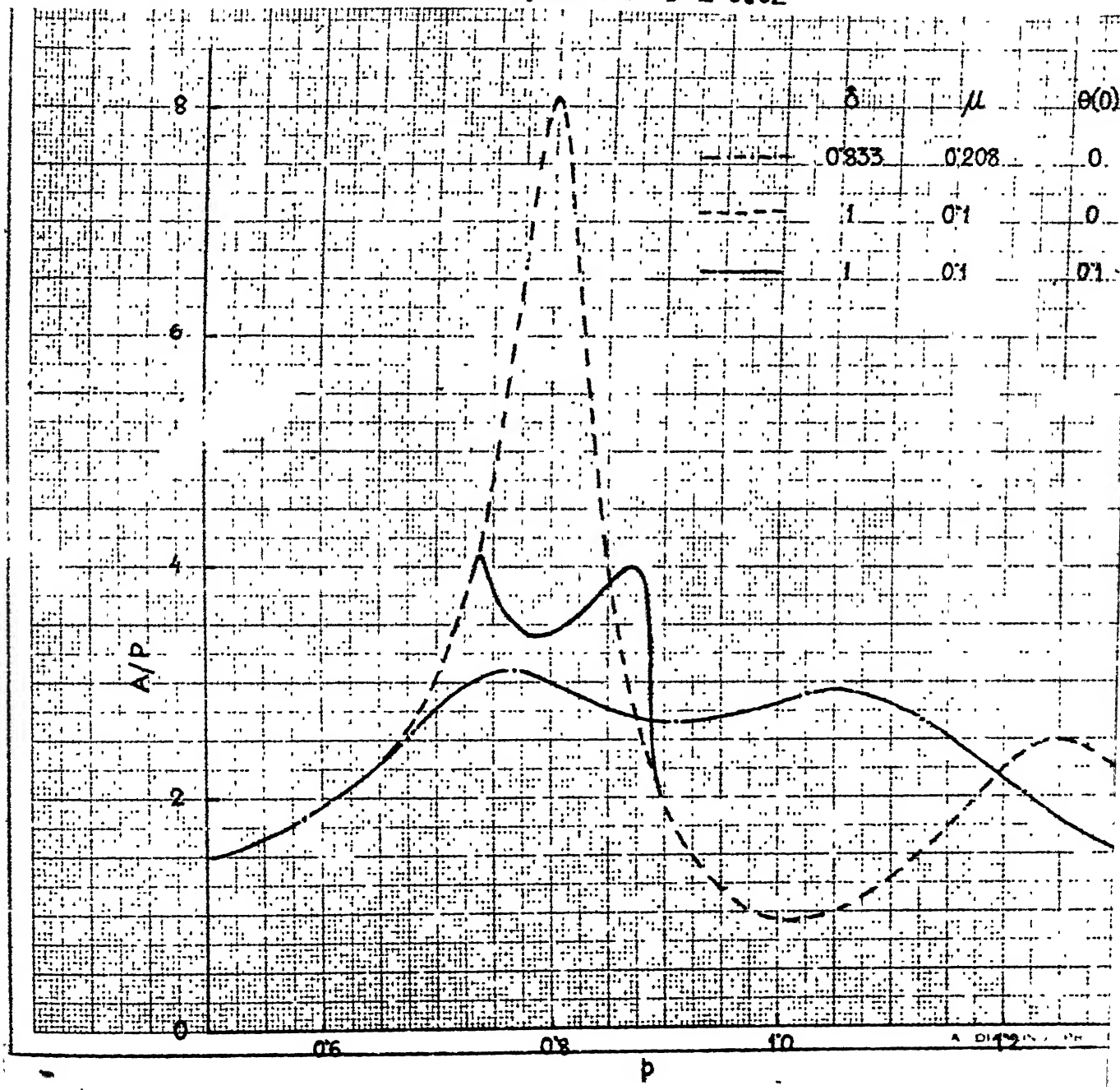

mass is given an additional degree of freedom in rotation, its effect on the primary response will be different. To study this effect near $p = 0.8$, the elastic pendulum is tuned so as to cause internal resonance near this excitation frequency.

To this end $\bar{q}$ is set as 0.4. The integrated results are obtained with $\theta(0) = 0.1$ (all other initial conditions are zero). These responses are found to be harmonic. The firm line in Fig. 6.6 (b) shows the amplitude of the primary when the pendulum also oscillates harmonically (i.e. the static equilibrium position of the pendulum is unstable). These amplitudes of the pendulum motion are shown in Fig. 6.6 (a). Outside the primary unstable region ($p \leq 0.735$ and $p \geq 0.89$) the static equilibrium position of the pendulum is stable and the system responds like an auxiliary mass damper. Because of the high damping in the pendulum, the overhang regions are almost nonexistent. The pendulum motion is seen to suppress the peak at $p = 0.8$.

The amplitudes of the relative displacement of the auxiliary mass (expressed as $\frac{Z}{P}$) are shown in Fig. 6.7. In this figure the representation of each curve is same as in Fig. 6.6 (b). It may be noted that detuning of δ and μ, from their optimum values, results in a high peak near $p = 0.8$ which again is suppressed by providing the additional degree of freedom (θ - coordinate) to the auxiliary mass.

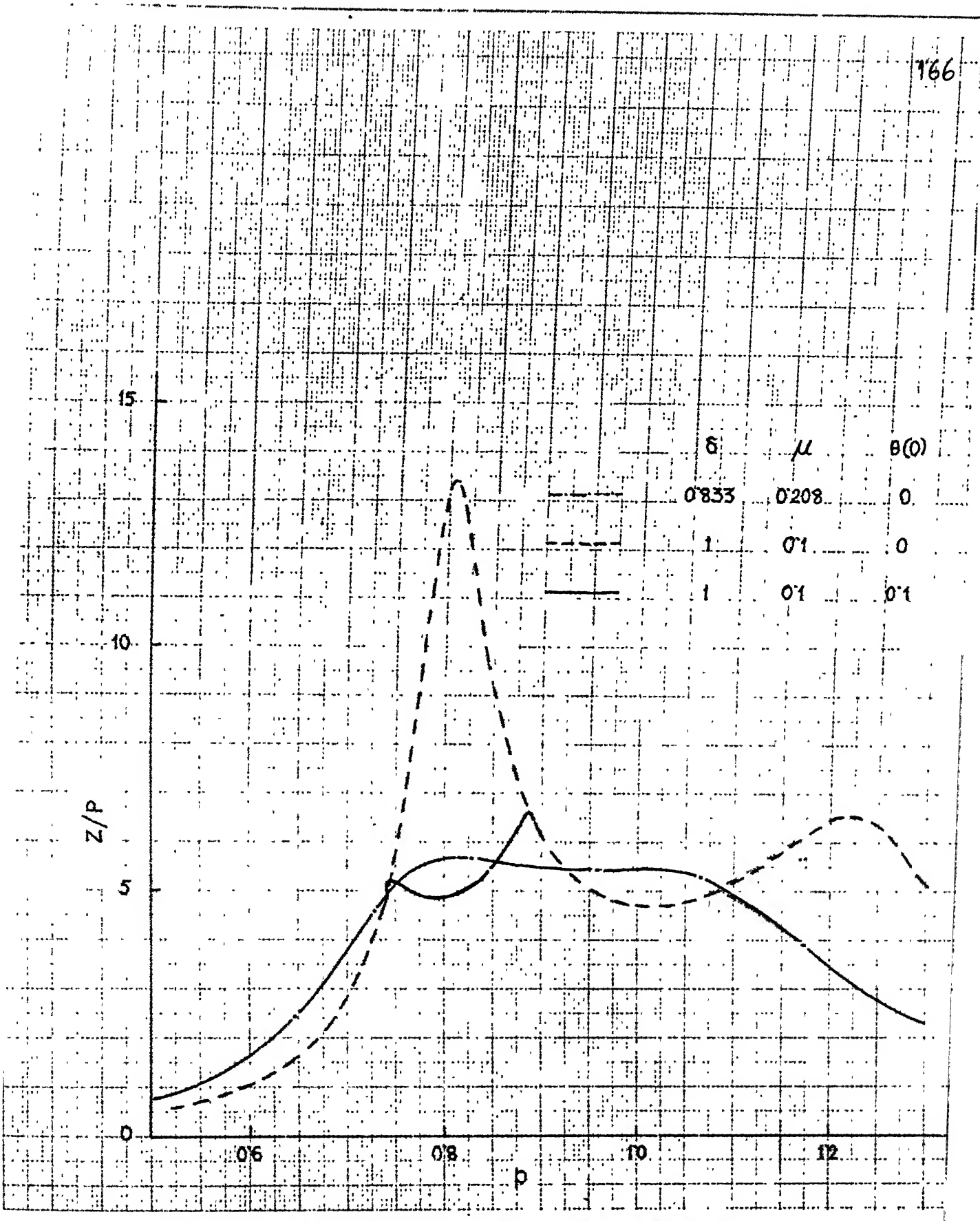

FIG. 6.7 AMPLITUDE OF LONGITUDINAL MOTION OF ELASTIC PENDULUM VERSUS EXCITATION FREQUENCY : P = 0.02

CHAPTER 7

CONCLUSIONS

This work concentrates mainly on a two degree - of - freedom autoparametric system under a harmonic excitation. The major objective is to determine the regions and nature of the harmonic and nonharmonic responses. The method of harmonic balance is used to obtain different order approximate results and these results are verified by numerical integrations. The major conclusions of the work are listed below.

1. The method of harmonic balance is sufficient to predict the existence and stability of the harmonic or near harmonic steady states. The amplitude and the stability conditions are obtained in closed form only for the first order approximations.

2. Only for sufficiently small excitations, the first order approximation (which essentially solves the approximate equations of motion with quadratic nonlinearities) yields correct results.

3. The higher order approximations reveal that (i) the primary amplitude is not independent of the excitation amplitude and (ii) the stability behaviour predicted by the first order approximation may be incorrect.

4. For the system having a spring controlled pendulum, with certain critical values of the amplitude and frequency of excitation, the stable harmonic motion bifurcates to one unstable harmonic motion and another stable amplitude modulated periodic state. The bifurcation is associated with a jump in the amplitude values.

5. For the system having a gravity controlled pendulum, with certain critical values of the forcing amplitude, following two types of branching (depending on the frequency) of the stable harmonic motion are possible:

(i) With a moderate excitation the stable harmonic motion branches out to one (or more) unstable harmonic state(s) and one (or more) amplitude modulated periodic motion(s). In this branching the amplitudes do not increase sharply. The amplitude modulated states are weakly stable and the modulation periods can vary over a wide range.

(ii) The stable harmonic motion branches out to one (or more) unstable harmonic state(s) and another chaotic state. The transition from the stable harmonic motion to chaotic motion is associated with sharp increase in the amplitudes.

6. For the combinations of forcing amplitude and frequency, resulting in chaotic states, the numerical integrations do not converge and the responses are completely non-periodic though remaining bounded. In such cases a meaningful description of the integrated responses is possible through the statistical analysis.

7. Random (or nonreproducible) responses are obtained experimentally with certain combinations of the forcing frequency and amplitude for which the numerical integrations also do not converge.

8. The pendulum in the two degree-of-freedom system exhibits limited absorber action. The major disadvantage of this absorber is that the effective frequency range, the level of the neutralizing effect and the optimum value of the absorber damping depend upon the excitation amplitude.

9. With a nonoptimal auxiliary mass damper, the peaks in the responses may be suppressed by providing the secondary with an additional degree of freedom in rotation (so that it behaves like an elastic pendulum).

REFERENCES

1. McLachlan, N.W., Theory and Application of Mathieu Functions, Dover Publications, New York, 1964.

2. Magnus, W. and Winkler, S., Hill's Equation, Wiley, New York, 1966.

3. Bolotin, V.V., The Dynamic Stability of Elastic Systems, Holden - Day, San Francisco, 1964.

4. Ibrahim, R.A. and Barr, A.D.S., "Parametric Vibration, Part I : Mechanics of Linear Problems," The Shock and Vibration Digest, 10 (1), pp. 15 - 29, 1978.

5. Ibrahim, R.A. and Barr, A.D.S., "Parametric Vibration, Part II : Mechanics of Nonlinear Problems," The Shock and Vibration Digest, 10 (2), pp. 9-24, 1978.

6. Ibrahim, R.A., "Parametric Vibration, Part III : Current Problems (1)," The Shock and Vibration Digest, 10 (3), pp. 41-57, 1978.

7. Ibrahim, R.A., "Parametric Vibration, Part IV : Current Problems (2)," The Shock and Vibration Digest, 10 (4), pp. 19-47, 1978.

8. Ibrahim, R.A. and Roberts, J.W., "Parametric Vibration, Part V : Stochastic Problems," The Shock and Vibration Digest, 10 (5), pp. 17-38, 1978.

9. Nayfeh, A.H. and Mook, D.T., Nonlinear Oscillations, John Wiley & Sons, New York, 1979.

10. Evan - Iwanowski, R.M., Resonance Oscillations in Mechanical Systems, Elsevier Scientific Publishing Company, New York, 1976.

11. Skalak, R. and Yarymovych, M.I., "Subharmonic Oscillations of a Pendulum," Journal of Applied Mechanics, Trans. ASME, 27, pp 159 - 164, 1960.

12. Caughey, T.K., "Subharmonic Oscillations of a Pendulum," Journal of Applied Mechanics, Trans. ASME, 27, pp. 754-755, 1960.

13. Caughey, T.K., "Hula - Hoop : An Example of Heteroparametric Excitation," American Journal of Physics, 28, pp 104 - 109, 1960.

14. Struble, R.A., "Oscillations of a Pendulum Under Parametric Excitation," Quarterly of Applied Mathematics, 21, pp. 121 - 131, 1963.

15. Struble, R.A., "On the Oscillations of a Pendulum Under Parametric Excitation," Quarterly of Applied Mathematics, 22, pp. 157 - 159, 1964.

16. Chester, W., "The Forced Oscillations of a Simple Pendulum," Journal of The Institute of Mathematics and Its Applications, 15, pp. 289 - 306, 1975.

17. Sevin, E., "On the Parametric Excitation of a Pendulum Type Vibration Absorber," Journal of Applied Mechanics, Trans. ASME, 28, pp. 330 - 334, 1961.

18. Struble, R.A. and Heinbockel, J.H., "Energy Transfer in a Beam - Pendulum System," Journal of Applied Mechanics, Trans. ASME, 29, pp 590 - 592, 1962.

19. Struble, R.A. and Heinbockel, J.H., "Resonant Oscillations of a Beam - Pendulum System," Journal of Applied Mechanics, Trans. ASME, 30, pp. 181 - 188, 1963.

20. Haxton, R.S. and Barr, A.D.S., "The Autoparametric Vibration Absorber," Journal of Engineering for Industry, Trans. ASME, 94 (1), pp. 119 - 125, 1972.

21. Kane, T.R. and Kahn, M.E., "On a Class of Two Degree - of - Freedom Oscillations," Journal of Applied Mechanics, Trans. ASME, 35, pp. 547 - 552, 1968.

22. Van der Burgh, A.H.P., "On the Higher Order Asymptotic Approximation for the Solutions of the Equation of Motion of an Elastic Pendulum," Journal of Sound and Vibration, 42 (4), pp. 463 - 475, 1975.

23. Van der Burgh, A.H.P., "Some Comments on the Asymptotic Theory of Nonlinear Resonance for the Elastic Pendulum," Journal of Sound and Vibration, 46 (2), p 295, 1976.

24. Mettler, E., "Higher Approximations in the Theory of the Elastic Pendulum with Internal Resonance, "Zeitschrift Für Angewandte Mathematik und Mechanik, 55, pp. 69 - 82, 1975.

25. Ryland II, G. and Meirovitch, L., "Stability Boundaries of a Swinging Spring with Oscillating Support," Journal of Sound and Vibration, 51 (4), pp. 547 - 560, 1977.

26. Sethna, P.R., "Vibrations of Dynamical Systems with Quadratic Nonlinearities," Journal of Applied Mechanics, Trans. ASME, 32, pp. 576 - 582, 1965.

27. Miles, J.W., "Stability of Forced Oscillations of a Spherical Pendulum," Quarterly of Applied Mathematics, 20, pp. 21 - 32, 1962.

28. Yamamoto, T. and Yasuda, K., "On the Internal Resonance in a Nonlinear Two - Degree - of - Freedom System," Bulletin of the Japan Society of Mechanical Engineers, 20 (140), pp. 168 - 175, 1977.

29. Sethna, P.R. and Bajaj, A.K., "Bifurcations in Dynamical Systems with Internal Resonance," Journal of Applied Mechanics, Trans. ASME, 45, pp. 895 - 902, 1978.

30. May, R.M., "Simple Mathematical Models with Very Complicated Dynamics," Nature, 261, pp. 459 - 467, 1976.

31. Lorenz, E.N., "Deterministic Nonperiodic Flow," Journal of the Atmospheric Sciences, 20, pp. 130 - 141, 1963.

32. Holmes, P.J., "A Nonlinear Oscillator with a Strange Attractor," Philosophical Transactions of Royal Society, London, 292 (1394), pp. 419 - 448, October 1979.

33. Moon, F.C. and Holmes, P.J., "A Magnetoelastic Strange Attractor," Journal of Sound and Vibration, 65 (2), pp. 276 - 296, 1979.

34. Moon, F.C., "Experiments on Chaotic Motions of a Forced Nonlinear Oscillator: Strange Attractors," Journal of Applied Mechanics, Trans. ASME, 47, pp. 638 - 644, 1980.

35. Mumford, W.W., "Some Notes on the History of Parametric Transducers," Proceedings of the Institute of Radio Engineers, 48 (5), pp. 848 - 853, 1960.

36. Rodgers, P.W., "Sub-resonant Response of a Mechanical System Parametrically Excited at Its Resonant Frequency," Nature, 207 (4999), p. 853, 1965.

37. Rodgers, P.W., "Parametric Phenomena as Applied to Vibration Isolators and Mechanical Amplifiers," Journal of Sound and Vibration, 5 (3), pp. 489 - 498, 1967.

38. Eisinger, K. and Merchant, H.C., "Amplitude Modulation of a Forced System by Parameter Variation," Journal of Applied Mechanics, Trans. ASME, 46, pp. 191 - 196, 1979.

39. Eisinger, K. and Merchant, H.C., "Clamped Beam Parametric Amplifier," Journal of Applied Mechanics, Trans. ASME, 46, pp. 197 - 202, 1979.

40. Bogoliubov, N.N. and Mitropolsky, Y.A., Asymptotic Methods in the Theory of Nonlinear Oscillations, Gordon and Breach, New York, 1961.

41. Struble, R.A., Nonlinear Differential Equations, McGraw-Hill, New York, 1962.

42. Nayfeh, A.H., Perturbation Methods, John Wiley & Sons, New York, 1973.

43. Whittaker, E.T. and Watson, G.N., A Course of Modern Analysis, Cambridge University Press, 1958.

44. Krishnamurthy, E.V. and Sen, S.K., Computer - Based Numerical Algorithms, Affiliated East-West Press, New Delhi, 1976.

45. Tables Relating to Mathieu Functions : Characteristic Values, Coefficients, and Joining Factors, National Bureau of Standards, Applied Mathematics Series 59, U.S. Government Printing Office, Washington, 1967.

46. Ralston, A. and Wilf, H.S., Mathematical Methods for Digital Computers, John Wiley & Sons, New York, 1962.

47. IBM Application Program, System/360 Scientific Subroutine Package, (360 A - CM - 03 X) Version II, IBM Technical Publications Department, New York, 1967.

48. Bendat, J.S. and Piersol, A.G., Random Data : Analysis and Measurement Procedures, Wiley, New York, 1971.

49. Den Hartog, J.P., Mechanical Vibrations, McGraw-Hill, New York, 1956.

APPENDIX A-1

DEFINITIONS USED IN STATISTICAL ANALYSIS PRESENTED IN CHAPTER 5

Various definitions and relations used in the statistical analysis are taken from reference [48].

A single time history representing a random phenomenon is called a sample function (or a sample record when observed over a finite interval). The collection of all possible sample functions which the random phenomenon might have produced is called a random process or a stochastic process.

For a given random process $\{u(t)\}$, where the symbol $\{\ \}$ is used to denote an ensemble of sample functions, the mean value $\mu_u(t_1)$ and the autocorrelation function $R_u(t_1, t_1 + \tau)$ can be found by taking the ensemble average at time t_1. When $\mu_u(t_1)$ and $R_u(t_1, t_1 + \tau)$ do not vary with t_1, the random process $\{u(t)\}$ is said to be weakly stationary. If all the possible moments and joint moments are time invariant, the random process is said to be strongly stationary.

If for a given random process the time - averaged mean value and autocorrelation function are equal to the corresponding ensemble averaged values, the process is said

to be a weakly ergodic random process. For a strongly ergodic process all the ensemble averaged statistical properties are deducible from corresponding time averages. A sample record obtained from an ergodic process will be stationary.

APPENDIX A-2

BASIC DESCRIPTIVE PROPERTIES OF A RANDOM DATA

For an ergodic random process $\{u(t)\}$ various parameters are defined as follows:

(i) Mean value μ_u is given by

$$\mu_u = \underset{T \to \infty}{\text{Lt.}} \frac{1}{T} \int_0^T u(t)\, dt \qquad \text{(A-2.1)}$$

(ii) Variance σ_u^2 is given by

$$\sigma_u^2 = \underset{T \to \infty}{\text{Lt.}} \frac{1}{T} \int_0^T (u(t) - \mu_u)^2\, dt \qquad \text{(A-2.2)}$$

(iii) Autocorrelation function $R_u(\tau)$ is given by

$$R_u(\tau) = \underset{T \to \infty}{\text{Lt.}} \frac{1}{T} \int_0^T u(t)\, u(t+\tau)\, dt\,, \qquad \text{(A-2.3)}$$

where τ is the time displacement.

$R_u(\tau)$ is a real valued even function with a maximum at $\tau = 0$. A transformed deterministic data with zero mean has $R_u(\tau)$ which persists over all τ, as opposed to the random data for which $R_u(\tau)$ approaches zero. Thus a study of an autocorrelogram can reveal the deterministic trends in apparently random data.

(iv) Power spectral density (PSD) function establishes the frequency composition of the random data. One sided PSD function can be defined as the general frequency composition of the data in terms of the spectral density of its mean square value. By this definition PSD is evaluated directly from the data points. Alternate definition of PSD function is in terms of Fourier transform of the autocorrelation function. This gives a two sided PSD function as

$$S_u(f) = \int_{-\infty}^{\infty} R_u(\tau) \exp(-2i\pi f \tau)\, d\tau , \qquad (A\text{-}2.4)$$

where f is the frequency at which S_u is being evaluated and $-\infty < f < \infty$.

For f varying over positive range only, the one sided PSD function is

$$G_u(f) = 4 \int_{0}^{\infty} R_u(\tau) \cos(2\pi f \tau)\, d\tau ; \qquad 0 \leq f < \infty . \qquad (A\text{-}2.5)$$

APPENDIX A-3

RUN TEST TO CHECK THE HYPOTHESIS OF STATIONARITY OF A SAMPLE RECORD

The stationarity of a random process is tested by investigating a single record $u(t)$ as follows:

(i) The same record is divided into J equal time intervals where the data in each interval may be considered independent.

(ii) Variance, σ_u^2 is computed for each interval. Omitting the subscript u, these values are aligned in time sequence as $\sigma_1^2, \sigma_2^2, \sigma_3^2, \cdots, \sigma_J^2$.

(iii) Finally this sequence is tested for the presence of underlying trends or variations other than those due to expected sampling variations. This is done by run test. Run test uses a nonparametric approach which does not require a knowledge of the sampling distributions of data parameters. The run test is performed as follows:

Let it be hypothesized that each variance in the sequence ($\sigma_1^2, \sigma_2^2, \cdots, \sigma_J^2$) is an independent sample value of a random variable. If this hypothesis is true, the variations in the sequence of sample values will be random and display no trend. Hence the

number of runs in the sequence relative to, say, median value will be as expected for a sequence of independent random observations of the random variable, which is presented in the Table in appendix A-4. If the number of runs is significantly different from the expected number given in the Table in appendix A-4, the hypothesis of stationarity would be rejected.

APPENDIX A-4

Table for Percentage Points of Run Distribution

Values of $r_{n;\alpha}$ such that Prob ($r_n > r_{n;\alpha}$) = α, where $n = \frac{J}{2}$,

J = Number of observations

$n = \frac{J}{2}$	α					
	0.99	0.975	0.95	0.05	0.025	0.01
5	2	2	3	8	9	9
10	5	6	6	15	15	16
15	9	10	11	20	21	22
20	13	14	15	26	27	28
25	17	18	19	32	33	34
30	21	22	24	37	39	40
35	25	27	28	43	44	46
40	30	31	33	48	50	51
45	34	36	37	54	55	57
50	38	40	42	59	61	63

APPENDIX A-5

DESCRIPTIONS OF THE INSTRUMENTS USED IN THE EXPERIMENT

1. Vibration Fatigue Testing Machine
   Model 150-VP-T (Vertical)
   All American Tool & Manufacturing Company

2. Vibration Pickup
   Type 1560 - P52
   General Radio Company

3. Vibration Meter
   Type 1553-A
   General Radio Company

4. Visicorder Oscillograph
   Model 906T - 1790F00
   Honcy Well

5. Columbia Model No. 502-1 Accelerometer

6. Electrostatic Charge Amplifier
   Model 566 M3 Multi-range
   Kistler Instrument Corporation

7. Digital Universal Counter and Timer
   Model - 613
   Yamuna